DEVELOPMENT OF CHALCOPYRITE CRYSTALS FOR NONLINEAR OPTICAL APPLICATIONS

R. F. Begley, et al

Stanford University

Prepared for:

Air Force Materials Laboratory
Advanced Research Projects Agency

1 December 1974

UNCLASSIFIED

SECURITY CLASSIFICATION OF THIS PAGE *(When Data Entered)*

REPORT DOCUMENTATION PAGE

READ INSTRUCTIONS BEFORE COMPLETING FORM

1. REPORT NUMBER: AFML-TR-74-240	2. GOVT ACCESSION NO.
3. RECIPIENT'S CATALOG NUMBER: AD-A007 838	
4. TITLE *(and Subtitle)*: Development of Chalcopyrite Crystals for Nonlinear Optical Applications	5. TYPE OF REPORT & PERIOD COVERED: Final Report, 30 June 72 - 31 Oct. 74
	6. PERFORMING ORG. REPORT NUMBER: M.L. 2387
7. AUTHOR(s): R. F. Begley, R. L. Byer, D. S. Chemla, M. M. Choy, R. L. Herbst, R. S. Feigelson, and S. Ciraci	8. CONTRACT OR GRANT NUMBER(s): F33615-72-C-2011
9. PERFORMING ORGANIZATION NAME AND ADDRESS: Microwave Laboratory, W.W. Hansen Laboratories of Physics, Stanford University, Stanford, CA 94305	10. PROGRAM ELEMENT, PROJECT, TASK AREA & WORK UNIT NUMBERS: PE61101E, ARPA Order 1636, JO #16360001
11. CONTROLLING OFFICE NAME AND ADDRESS: Advanced Research Projects Agency, 1400 Wilson Boulevard, Arlington, VA 22209	12. REPORT DATE: 1 December 1974
	13. NUMBER OF PAGES: 144
14. MONITORING AGENCY NAME & ADDRESS *(if different from Controlling Office)*: Air Force Materials Laboratory, Air Force Systems Command, Wright-Patterson AFB, OH 45433	15. SECURITY CLASS. *(of this report)*: Unclassified
	15a. DECLASSIFICATION/DOWNGRADING SCHEDULE

16. DISTRIBUTION STATEMENT *(of this Report)*

Approved for public release; distribution unlimited

17. DISTRIBUTION STATEMENT *(of the abstract entered in Block 20, if different from Report)*

18. SUPPLEMENTARY NOTES

19. KEY WORDS *(Continue on reverse side if necessary and identify by block number)*

chalcopyrites; nonlinear optics; crystal growth; $CdGeAs_2$; $AgGaSe_2$; $AgGaS_2$; second harmonic generation; third harmonic generation; fourth harmonic generation; CO_2 laser; TEA laser; nanosecond laser pulses.

20. ABSTRACT *(Continue on reverse side if necessary and identify by block number)*

This final report summarizes recent progress in the growth of three chalcopyrite crystals, $CdGeAs_2$, $AgGaSe_2$ and $AgGaS_2$. Recent applications of these crystals to the generation of tunable infrared radiation has been more actively pursued as a result of a number of important requirements for tunable sources.

The bulk of this final report is part of Dr. Begley's Ph.D. thesis and treats in detail the theory of nonlinear interactions in solids. The treatment

DD FORM 1 JAN 73 1473 EDITION OF 1 NOV 65 IS OBSOLETE

UNCLASSIFIED

SECURITY CLASSIFICATION OF THIS PAGE *(When Data Entered)*

20. (continued)

includes a discussion of third and fourth harmonic generation.

Recent work in $AgGaSe_2$ for infrared generation by mixing is presented as a reprint in Appendix III. Also included in Appendix IV is a preprint of a paper describing a new model for the calculation of second order nonlinear susceptibilities. The Bond Orbital Model is a physically descriptive model which should prove useful for estimating nonlinear properties of new semiconducting crystal compounds.

This is a final report for a program which ran over a two-year period but which formed an extension of an earlier three-year program. The accomplishments of this program have been the growth and characterization of the chalcopyrite crystals $CdGeAs_2$, $AgGaSe_2$ and $AgGaS_2$ and their application to the generation of infrared radiation by second, third and fourth harmonic generation, and by mixing over the spectral range from 1 μm to 18 μm.

NOTICE

When Government drawings, specifications, or other data are used for any purpose other than in connection with a definitely related Government procurement operation, the United States Government thereby incurs no responsibility nor any obligation whatsoever; and the fact that the government may have formulated, furnished, or in any way supplied the said drawings, specifications, or other data, is not to be regarded by implication or otherwise as in any manner licensing the holder or any other person or corporation, or conveying any rights or permission to manufacture, use, or sell any patented invention that may in any way be related thereto.

This report has been reviewed and cleared for open publication and/or public release by the appropriate Office of Information (OI) in accordance with AFR 19-17 and DODD 5320.9. There is no objection to unlimited distribution of this report to the public at large, or by DDC to the National Technical Information Service (NTIS).

Vincent L. Donlan
Project Engineer

FOR THE COMMANDER

Paul W. Elder, Maj, USAF
Chief, Laser Hardened Materials Branch
Air Force Materials Laboratory

Copies of this report should not be returned unless return is required by security considerations, contractual obligations, or notice on a specific document.

TABLE OF CONTENTS

TABLE OF CONTENTS (Continued)

LIST OF FIGURES

LIST OF FIGURES (Cont'd)

I. GENERAL INTRODUCTION

This work was undertaken over a period of three years, during which time research in nonlinear optics was increasingly concerned with both phenomena of higher order than $\chi^{(2)}$ nonlinearities and with applications of nonlinear optical techniques to spectroscopic problems.

This final report discusses progress made in the growth and application of the chalcopyrite crystals $CdGeAs_2$, $AgGaSe_2$ and $AgGaS_2$ to the generation of tunable infrared radiation. The bulk of this report is work that comprised R.F. Begley's Ph.D. thesis. However, the Appendices include work of Mr. M.M. Choy, Dr. D. Chemla, Dr. R.L. Herbst and Dr. S. Ciraci. The recent tremendous need for tunable infrared radiation reaffirms our early expectations that the chalcopyrite crystals will make an important contribution as new nonlinear optical materials.

A. NONLINEAR OPTICAL PROCESSES

The first part of this report considers the development of high peak power, short pulse, tunable infrared sources based on nonlinear optical processes in semiconductor materials. The primary laser source considered is the atmospheric pressure TEA-CO_2 laser, whose high efficiency, large output powers and relatively small operating cost make it an ideal basis for high power, tunable infrared devices.

The principal nonlinear material considered is $CdGeAs_2$, a chalcopyrite crystal with $\bar{4}2$ m symmetry. The linear and nonlinear optics properties of this material have been examined by several workers.[1-4] Due to its large

birefringence, $CdGeAs_2$ can be phasematched for second, third, and fourth harmonic generation within a large part of its transparency range from 2.4 to 18 μm. In addition, this crystal can be phasematched for difference frequency mixing of a CO and CO_2 laser to generate wavelengths between 11.4 and 16.8 μm.[5] When pumped with 5.3 μm, $CdGeAs_2$ looks promising as a parametric oscillator source covering the range from 7 to 18 μm.[4] Moreover, this crystal has the highest figure of merit for second order nonlinear interactions of all materials, with the exception of tellurium. Figure 1[6] illustrates the transparency ranges and figures of merit of all nonlinear crystals currently in use. Finally, $CdGeAs_2$ has a large burn density of 33 MW/cm^2 for a 200 nsec long pulse from a TEA-CO_2 laser.[4] These last two facts point to the possibility of doing very efficient nonlinear interactions in quite small crystals. We have, for example, measured second harmonic conversion efficiencies of 2% and conversion to third harmonic of 10^{-6} in a 2 mm long crystal using a 50 KW, 200 nsec pulse from a CO_2 laser.[3] If we extrapolate to a 1 nsec pulse with 10^8 W peak power and a 1 cm long crystal, we predict theoretical conversion efficiencies of 60% for second harmonic and 30% for third harmonic generation.

Such large conversion efficiencies indicate that both three and four frequency parametric processes can be well above threshold in just a few millimeters of material. The three frequency parametric process can be phasematched, as mentioned above. The four frequency parametric process, using two photons of 10.6 μm as a two frequency pump to generate both a longer and a shorter wave, is phasematched only very close to 10.6 μm.

The calculated parametric gains of several nonlinear materials with a length of 1 cm and an input pump intensity of 1 MW/cm^2 are shown in Fig. 2.[6]

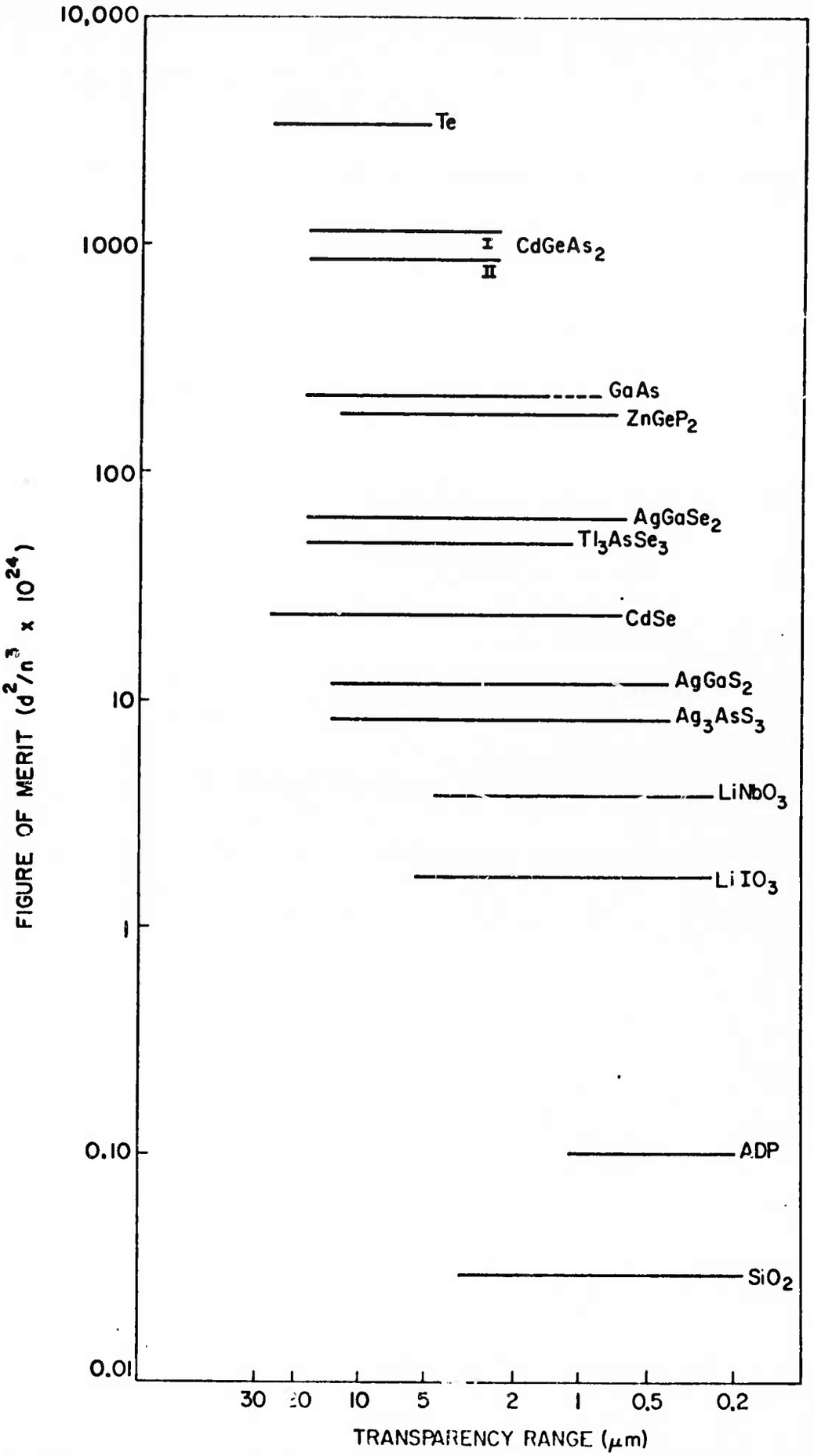

FIGURE 1. Figures of merit and transparency ranges for nonlinear optical materials.

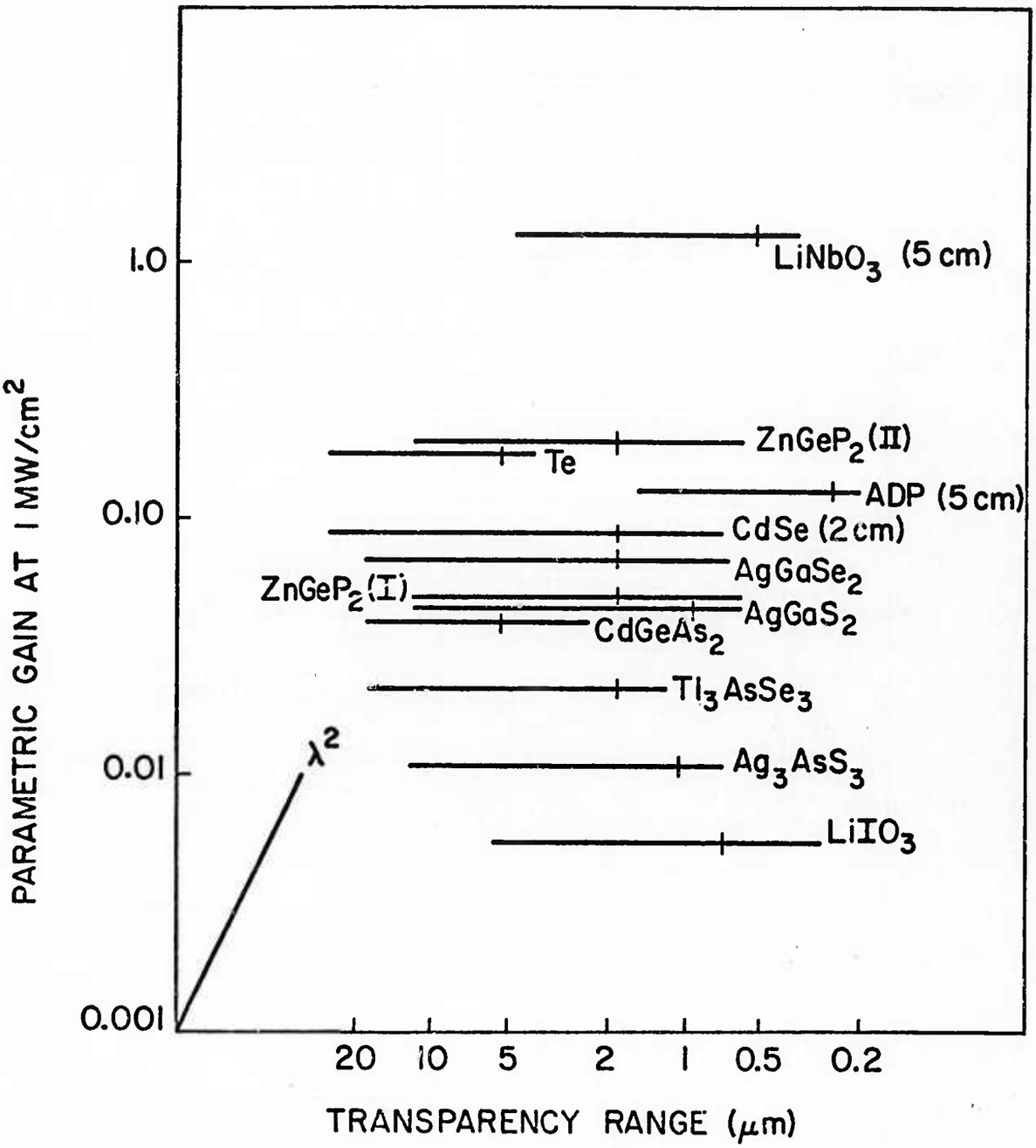

FIGURE 2--Parametric gain at 1 MW/cm^2 pump intensity for nonlinear optical materials.

For $CdGeAs_2$, a 5% gain at 1 MW/cm^2 implies a gain of approximately 1.5 at 30 MW/cm^2 which is just below the burn density for 200 nsec long pulses. For a 1 nsec pulse with 10^8 W/cm^2 we reach a gain of 5 in a 1 cm long crystal. Burn densities of 1 GW/cm^2 reported in p-type germanium[8] with a 1.7 nsec pulse raise the exciting possibility that burn densities in $CdGeAs_2$ may be about the same with 1 nsec pulses. For a 1 GW/cm^2 input intensity super-radiant gains of nearly 50 in a 1 cm $CdGeAs_2$ oscillator crystal are possible.

In order to fully evaluate the potentials of this material for efficient nonlinear optics we have constructed two CO_2 laser systems. The first device consists of a pin discharge atmospheric pressure laser oscillator, which is modelocked with a germanium acousto-optic modulator. The modelocked pulse train, consisting of twenty 1 nsec wide pulses, each separated by 10 nsec, is passed through an electro-optic selector arrangement which picks out a single 1 nsec pulse. That pulse is in turn amplified in a three pass CO_2 amplifier to reach a peak power of 10^7 - 10^8 W.

The second laser device is a high pressure, 1 meter long CO_2 laser oscillator which operates between 5 and 10 atmospheres. At these pressures the individual rotational lines are so pressure broadened that they overlap significantly. By making a three mirror cavity, with a diffraction grating as a tuning element, the output of this laser can be continuously tuned across the 9 to 11 μm range of the CO_2 molecule.

Four aspects of the work performed at Stanford are covered in this report. First, the crystal growth of $CdGeAs_2$, $AgGaSe_2$, and $AgGaS_2$ are described. Second, the design and operation of the 1 nsec system is discussed in detail. Third, a theoretical treatment is provided, both

for higher order nonlinear optical processes in $CdGeAs_2$, and for the origins of its large third order nonlinear susceptibility.[7] Finally, a description of the experimental work performed to date with this source is given. Saturation mechanisms, particularly free carrier absorption, are discussed.

At this point one might ask what applications require both high peak powers and tunability from a source operating at wavelengths from 2 to 20 μm. We can separate the applications of such sources into three categories: spectroscopy, chemical kinetic studies, and optical pumping studies.

Perhaps the most active area of laser spectroscopy at present is the study of vibrational rotational spectra of molecules, many of whose lines lie in the near infrared. Such spectra can be used, for example, as indicators of the composition of the atmosphere by remote air pollution detection schemes.[9,10] A second, and perhaps much less explored area is two photon absorption spectroscopy.

Most optical spectroscopy of solids,[11] for example, has been done by reflectivity techniques. Since the first experiments on two photon absorption near the fundamental absorption edge using visible and ultraviolet sources,[12-17] it has been clear that this technique allows one to probe the properties of bulk materials as well as of the surface states. The principal advantage of this technique is that each photon lies within the transparency range of the material. Tunable infrared sources then should have considerable application in two photon spectroscopy of semiconductors whose band gap energies lie in the near infrared. Moreover, high peak power sources should allow studies of nonlinear interactions not accessible by conventional spectrometers. Third order nonlinearities, as we shall see later, are

sensitive to the shapes of the energy bands, for example.[18]

Applications of lasers to chemistry have been reviewed by Moore.[19] Vibrational and rotational relaxation processes, as well as energy transfer mechanisms, can be studied with tunable infrared sources with pulses in the nanosecond and picosecond regimes. The question of inducing chemical reactions by selectively exciting vibrational levels has received much attention, particularly with regard to isotope separation.

Finally, optical pumping of high pressure gases appears to be an important technique for the generation of wavelengths across both the near and far infrared with pulse widths of 1 nsec and shorter.[20-27] With high peak power tunable sources one can now consider multiphoton pumping upper vibrational levels of simple molecules, exactly on resonance, to produce lasing action at a variety of wavelengths in the infrared.

An excellent review on infrared tunable sources and current spectroscopy research is given by Hinkley, Nill and Blum.[28] A table summarizing their comparison of performance characteristics of various tunable infrared sources is shown in Table I.

Important materials used in nonlinear optics devices are tabulated in Table II. Of the approximately forty chalcopyrite crystals only four are used for nonlinear optics: $ZnGeP_2$, $AgGaS_2$, $CdGeAs_2$ and $AgGaSe_2$. The enormous output powers and high efficiency of CO_2 lasers, coupled with the large nonlinear figure of merit of $CdGeAs_2$, make this particular combination a very promising source for high power, tunable infrared radiation.

TABLE I

TUNABLE INFRARED SOURCES

Source	Wavelength Range (μm)	Highest Resolution (cm^{-1})	Output Power
Semiconductor Diode Laser	1 - 34	3×10^{-6}	100 W pulsed
Spin-Flip Raman Lasers	5 - 16 9 - 14	3×10^{-5} 3×10^{-2}	1 KW pulsed
Gas Lasers Zeeman Tuned High Pressure CO_2	 3 - 9 9 - 11	 3×10^{-3} 3×10^{-2}	 1 - 10 mw cw 10-100 MW pulsed
Nonlinear Optics	0.3 - 30 μ	0.3×10^{-2}	1 μw - 1 MW

TABLE II

NONLINEAR OPTICAL DEVICES

Source	Wavelength Range (μm)	Material	Pump
Parametric Oscillator	0.4 - 4	$LiIO_3$	Ruby
	0.4 - 3.6	$LiNbO_3$	Nd:Glass/YAG
	1.2 - 8.5	Ag_3AsS_3	Nd:$CaWO_4$
	3.4 - 7.9	CdSe	Dy:CaF_2
	9.8 - 10.4	CdSe	Nd:YAG
Difference Frequency Generation	3.0 - 4.5	$LiNbO_3$	Ruby/dye
	3.2 - 5.6	Ag_3AsS_3	Ruby/dye
	4.1 - 5.2	$LiIO_3$	Ruby/dye
	10.1 - 12.7	Ag_3AsS_3	Ruby/dye
	4.6 - 12.0	*$AgGaS_2$	Ruby/dye
	7.0 - 15.0	*$AgGaSe_2$	Nd:YAG
	11.4 - 16.8	*$CdGeAs_2$	CO/CO_2
Two Photon Mixing	9.0 - 11.0	GaAs	CO_2/Klystron
Four Photon Mixing	2.0 - 24.0	K vapor	Dye/dye

*Chalcopyrites

B. CRYSTAL GROWTH

1. $CdGeAs_2$

During this program we have evaluated three growth techniques for $CdGeAs_2$, vertical Bridgeman growth, Czolchralski growth, and growth from Bismuth-Cd solution. Our results show that $CdGeAs_2$ self nucleates on the container walls and grows rapidly in a nearly dendritic way. These experiments suggest that serious consideration be given to an oven design with a very steep gradient or to the proper design of a Czolchralski growth furnace for $CdGeAs_2$. During the study program we did obtain a single crystal approximately 1 cm × 1 cm × 15 mm in size. When fabricated, this crystal yielded an oriented crystal 6 mm long by 8 mm × 8 mm area. We are now evaluating this crystal for CO_2 laser second harmonic generation (SHG). The enormous nonlinearity of $CdGeAs_2$ make further growth studies important if future advantage is to be taken of this unique material.

2. $AgGaSe_2$ and $AgGaS_2$

In a previous progress report we included a preprint of the paper "Growth of $AgGaSe_2$ for Infrared Applications" by R. K. Route, R.S. Feigelson, and R. J. Raymakers.[29] This paper described the growth of single crystal $AgGaSe_2$. Since then, we have extended our work to include the growth of $AgGaS_2$ and have successfully grown single crystals up to 1 cm diameter by 1 cm in length.

During our previous growth work, we noted the consistent poor optical quality of both $AgGaSe_2$ and $AgGaS_2$ due to optical scattering centers. For example, the measured optical loss at 1.15 μm due to scattering was 2 cm^{-1} for both crystals.

In an attempt tc improve the optical quality we tried two growth modifications. The first was to dope $AgGaSe_2$ with Tl in order to improve the growth rate. This procedure proved not to be of value. The second was to rapidly quench the crystals from a high temperature ($\sim 700^{o}C$) to room temperature. The quenching procedure did improve the optical quality by an order of magnitude reducing the loss to near 0.2 cm^{-1} – 0.1 cm^{-1} at 1.15 μm.

This remarkable improvement in crystal quality has led to a careful study of the quenching process. The work is still in progress but the main points are clear. Both $AgGaSe_2$ and $AgGaS_2$ suffer a phase separation upon slow cooling which leads to optical scatter centers. The phase separation occurs near $700^{o}C$ for $AgGaSe_2$. Crystals can be cycled through the quenching process and reproduce the desired optical quality improvement. And, finally, large single crystals can be quenched without cracking. The details of this important crystal quality breakthrough are being studied and prepared for publication.

II. THE TEA-CO_2 LASER SYSTEM

A. INTRODUCTION

The literature on CC_2 lasers, both conventional low pressure and pulsed atmospheric TEA discharges, is vast. This report describes the high peak power short pulse laser system engineered at Stanford. The description of the 1 nsec system is more from a practical construction point of view, and ample reference to the existing literature is provided to supplement the theoretical aspects of the first system's operation. A discussion of a 10 atmosphere CO_2 laser designed at Stanford, and an alternative scheme to laser triggered spark gap switching is given elsewhere.[30]

B. 1 nsec TEA-CO_2 LASER-AMPLIFIER SYSTEM

1. Background

This laser system was engineered and constructed with two objectives in mind: first, to study higher order nonlinear optical processes which become very efficient when high peak power pulses are used. However, since all materials will burn at approximately 1 - 4 J/cm^2 input energy density, it is necessary to reduce the laser pulse width to limit the total energy. Secondly, it was necessary to answer the many questions that needed investigation, particularly in producing stable, large volume gas discharges at high pressures and in producing short pulses at 10.6 μm. Laser development in this field in the past four years has been impressive, with output powers now in the gigawatt range and energies of 300 J in one nanosecond long pulses.

There are several excellent review articles[31-33] that describe the development of CO_2 lasers from the first cw laser of Patel[34] to the present 300 J system in Canada.[35]

The basic problem of providing uniform electrical discharges in large volumes of high pressure (1 - 20 atmospheres) gases has been attacked in many ways. Electrode structures for transverse excitation range from pin discharge geometries,[36-38] three electrode structures[39-43] and resistive electrodes,[44-45] to more exotic structures,[46-48] including electron beam controlled discharges,[49] which are not discussed here. An alternative approach to electron beam pumping for producing stable, large volume discharges is the use of ultraviolet radiation to preionize the laser medium.[50-59] Measurements of the electrical characteristics,[60] of the spatial and temporal behavior of the gain,[61-64] and of the spectral content[65] of TEA-CO_2 discharges have been made by several workers. Finally, several authors have attempted to fit theoretical models to TEA-CO_2 laser characteristics.[66-71] Two 1 nsec CO_2 laser systems of comparable design, although with higher output powers, have been discussed in the literature.[72-74]

2. Design and Operation

The overall system design is shown schematically in Fig. 3.

a. Laser Oscillator

The pin discharge oscillator is similar in design to one built by Robinson.[36] It consists of 400 - 1,000 Ω resistors connected in parallel for a cathode and an aluminum plate for an anode. We obtained a stable, arc-free oscillator when the resistors were cut off with equal length tips and both electrodes are mounted on a plexiglas frame to keep them parallel. The 10-meter curvature, high reflecting mirror is internal to the laser tube.

GENERAL LAYOUT OF 1 nsec TEA LASER SYSTEM

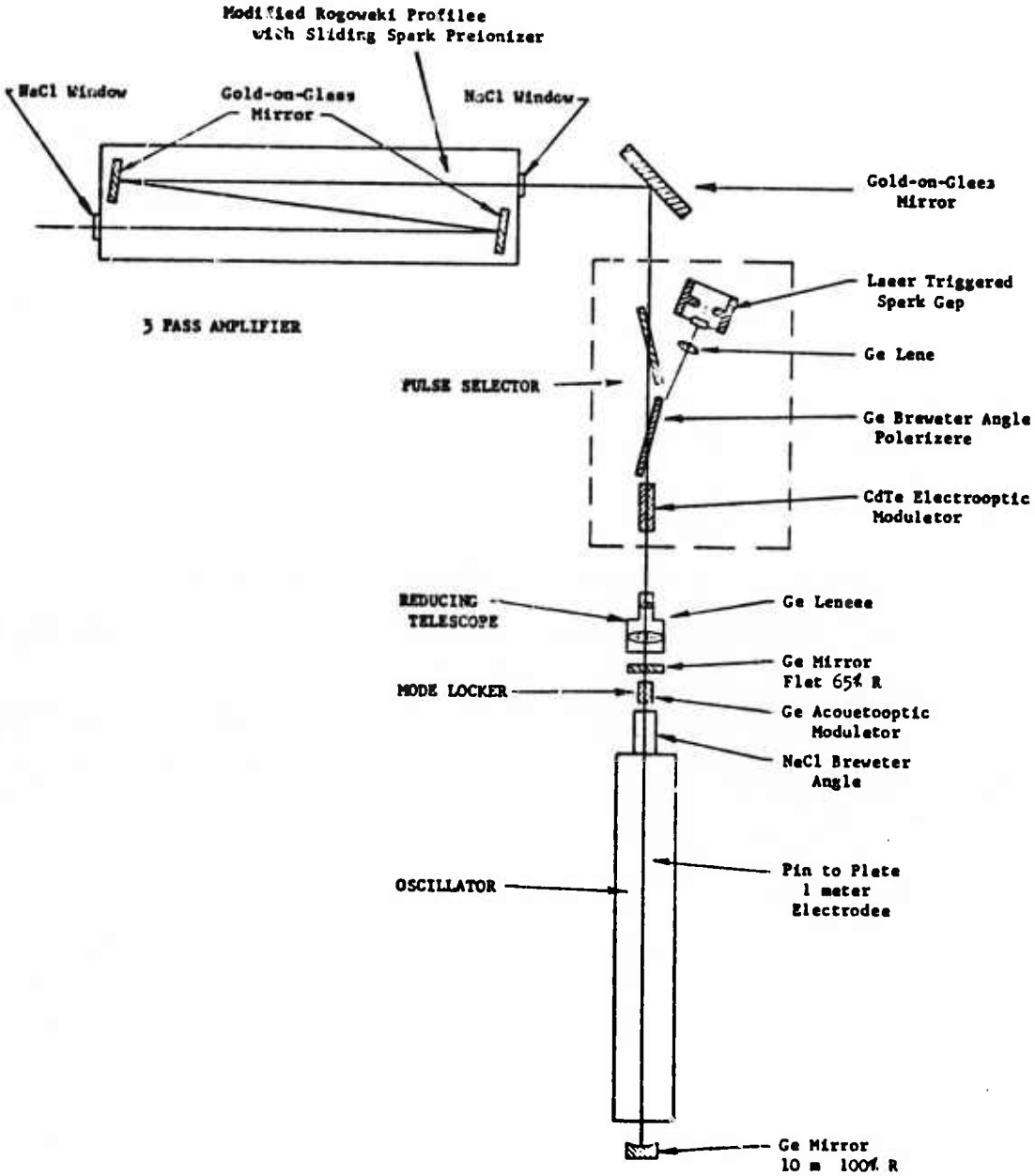

FIGURE 3. General layout of 1 nsec TEA laser system.

A sodium chloride window at Brewster's angle provides polarized output and an adjustable aperture maintains TEM_{oo} mode operation. The output mirror is a flat 65% reflecting germanium mirror located 141.61 cm from the high reflector. Output pulses from such an oscillator are typically 200 nsec in duration and 0.5 - 1.0 MW peak power in TEM_{oo} mode, at a repetition rate of several pulses per second.

Since the oscillator has been used for higher order nonlinear optics processes investigations, we wanted as stable an output pulse as possible. At low enough gains, namely when the discharge voltage is low or the mirrors slightly detuned, no mode beating occurs and this oscillator runs at approximately 5% peak-to-peak stability over sixty minutes of operation. Figure 4 shows the results of a measurement of the laser stability. We used a crystal of $CdGeAs_2$ to produce THG of the laser output. The third harmonic signal was monitored as a function of time and shows 15% peak-to-peak fluctuations. Moreover, by doing SHG in the same crystal and allowing the fundamental laser frequency to mix with the SHG signal, we again generate a 3ω signal. Here, however, the fluctuations should be proportional to twice the laser fluctuations rather than three times, as in the THG case. The result of these measurements is that the laser operates in TEM_{oo} mode at 5% peak-to-peak stability over long periods of time. At higher voltages, and with proper alignment mode beating occurs and the laser output stability degrades considerably. Finally, when completely modelocked, the pulse-to-pulse stability is again about 5% .

b. Modelocking

The modelocker consists of a germanium acousto-optic modulator[75-76] block driven by a 36° y-cut $LiNbO_3$ transducer operating as a Bragg

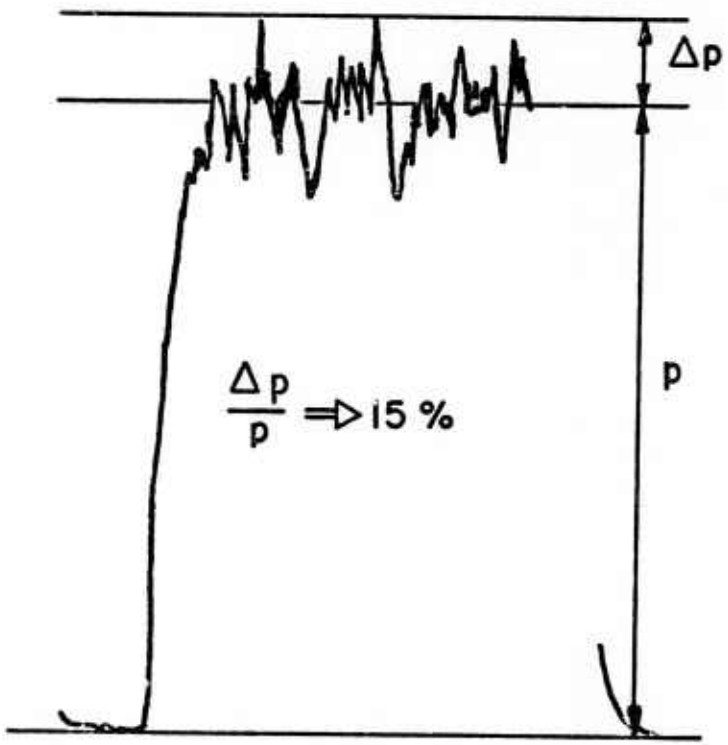

FLUCTUATIONS OF DIRECT THG

$\omega + \omega + \omega \Rightarrow 3\omega$

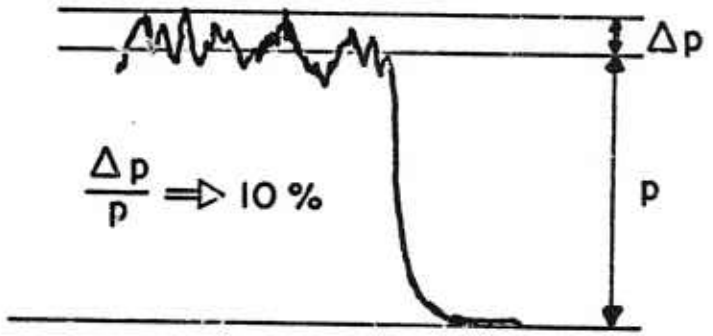

FLUCTUATIONS OF MIXING THG

$\omega + 2\omega \Rightarrow 3\omega$

$\Rightarrow$ LASER FLUCTUATIONS $\frac{\Delta p}{p} \Rightarrow 5\%$

FIGURE 4--Laser stability shown by observing fluctuations in 3ω signals.

deflector (θ_B = 41.4' inside and 2° 46' outside the crystal). Light enters the modulator in the [110] direction polarized along the [111] direction for maximum interaction. The acoustic driving frequency 50.313 MHz is half the cavity mode frequency (c/2L). In designing such a modulator with high index of refraction material (n = 4.00 at 10.6 μm in Ge), one must consider alternative designs to Brewster angle cut pieces (θ_B = 76° in Ge) in order to make reasonably small modulators. By making plane parallel faces the size of the modulator is reduced considerably but etalon effects may be introduced into the laser cavity. By anti-reflection coating the modulator faces, the bandwidth of this etalon can be made several times larger than that of the laser cavity[77] and therefore reduce the problem of cavity instability. The same modulator with no anti-reflection coating seriously affects laser stability, since the bandwidths are then comparable. Figure 5 shows the pulse train detected by a fast strontium barium niobate (SBN) pyroelectric detector[78] and displayed on a Tektronix 7904 oscilloscope. The upper trace shows a superposition of 10 modelocked pulse trains, illustrating both very clean modelocking and small peak-to-peak fluctuations. The lower trace shows a 2 nsec pulse width which is the limiting resolution of the 7904 plug-in. The actual pulses are 1 nsec wide.

c. Pulse Selector

The train of 1 nsec pulses, separated by 10 nsec, passes through a pulse selector consisting of a CdTe electro-optic crystal,[79-82] a crossed polarizer, laser triggered spark gap,[83-84] and coaxial cable charged to the correct voltage. The modelocked train enters the electro-optic crystal, reflects off the Ge Brewster angle plate polarizer and triggers the pressurized spark gap. A length of coaxial cable, charged to twice the

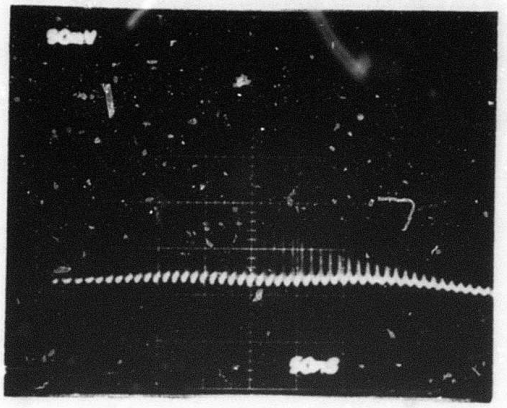

(a)

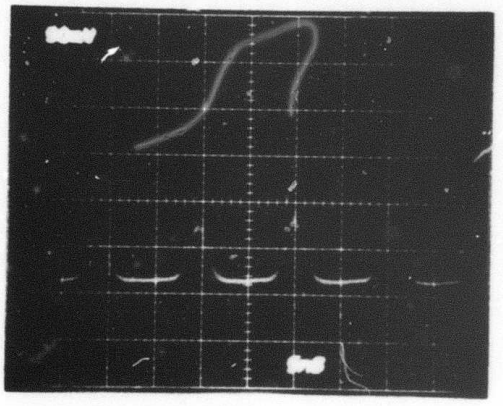

(b)

FIGURE 5. (a) Modelocked CO_2 pulse; (b) individual pulses, resolution limited by oscilloscope preamp bandwidth.

half wave voltage of the electro-optic crystal, then discharges across the crystal. By picking the length and impedance of the cable correctly (in this case 2 ft of 73 Ω cable), one can impress a square wave of approximately 1 nsec rise and fall times and 10 nsec base width on the crystal. The polarization of a single 1 nsec pulse is then changed by 90°, allowing it to pass through the Ge polarizer and out to the CO_2 amplifier. The CdTe electro-optic crystal is 46 mm long and 5 × 5 mm in cross section. The half wave voltage is 4.35 kV, so the transmission line must be charged to at least 8.7 kV (twice what appears across the crystal). Light propagates in the [110] direction in the crystal, with both electrical pulse and light polarization along the [$\bar{1}$10] direction for maximum interaction.[82] The CdTe crystal is mounted in a brass plate electrode structure designed to match the characteristic 73 Ω impedance of the transmission line.[85]

The pulse selector assembly is by far the most unstable part of this entire system. It is quite difficult to trigger the spark gap reliably over more than 100 pulses without readjustment of the laser focus. More importantly, however, such a fast spark discharge radiates very high frequency noise (1 - 10 GHz) which makes detection of the switched out 1 nsec laser pulse very difficult on any fast detector. By using a slow but sensitive pyroelectric detector as an energy monitor we have observed stable switching of pulses from the modelocked pulse train. By replacing the spark gap with a completely electronic detection and switching system, it appears possible to make a noise free, reliable pulse selector. A suggested design is discussed in reference 30.

d. Amplifier

The single 1 nsec pulse then passes through a three pass, modified Rogowski profile CO_2 amplifier.[86] To make the discharge more uniform, two arrays of spark sources called "sliding sparks"[87-89] line the sides of the electrode structure. The spark sources were made in a transmission line geometry to allow easy handling. By milling a pattern of rectangular tabs on the top of double copper clad circuit board, one creates a transmission line with gaps, which can be modeled as an array of capacitors coupled together by the stray capacitance of each gap. A pulse propagates on this line by arcing across each gap, thus emitting UV radiation into the laser plasma. The geometry of the electrodes for both laser oscillator and amplifier is shown in Fig. 6. The amplifier has two internal mirrors made by depositing gold coatings on flat glass so that the amplifier can be used for 1, 2, 3 or 5 passes. We have measured the single pass gain to be 1%/cm of excited volume. Typical CO_2 amplifier gains range from 1%/cm to 4%/cm, depending on gas mixture, electrode structure, preionization techniques, and discharge voltage. In this amplifier we are limited in voltage to 30 kV by our power supply and can only operate at 300 torr pressure. The measured gain is quite good under these circumstances. It would be necessary to modify the high voltage electronics to allow operation at higher voltages and pressures to raise the gain.

In contrast to the resistively ballasted oscillator which operates on CO_2 and He alone, the amplifier requires a 2 : 1 : 3 ratio of CO_2, N_2 and He to operate stably. Since both oscillator and amplifier power supplies are the same, it appears that the impedances of each electrode structure are not the same. The switching thyratron likes to look into a 50 Ω load; apparently

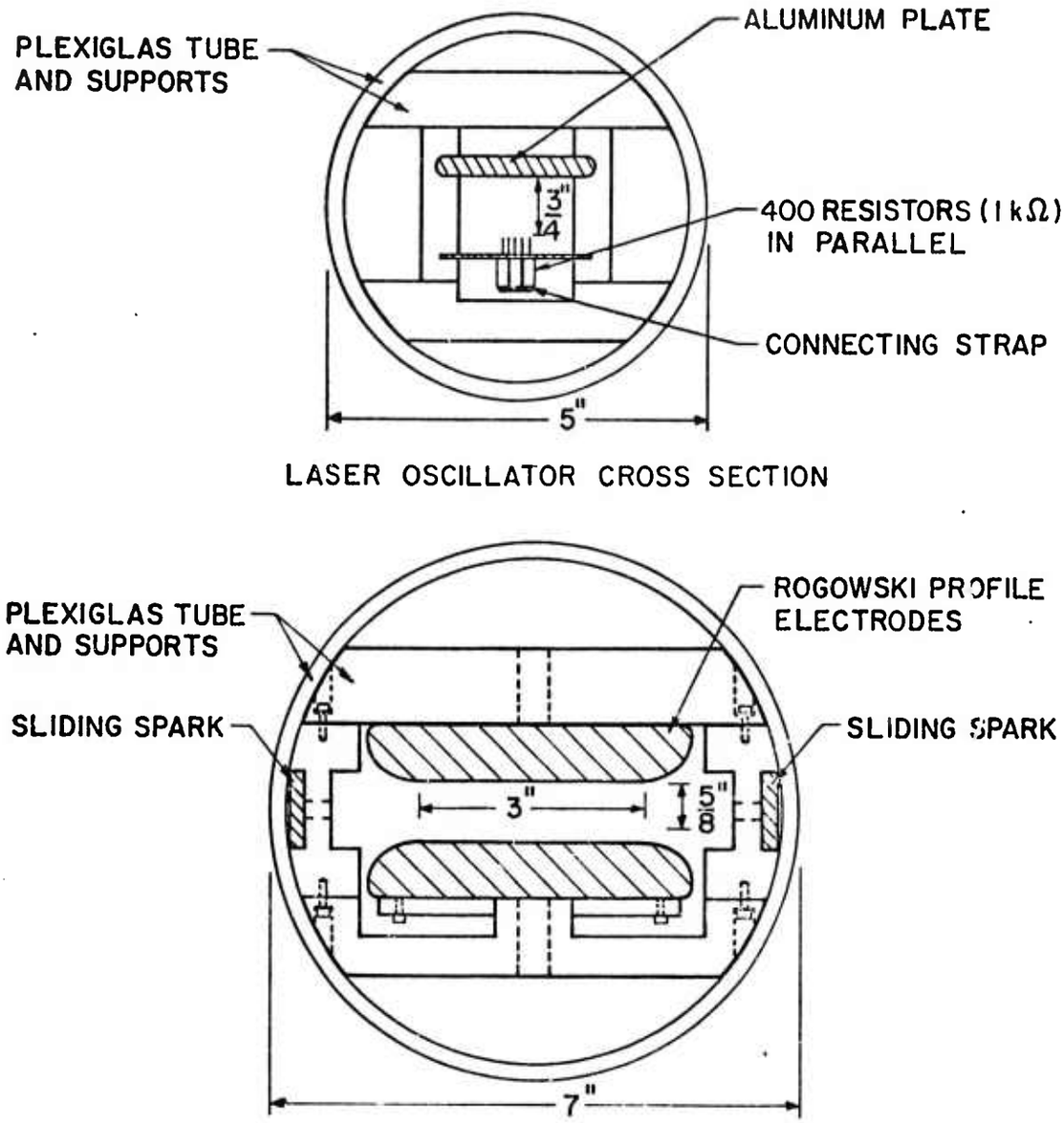

FIGURE 6. Oscillator and amplifier electrode structures.

by adding nitrogen to the amplifier medium we balance the capacitance of the electrode structure to make the amplifier look more like a 50 Ω load.

When properly impedance matched, both devices emit relatively little electrical noise by comparison to the laser triggered spark gap.

e. Electronics

The circuit diagrams for the system rate generator and master control, thyratron trigger circuits, and high voltage electronics are shown in Figs. 7 to 9. The modelocking electronics is not shown here. It consists of a standard Tektronix 190B signal generator operating at 25.157 MHz, and a Heathkit DX-60 transmitter modified to operate in pulse mode at twice the oscillator frequency. Since the effective impedance of the acousto-optic modelocker is 2.2 Ω, it is necessary to use a pi network to match the 50 Ω output impedance of the Heathkit transmitter.

Since we require 3.7 kV on the transmission line for operation of the CdTe electro-optic crystal, and we must maintain a rise time of 1-2 nsec, it seemed impossible at first to use an avalanche transistor array for the pulse selector electronics. Consequently we had to use a laser triggered spark gap as our fast switch. DC voltage is provided by a Variac and DC power pack. However, by using a transmission line transformer it now appears that an array of approximately 32 avalanche transistors can be used to generate 4-5 kV across the electro-optic crystal. A block diagram of the proposed electronics is shown in reference 30.

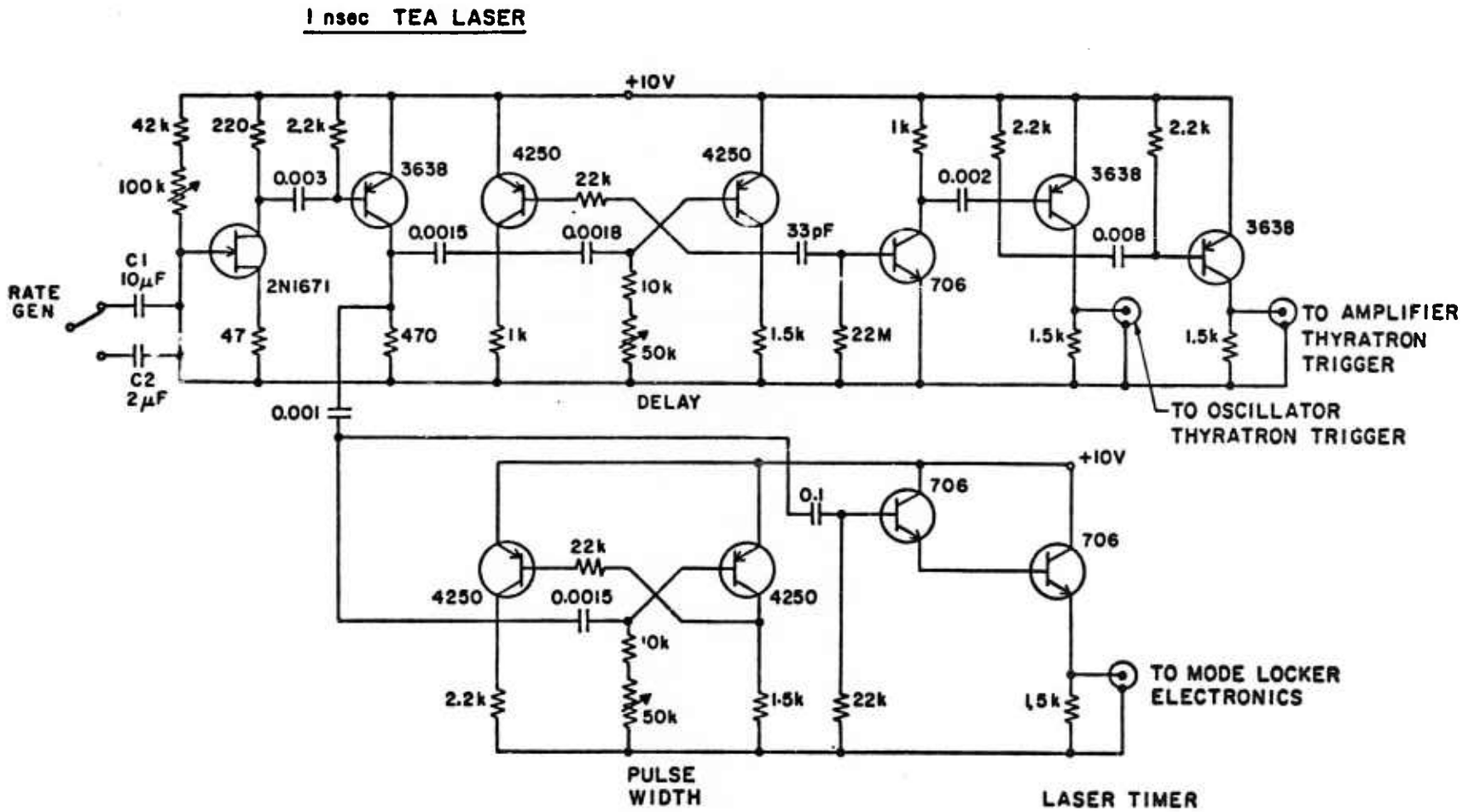

FIGURE 7. Master control circuit for 1 nsec laser system.

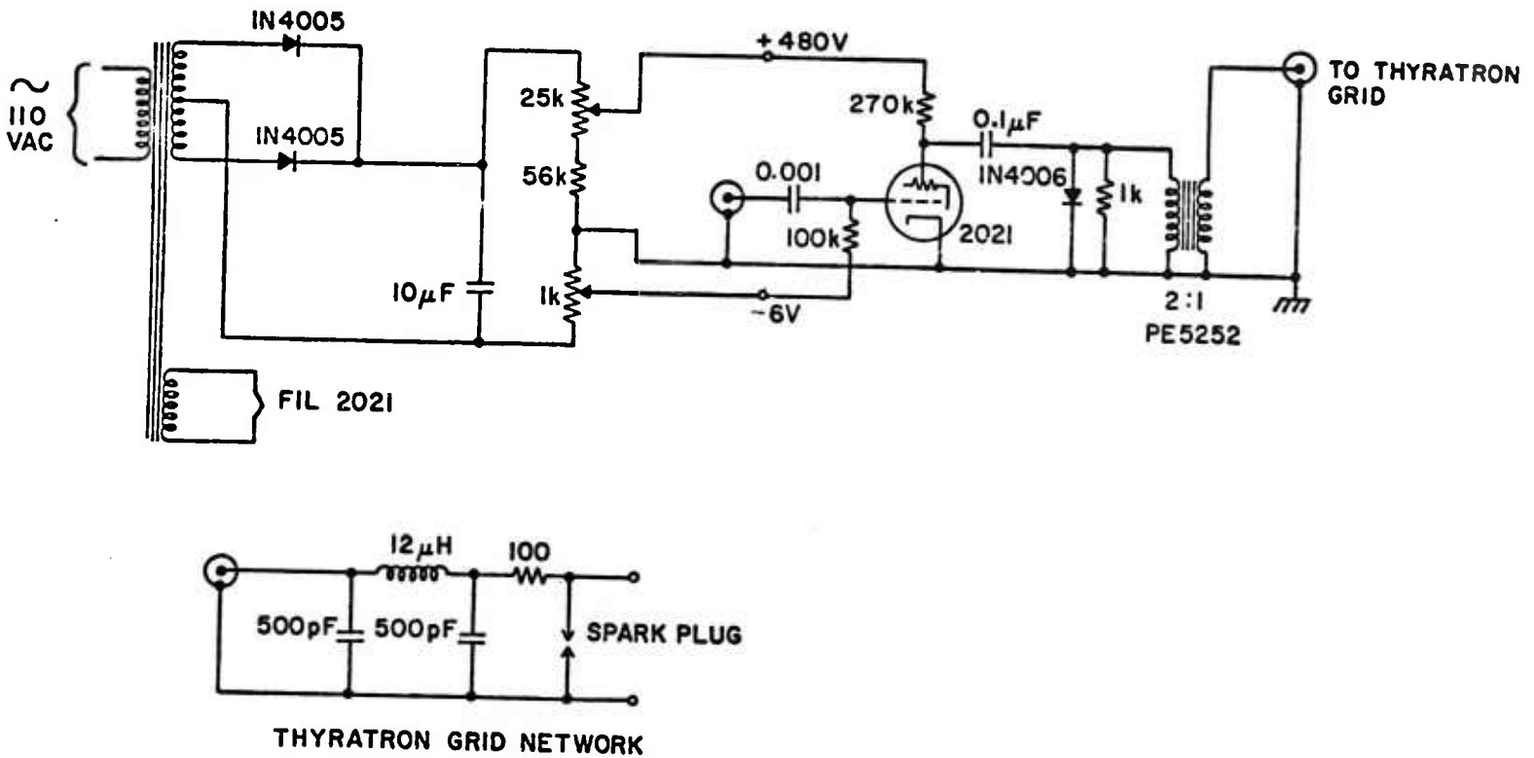

FIGURE 8. Thyratron trigger box.

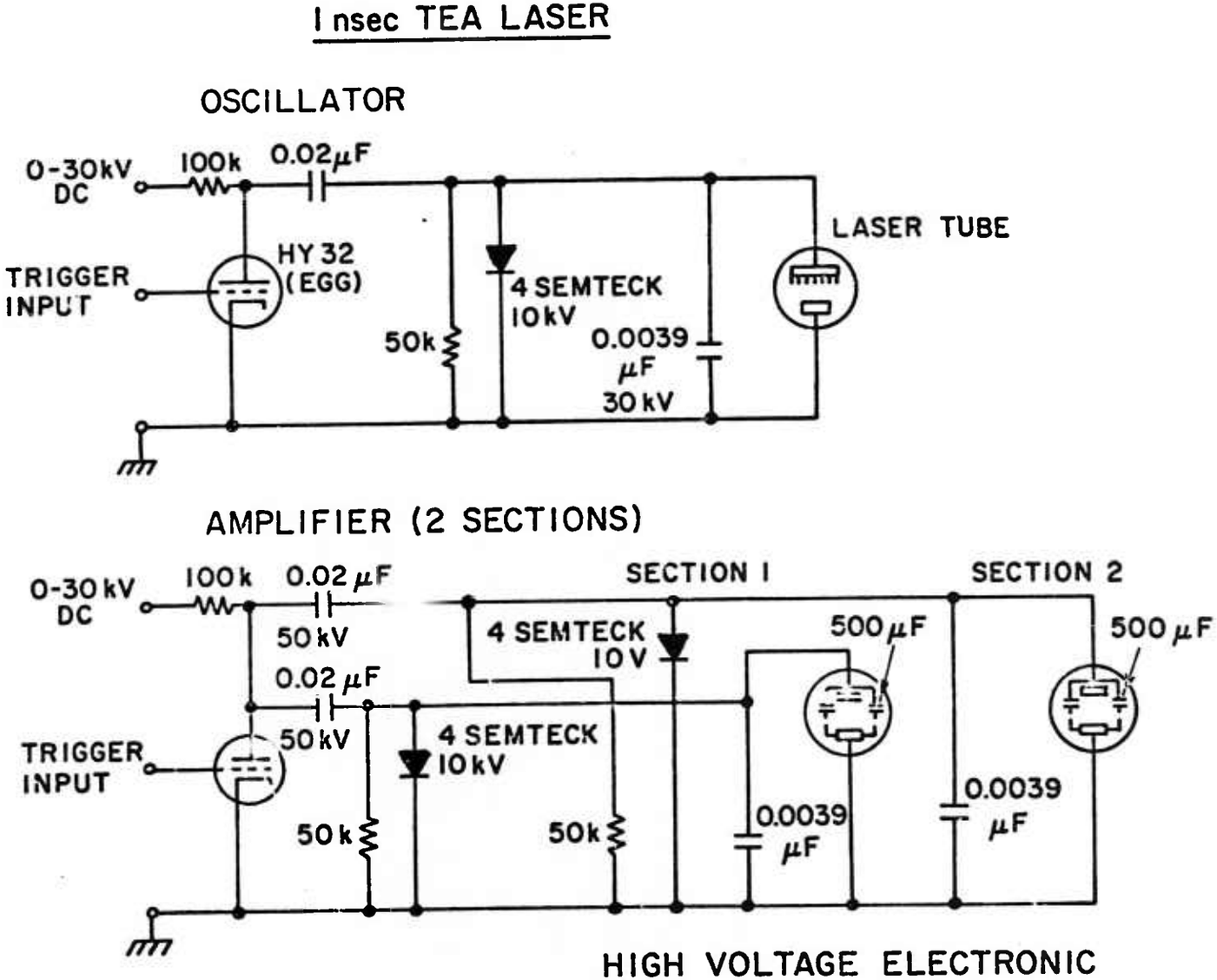

FIGURE 9. High voltage pulsed circuit.

III. NONLINEAR OPTICS THEORY

This section presents a theoretical treatment of higher order nonlinear optical processes in crystals witn $\bar{4}2$ m symmetry. It begins by determining the equations for second (SHG), third (THG) and fourth (FHG) harmonic generation in a crystal with absorption at the fundamental frequency ω and each of its harmonics 2ω, 3ω and 4ω. Also considered is the case of nonphasematched mixing to produce higher harmonics, namely $\omega + 2\omega \rightarrow 3\omega$, $\omega + 3\omega \rightarrow 4\omega$, and $2\omega + 2\omega \rightarrow 4\omega$. All equations are derived in cgs units.

A. SECOND, THIRD, AND FOURTH HARMONIC PROCESSES

1. Nonlinear Polarization Equations

Throughout, this discussion follows the works of Midwinter and Warner on second order[90] and third order[91] processes, keeping in mind that they are missing a factor of 2 for the case of second order mixing, and factors of 3 or 6 for third order mixing.[96]

We can write the general tensor equations for this crystal class for second, third and fourth harmonic generation processes as

$$P_i = d_{ijk} E_j E_k \tag{3.1a}$$

$$P_i = c_{ijk\ell} E_j E_k E_\ell \tag{3.1b}$$

$$P_i = b_{ijk\ell p} E_j E_k E_\ell E_p \tag{3.1c}$$

If we restrict ourselves to frequencies in the transparency range of the material and assume Kleinman symmetry,[92] the nonzero elements of the d, c, and b tensors can be determined and are shown in Fig. 10. The reduced subscript notation is explained in Fig. 11 for all three processes. In Appendix I a practical discussion is presented for calculating higher order nonlinear coefficient tensors from those of lower rank. Equations (3.1) are written out in detail as shown in Fig. 12. The cases of SHG and THG have been discussed by Kildal[4] and are simply summarized here. The case of FHG is treated in detail.

2. Fourth Harmonic Generation

a. Effective Coefficients

With the exception of Se, $CdGeAs_2$ is the only crystal that phase-matches for FHG in the infrared. From Fig. 10 we see that there are two independent, nonzero components of the FHG tensor for a crystal with $\bar{4}2m$ symmetry, assuming Kleinman symmetry. For convenience, let us define

$$b_{1(4)} = b_\alpha \quad b_{1(5)} = b_\beta \tag{3.2}$$

Then, from Figs. 10 and 12(b) we have

$$\begin{aligned} P_x &= b_\alpha [4E_y E_z^3] + b_\beta [4E_z E_y^3 + 12\, E_y E_z E_x^2] \\ P_y &= b_\alpha [4E_x E_z^3] + b_\beta [4E_z E_x^3 + 12\, E_x E_z E_y^2] \\ P_z &= b_\alpha [12E_x E_y E_z^2] + b_\beta [4E_x E_y^3 + 4E_y E_x^3] \end{aligned} \tag{3.3}$$

$$\begin{bmatrix} 0 & 0 & 0 & d_{14} & 0 & 0 \\ 0 & 0 & 0 & 0 & d_{14} & 0 \\ 0 & 0 & 0 & 0 & 0 & d_{14} \end{bmatrix} \quad \text{SHG}$$

$$\begin{bmatrix} c_{11} & 0 & 0 & 0 & 0 & c_{16} & 0 & c_{18} & 0 & 0 \\ 0 & c_{11} & 0 & c_{16} & 0 & 0 & 0 & 0 & c_{18} & 0 \\ 0 & 0 & c_{33} & 0 & c_{16} & 0 & c_{16} & 0 & 0 & 0 \end{bmatrix} \quad \text{THG}$$

$$\begin{bmatrix} 0 & 0 & 0 & b_{1(4)} & b_{1(5)} & 0 & 0 & 0 & 0 & 0 & 0 & 0 & b_{1(5)} & 0 & 0 \\ 0 & 0 & 0 & 0 & 0 & b_{1(4)} & b_{1(5)} & 0 & 0 & 0 & 0 & 0 & 0 & b_{1(5)} & 0 \\ 0 & 0 & 0 & 0 & 0 & 0 & 0 & b_{1(5)} & b_{1(5)} & 0 & 0 & 0 & 0 & 0 & b_{1(4)} \end{bmatrix} \quad \text{FHG}$$

FIGURE 10. Nonlinear coefficient tensors for 2ω, 3ω and 4ω processes in $\bar{4}2m$ crystals.

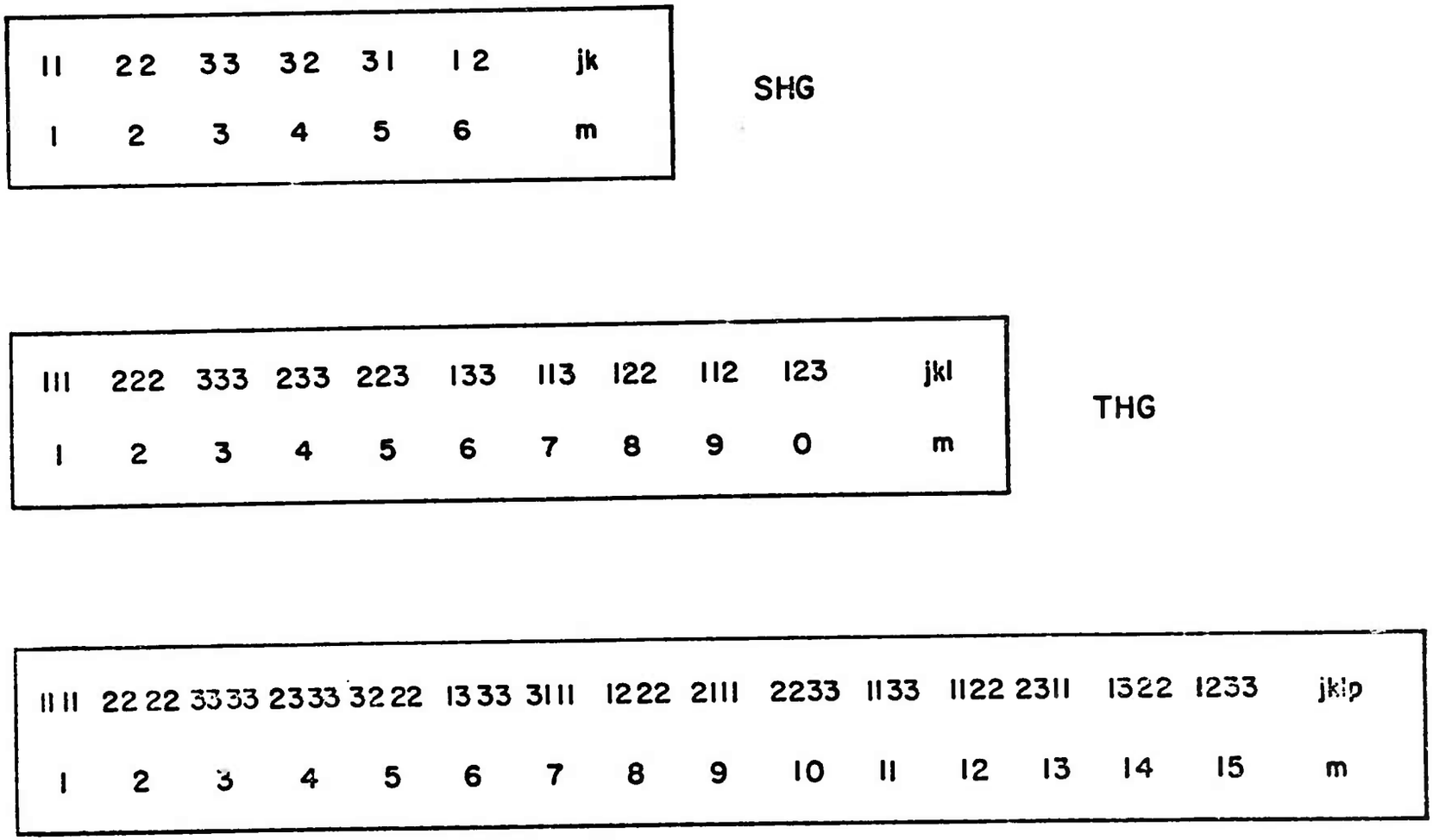

FIGURE 11. Reduced subscript notation for 2ω, 3ω, 4ω tensors.

$$\begin{pmatrix} P_x \\ P_y \\ P_z \end{pmatrix} = (d_{ijk}) \begin{pmatrix} E_x^2 \\ E_y^2 \\ E_z^2 \\ 2E_yE_z \\ 2E_zE_x \\ 2E_xE_y \end{pmatrix} \qquad \text{SHG}$$

$$\begin{pmatrix} P_x \\ P_y \\ P_z \end{pmatrix} = (c_{ijk\ell}) \begin{pmatrix} E_x^3 \\ E_y^3 \\ E_z^3 \\ 3E_yE_z^2 \\ 3E_y^2E_z \\ 3E_xE_z^2 \\ 3E_x^2E_z \\ 3E_xE_y^2 \\ 3E_x^2E_y \\ 6E_xE_yE_z \end{pmatrix} \qquad \text{THG}$$

FIGURE 12(a). Tensor equations for 2ω, 3ω nonlinear polarizations.

and

$$\begin{pmatrix} P_x \\ P_y \\ P_z \end{pmatrix} = (b_{ijk\ell p}) \begin{pmatrix} E_x^4 \\ E_y^4 \\ E_z^4 \\ 4E_yE_z^3 \\ 4E_zE_y^3 \\ 4E_xE_z^3 \\ 4E_zE_x^3 \\ 4E_xE_y^3 \\ 4E_yE_x^3 \\ 6E_y^2E_z^2 \\ 6E_x^2E_z^2 \\ 6E_x^2E_y^2 \\ 12E_yE_zE_x^2 \\ 12E_xE_zE_y^2 \\ 12E_xE_yE_z^2 \end{pmatrix} \qquad \text{FHG}$$

FIGURE 12(b). Tensor equations for 4ω nonlinear polarization.

For FHG we have four possible types of phasematching situations. They are given below with the corresponding index matching equations for a positive birefringent crystal.

$$
\begin{array}{lll}
\text{Type I} & e + e + e + e \rightarrow o & 4n_e(\theta,\omega) = 4n_o(4\omega) \\
\text{Type II} & e + e + e + o \rightarrow o & 3n_e(\theta,\omega) + n_o(\omega) = 4n_o(4\omega) \\
\text{Type III} & e + e + o + o \rightarrow o & 2n_e(\theta,\omega) + 2n_o(\omega) = 4n_o(4\omega) \\
\text{Type IV} & e + o + o + o \rightarrow o & n_e(\theta,\omega) + 3n_o(\omega) = 4n_o(4\omega)
\end{array}
\qquad (3.4)
$$

Here e and o refer to extraordinary and ordinary waves. Only the first two types phasematch in $CdGeAs_2$.

We must now calculate the effective nonlinear coefficients for the Type I and Type II processes. From Eq. (3.4) for the Type I process it is evident that

$$
P(4\omega) = P_o(4\omega) = \begin{pmatrix} \sin\phi \\ -\cos\phi \\ o \end{pmatrix} \qquad P(4\omega)
$$

$$
E(\omega) = E_e(\omega) = \begin{pmatrix} -\cos\theta\cos\phi \\ -\cos\theta\sin\phi \\ \sin\theta \end{pmatrix} \qquad E(\omega) \qquad (3.5)
$$

The geometry is explained in Fig. 13. Combining Eqs. (3.3) and (3.5) we have

$$
\frac{P_x}{E^4} = -4b_\alpha \sin^3\theta\cos\theta\sin\phi - 4b_\beta[\cos^3\theta\sin\theta\sin^3\phi + 3\cos^3\theta\sin\theta\cos^2\phi\sin\phi]
$$

$$
\frac{P_y}{E^4} = -4b_\alpha \sin^3\theta\cos\theta\cos\phi - 4b_\beta[\cos^3\theta\sin\theta\cos^3\phi + 3\cos^3\theta\sin\theta\sin^2\phi\cos\phi] \qquad (3.6)
$$

Since

$$P_o = \begin{pmatrix} \sin\phi \\ \cos\phi \\ 0 \end{pmatrix} \quad P = P_x \sin\phi - P_y \cos\phi$$

we have

$$\frac{P_x \sin\phi}{E^4} = -\left[4b_\alpha \sin^3\theta\cos\theta + 4b_\beta \cos^3\theta\sin\theta(\sin^2\phi + 3\cos^2\phi)\right]\sin^2\phi$$

$$\frac{-P_y \cos\phi}{E^4} = \left[4b_\alpha \sin^3\theta\cos\theta + 4b_\beta \cos^3\theta\sin\theta(3\sin^2\phi + \cos^2\phi)\right]\cos^2\phi \qquad (3.7)$$

We define the FHG effective coefficient as $P_o(4\omega) = b_{eff} E^4(\omega)$ and from Eq. (3.7) we determine it to be

$$\boxed{b_{eff}(I) = 2[b_\alpha \sin^2\theta + b_\beta \cos^2\theta]\sin 2\theta \cos 2\phi} \qquad (3.8)$$

for Type I phasematching in crystals with $\bar{4}2\,m$ symmetry. It should be noted that for $\bar{4}3\,m$ symmetry this expression reduces to $b_{eff}(\bar{4}3\,m) = 2b_\alpha \sin 2\theta\cos 2\phi$. In a similar way we calculate the Type II effective coefficient to be

$$\boxed{b_{eff}(II) = 4[b_\alpha \sin^2\theta + b_\beta \cos^2\theta]\sin\theta \sin 2\phi[\sin^3\rho\cos\rho]} \qquad (3.9)$$

The angles θ, ϕ, and ρ are again defined by Fig. 13 and $E_e = E\sin\rho$. It is easy to show that the expression $\sin^3\rho\cos\rho$ is maximized when $\rho = \pm\frac{\pi}{3} + n\pi$, in which case $4\sin^3\rho\cos\rho = \frac{3\sqrt{3}}{4}$. Moreover, $\cos 2\phi$ is maximum for $\phi = 0$, whereas $\sin 2\phi$ is maximum for $\phi = \frac{\pi}{4}$. Therefore

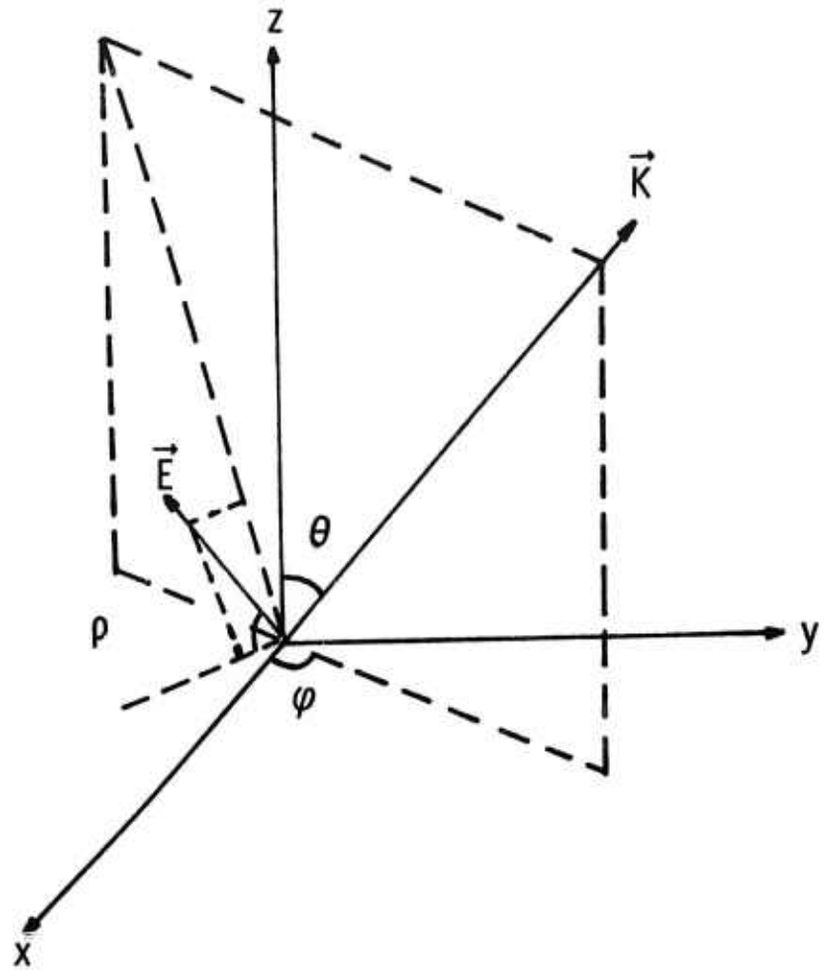

FIGURE 13. Geometry of angles θ, ϕ, ρ used in harmonic generation calculations.

the maximized equations in terms of θ alone are

$$\text{Type I} \quad P(4\omega) = 2[b_\alpha + (b_\beta - b_\alpha)\cos^2\theta]\sin 2\theta\, E^4(\omega)$$

$$\text{Type II} \quad P(4\omega) = \frac{3\sqrt{3}}{4}[b_\alpha + (b_\beta - b_\alpha)\cos^2\theta]\sin\theta\, E^4(\omega) \tag{3.10}$$

From index of refraction data due to Boyd[93] we calculate a phasematching angle for $\lambda = 10.6\ \mu m$ of $\theta_m = 67.85^\circ$ in which case

$$\text{Type I} \quad P(4\omega) = 1.406\,[b_\alpha + .142(b_\beta - b_\alpha)]\,E^4(\omega)$$

or

$$\boxed{\text{Type I} \quad P(4\omega) \approx 1.406\ b_\alpha\ E^4(\omega)} \tag{3.11}$$

for $\lambda = 10.6\ \mu m$. Two problems arise in looking at this phasematching process. There is a good possibility of wave vector walk-off in any crystal long enough to give appreciable signal. One can possibly generate 4ω by mixing $3\omega + \omega \rightarrow 4\omega$ since THG is phasematched theoretically at 64° for $\lambda = 10.6\ \mu m$ and the two processes could overlap. From Boyd's index data the turning point of the Type II FHG curve occurs at $\lambda = 13\ \mu m$ and $\theta_m = 82^\circ$. In this case

$$\boxed{\text{Type II} \quad P(4\omega) \approx 1.29\ b_\alpha\ E^4(\omega)} \tag{3.12}$$

for $\lambda = 13\ \mu m$. Even though the Type II process has the advantage of being phasematched close to 90° so that walk-off is not a problem, it is nevertheless quite difficult at present to consider generating enough radiation at $13\ \mu m$ to actually observe the Type II - FHG process.

Since the index of refraction measurements for this crystal are not yet that accurate, we must consider these FHG calculations as approximate. However, the fortunate proximity of phasematched Type II - THG with Type I - FHG bears further investigation. In the case of producing 3ω by mixing $2\omega + \omega \rightarrow 3\omega$, the THG output depended on the SHG signal.[7] Similarly, here it is possible to consider the mixing process $3\omega + \omega \rightarrow 4\omega$ where the FHG output will depend on the THG signal. We have in fact observed FHG due to this mixing process.

b. FHG Power and Conversion Efficiency

We can calculate the FHG power at phasematching, taking into account the properties of a focused beam and the transmission of the crystal faces. Since for all crystal sizes of interest here the effective length of the focal region is much larger than the crystal length, we can use a plane wave analysis.[94-97] The electric field in a medium can be written in this approximation as

$$E(\omega) = A(z,\omega) \exp(-\tfrac{1}{2} \alpha_1 z) \exp[i(k_1 z - \omega t)] \qquad (3.13)$$

for propagation along some direction z. The FHG polarization is given then by

$$P^{NL}(4\omega) = b_{eff} A^4(\omega) \exp(-2\alpha_1 Z) \exp[i(4k_1 z - 4\omega t)] \qquad (3.14)$$

In the thin slab between z' and $z' + d z'$, the increment of the FHG signal can be obtained from Maxwell's equations and is given by[94-97]

$$dA(z,4\omega) = \frac{2\pi i}{n_4} \left(\frac{\omega_4}{c}\right) P^{NL}(4\omega) \exp(-ik_4 z' + i\, 4\omega\, t) dz' \qquad (3.15)$$

where the geometry is shown in Fig. 14 and n_4 is the refractive index at $\omega_4 = 4\omega$. This generated signal is somewhat absorbed in the $(\ell - z')$

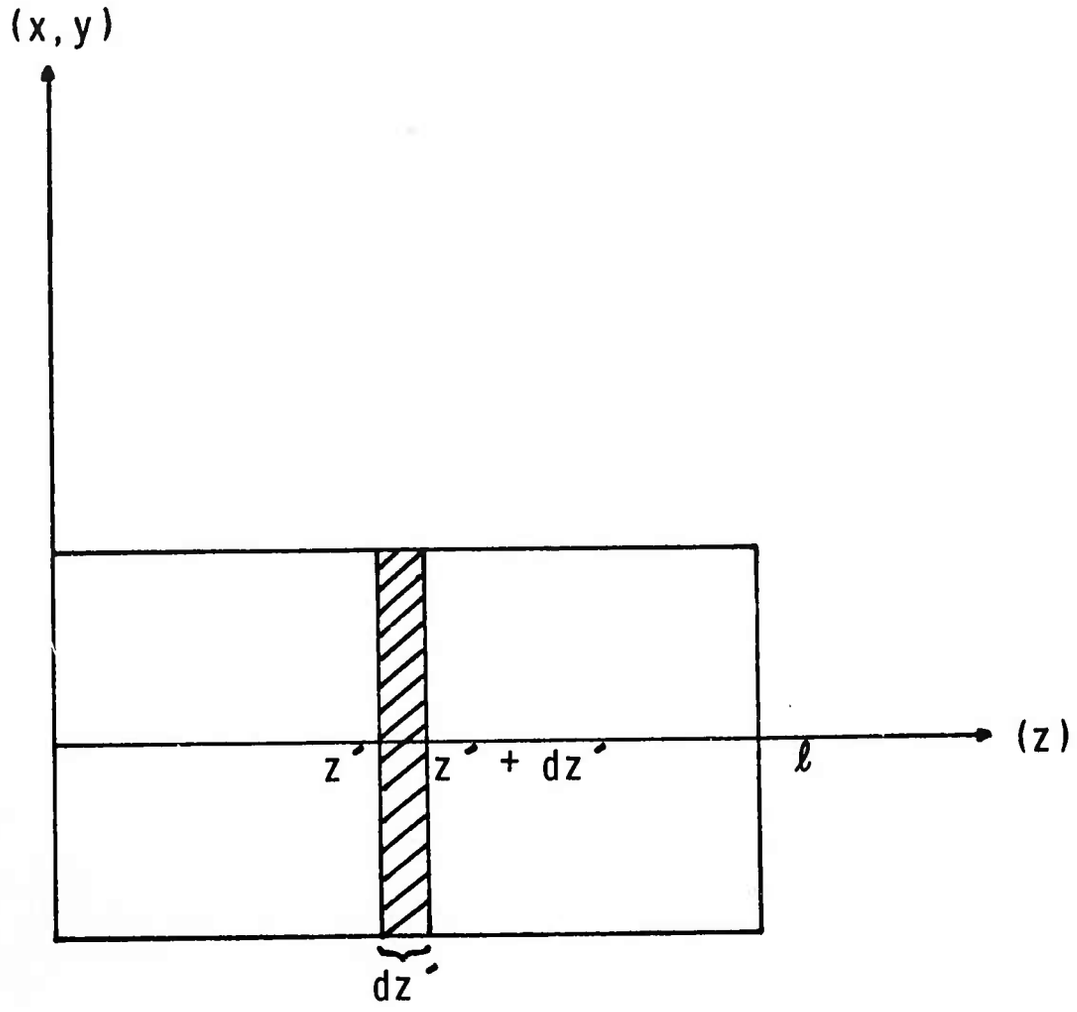

FIGURE 14. Generation of the harmonic wave in a thin slab within a sample.

distance remaining in the material. Consequently the increment in the FHG signal at the end of the crystal, due to that produced in the thin slab, is given by

$$dA(z,4\omega) = \frac{2\pi i}{n_4}\frac{\omega_4}{c} P^{NL}(4\omega)\exp(-ik_4 z')\exp[-\tfrac{1}{2}\alpha_4(\ell - z')]dz' \exp(i4\omega t) \qquad (3.16)$$

or

$$dA(z,4\omega) = \left[\frac{2\pi i}{n_4}\frac{\omega_4}{c} b_{eff} A^4(\omega)\right] \exp(-\tfrac{1}{2}\alpha_4\ell)\exp(-\Delta\alpha z')\exp(i\Delta k z')dz'\exp(i4\omega t) \qquad (3.17)$$

where

$$\Delta\alpha = 2\alpha_1 - \tfrac{1}{2}\alpha_4 \quad \text{and} \quad \Delta k = 4k_1 - k_4 \ .$$

Ignoring the time dependence we have

$$A(\ell,4\omega) = \int_0^{\ell} dA(4\omega) = \left[\frac{2\pi i}{n_4}\frac{\omega_4}{c} b_{eff} A^4(\omega)\exp(-\tfrac{1}{2}\alpha_4\ell)\right] \int_0^{\ell} \exp(i\Delta k - \Delta\alpha)z'dz' \qquad (3.18)$$

Integrating, we get

$$A(\ell,4\omega) = \left[\frac{2\pi i}{n_4}\frac{\omega_4}{c} b_{eff} A^4(\omega)\exp(-\tfrac{1}{2}\alpha_4\ell)\right] \left[\frac{\exp(i\Delta k - \Delta\alpha)\ell - 1}{(i\Delta k - \Delta\alpha)}\right] \qquad (3.19)$$

Now

$$|E(\ell,4\omega)|^2 = |A(\ell,4\omega)|^2 = A(\ell,4\omega)A^*(\ell,4\omega)$$

$$|E(\ell,4\omega)|^2 = 2\left[\frac{2\pi\omega_4}{n_4 c} b_{eff} A^4(\omega)\right]^2 \exp(-\alpha_4\ell)\exp(-\Delta\alpha\ell)\left[\frac{\cosh(\Delta\alpha\ell) - \cos(\Delta k\ell)}{(\Delta k)^2 + (\Delta\alpha)^2}\right] \qquad (3.20)$$

We can write the power generated at 4ω as $P(4\omega)=A<S>$ where S is the Poynting vector $S = \frac{c}{8\pi} |E|^2$ and $A = \frac{\pi w_4^2}{2}$ for a Gaussian beam.

$$P(4\omega) = \frac{c}{16} w_4^2 |E(4\omega)|^2 = \frac{c}{16} w_4^2 |A(4\omega)|^2 \qquad (3.21)$$

where w_4 is the beam waist. Since the electric field amplitudes are related by transmission factors at the faces we can write

$$P(4\omega) = \left(\frac{c}{16} w_4^2\right)\left(\frac{2\pi\omega_4}{n_4 c} b_{eff}\right)^2 \left(t_1^4 t_4\right)^2 \left(\frac{16P(\omega)}{cw_1^2}\right)^4 \exp[-(2\alpha_1 + \tfrac{1}{2}\alpha_4)\ell]$$

$$\times\ 2\left[\frac{\cosh(\Delta\alpha\ell) - \cos(\Delta k\ell)}{(\Delta k)^2 + (\Delta\alpha)^2}\right] \qquad (3.22)$$

as the general expression for the FHG power coming out of a crystal. We have used the facts that $E(\omega)$ (inside) $= t_1 E(\omega)$ (outside) and $E(4\omega)$ (outside) $= \frac{1}{t_4} E(4\omega)$ (inside)[98] and that $-(\Delta\alpha + \alpha_4) = -(2\alpha_1 + \frac{1}{2}\alpha_4)$. If we consider the case of phasematching, $\Delta k \to 0$, then we can simplify the last term as follows

$$2\left[\frac{\cosh(\Delta k\ell) - \cos(\Delta k\ell)}{(\Delta k)^2 + (\Delta\alpha)^2}\right] \approx 2\left[\frac{1 + \frac{1}{2}(\Delta\alpha\ell)^2 - 1 + \frac{1}{2}(\Delta k\ell)^2}{(\Delta k)^2 + (\Delta\alpha)^2}\right]$$

$$\approx \ell^2 \qquad (3.23)$$

for $\Delta k \to 0$.

Therefore for phasematched FHG we have

$$P(4\omega) = \frac{16^3}{c^5}\left(\frac{w_4^2}{w_1^8}\right)\left(\frac{2\pi\omega_4}{n_4}\, b_{eff}\, \ell\right)^2\left(t_1^4 t_4\right)^2 P^4(\omega)\, \exp\left[-\tfrac{1}{2}(\alpha_4 + 4\alpha_1)\ell\right] \qquad (3.24)$$

Since $\omega_4 = 4\omega = 4\left(\frac{2\pi}{\lambda}\right)c$, we have for the generated FHG power

$$\boxed{P(4\omega) = \left(\frac{16}{c}\right)^3\left(\frac{w_4^2}{w_1^8}\right)\left(16\pi^2\right)\left(\frac{4\pi\, b_{eff}\, \ell}{n\lambda}\right)^2\left(t_1^4 t_4\right)^2 P^4(\omega)\, \exp\left[-\tfrac{1}{2}(\alpha_4 + 4\alpha_1)\ell\right]} \qquad (3.25)$$

where $t_1 = \frac{2}{1+n}$ and $t_4 = \frac{2n}{1+n}$ from the Fresnel equations,[98] and $n_4 = n$ for phasematching. The FHG conversion efficiency is given by

$$\boxed{\frac{P(4\omega)}{P(\omega)} = \left(\frac{16}{c}\right)^3\left(\frac{w_4^2}{w_1^8}\right)\left(16\,\pi^2\right)\left(\frac{4\pi\, b_{eff}\, \ell}{n\lambda}\right)^2\left(t_1^4 t_4\right)^2 P^3(\omega)\, \exp\left[-\tfrac{1}{2}(\alpha_4 + 4\alpha_1)\ell\right]} \qquad (3.26)$$

c. Angular Half Width

Kildal[4] has given a clear description of the calculation for the angular half width of generated SHG and THG signals. Such a measurement is important for several reasons. First it serves as a check on the type of process one is actually observing; mixing and harmonic generation, for example, have different angular tolerances. Second, it is an indication of the practical angular tolerance limits one encounters in turning a crystal to phasematch different input frequencies. Third, it serves as one

measure of the quality of the crystal. We can briefly summarize Kildal's work and extend it to the case of FHG. Let us return to Eq. (3.22) and assume that $\Delta\alpha = 0$ for simplicity. This equation reduces then to

$$P(4\omega) = \left(\frac{16}{c}\right)^3 \left(\frac{w_4^2}{8 w_1}\right)(16\pi^2) \left(\frac{4\pi\, b_{eff}\, \ell}{n\lambda}\right)^2 \left(t_1^4 t_4\right)^2 P^3(\omega)\, \mathrm{sinc}^2\left(\frac{\Delta k \ell}{2}\right) \quad (3.27)$$

The half width at half power is given when $\mathrm{sinc}^2 \frac{\Delta k \ell}{2} = \frac{1}{2}$ which occurs when $\frac{\Delta k \ell}{2} = 1.4$ radians or $\Delta k = 2.8/\ell$. Now we must calculate the variation of Δk with θ for each type of phasematching, where

$$\Delta k = \frac{\partial k(\theta)}{\partial \theta} \Delta\theta$$

Type I e+e+e+e → o $\quad \vec{\Delta k}_I = \vec{k}_4 - 4\vec{k}_1 = \vec{k}_4(4\omega) - 4\vec{k}_1(\omega,\theta)$

$$\text{or} \quad \vec{\Delta k}_I = -\frac{8\pi}{\lambda_1} \frac{\partial n_e(\theta)}{\partial \theta} \Delta\theta$$

Type II e+e+e+o → o $\quad \vec{\Delta k}_{II} = \vec{k}_4 - 4\vec{k}_1 = \vec{k}_4(4\omega) - 3\vec{k}_1(\omega,\theta) - \vec{k}_1(\omega)$

$$\Delta k_{II} = \frac{-6\pi}{\lambda_1} \frac{\partial n_e(\theta)}{\partial \theta} \Delta\theta \quad (3.28)$$

Now one can write $n_e(\theta)$ as

$$\frac{1}{n_e^2(\theta)} = \frac{\cos^2\theta}{n_o^2} + \frac{\sin^2\theta}{n_e^2} \quad (3.29)$$

and the Poynting vector walk-off angle η[98] as

$$\tan \eta = \frac{n_e^2(\theta)}{2} \left(\frac{1}{n_e^2} - \frac{1}{n_o^2} \right) \sin 2\theta \qquad (3.30)$$

From these two expressions one finds

$$\frac{\partial n_e(\theta)}{\partial \theta} = - n_e(\theta) \tan \eta \qquad (3.31)$$

Finally, for near normal incidence $\Delta\theta$ external = $n\Delta\theta$ internal. Combining this result with Eqs. (3.28) and (3.31) we find

$$\Delta\theta_{I\ ext} = \frac{\lambda}{8.98\ell \tan \eta}$$

$$\Delta\theta_{II\ ext} = \frac{\lambda}{6.73\ell \tan \eta} \frac{n_o(4\omega)}{n_e(\omega,\theta)} \qquad (3.32)$$

3. Summary of Harmonic Generation Results

At this point we can tabulate the results for SHG,[4] THG,[4] and FHG in a crystal with $\bar{4}2m$ symmetry. The effective nonlinear coefficients for the various phasematching conditions are given in Table 3. The expressions for output powers at the harmonic frequencies, in terms of the input power at ω, are shown in Table 4. Finally the angular half widths are given in Table 5. It should be noted that the widths get narrower as we go to higher order harmonics. The tuning curves for these three processes are shown in Figs. 15 and 16.

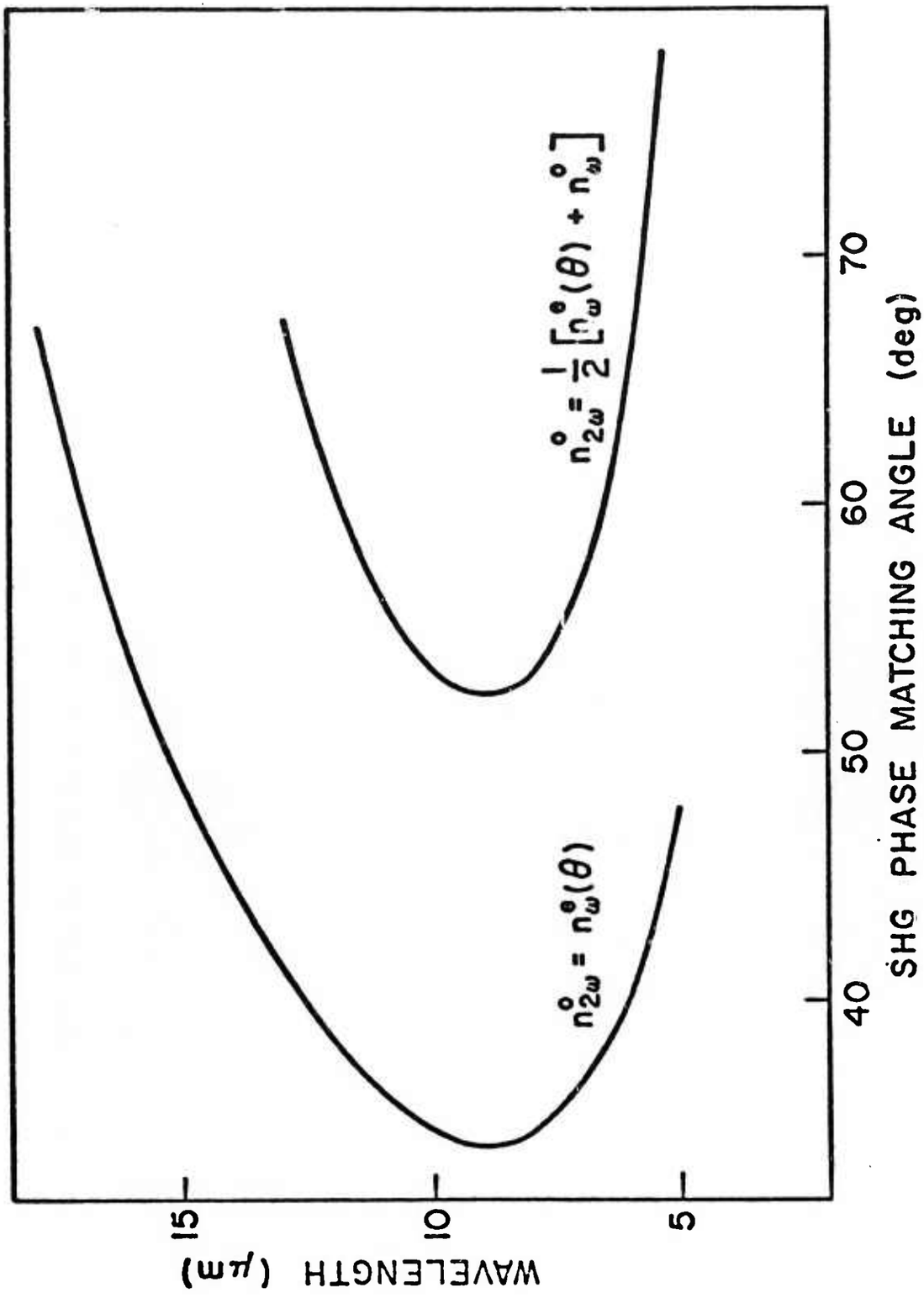

FIGURE 15. SHG angle tuning curves in $CdGeAs_2$.

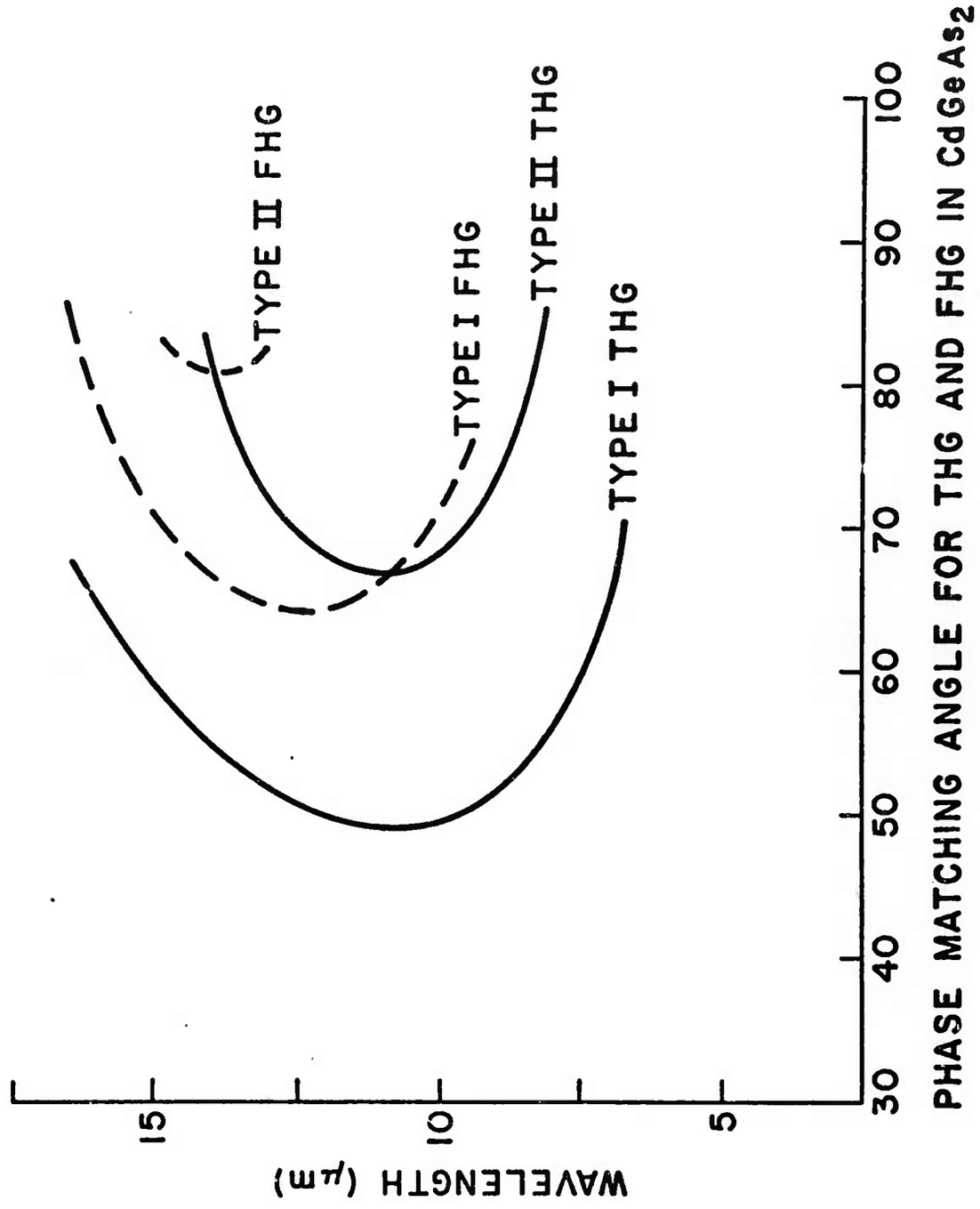

FIGURE 16. THG and FHG angle tuning curves in $CdGeAs_2$.

TABLE III

EFFECTIVE NONLINEAR COEFFICIENTS FOR HARMONIC GENERATION

Harmonic Type

SHG	I	$d_I = d_{14} \sin 2\theta \cos 2\phi$
	II	$d_{II} = -d_{14} \sin\theta \sin 2\phi \sin 2\rho$
THG	I	$c_I = -\frac{1}{4}(c_{11} - 3c_{18}) \cos^3\theta \sin 4\phi$
	II	$c_{II} = [\frac{1}{2}(c_{11} - 3c_{18}) \cos^2\theta \sin^2 2\phi + c_{16} \sin^2\theta + c_{18} \cos^2\theta] \cos\rho \sin^2\rho$
	III	$III = \frac{1}{4}(c_{11} - 3c_{18}) \cos\theta \sin 4\phi \sin\rho \cos^2\rho$
FHG	I	$b_I = 2[b_{1(4)} \sin^2\theta + b_{1(5)} \cos^2\theta] \sin 2\theta \cos 2\phi$
	II	$b_{II} = 4[b_{1(4)} \sin^2\theta + b_{1(5)} \cos^2\theta] \sin\theta \sin 2\phi [\sin^3\rho \cos\rho]$

where $P_I(2\omega) = d_I E^2(\omega)$, etc.,

TABLE IV

POWER EQUATIONS FOR HARMONICS

$P(2\omega) = \left(\frac{16}{c}\right)\left(\frac{w_2^2}{w_1^4}\right)\left(16\,\pi^2\right)\left(\frac{2\pi\, d_{eff}\, \ell}{n\,\lambda}\right)^2\left(t_1^2 t_2\right)^2 P^2(\omega)\, \exp[-\tfrac{1}{2}(\alpha_2 + 2\alpha_1)\,\ell]$
$P(3\omega) = \left(\frac{16}{c}\right)^2\left(\frac{w_3^2}{w_1^6}\right)\left(16\pi^2\right)\left(\frac{3\pi\, c_{eff}\, \ell}{n\,\lambda}\right)^2\left(t_1^3 t_3\right)^2 P^3(\omega)\, \exp[-\tfrac{1}{2}(\alpha_3 + 3\alpha_1)\,\ell]$
$P(4\omega) = \left(\frac{16}{c}\right)^3\left(\frac{w_4^2}{w_1^8}\right)\left(16\pi^2\right)\left(\frac{4\pi\, b_{eff}\, \ell}{n\,\lambda}\right)^2\left(t_1^4 t_4\right)^2 P^4(\omega)\, \exp[-\tfrac{1}{2}(\alpha_4 + 4\alpha_1)\,\ell]$

where $w_1 \rightarrow w_4$ are beam waists, $t_1 \rightarrow t_4$ are electric field transmission factors and $\alpha_1 \rightarrow \alpha_4$ are loss constants for beams with $\omega \rightarrow 4\omega$. ℓ is the effective interaction length.

TABLE V

ANGULAR HALF WIDTHS

SHG	I	$\Delta\theta_I = \dfrac{\lambda_1}{4.5\,\ell \tan\eta}$
	II	$\Delta\theta_{II} = \dfrac{\lambda_1}{2.25\,\ell \tan\eta} \dfrac{n_o(2\omega)}{n_e(\omega,\theta)}$
THG	I	$\Delta\theta_I = \dfrac{\lambda_1}{6.75\,\ell \tan\eta}$
	II	$\Delta\theta_{II} = \dfrac{\lambda_1}{4.5\,\ell \tan\eta} \dfrac{n_o(3\omega)}{n_e(\omega,\theta)}$
	III	$\Delta\theta_{III} = \dfrac{\lambda_1}{2.25\,\ell \tan\eta} \dfrac{n_o(3\omega)}{n_e(\omega,\theta)}$
FHG	I	$\Delta\theta_I = \dfrac{\lambda_1}{8.98\,\ell \tan\eta}$
	II	$\Delta\theta_{II} = \dfrac{\lambda_1}{6.73\,\ell \tan\eta} \dfrac{n_o(4\omega)}{n_e(\omega,\theta)}$

where ℓ = crystal length, λ_1 = input wavelength η = walk-off angle

B. MIXING PROCESSES

1. $\omega + 2\omega \rightarrow 3\omega$

There are two mixing processes that can generate 3ω and 4ω which should be discussed. The first process

$$\omega + 2\omega \rightarrow 3\omega \tag{3.33}$$

is not phasematched and occurs along the direction of phasematched SHG. By using two sources one at 10.6 μm and the other at 5.3 μm we can have phasematched mixing. In terms of ordinary and extraordinary polarizations the only combination of importance here is

$$\vec{E}_e(\omega) + \vec{E}_o(2\omega) \rightarrow \vec{E}_o(3\omega) \quad . \tag{3.34}$$

Because of positive birefringence, the harmonics must be ordinary waves. Moreover, only the extraordinary wave at ω will generate a mixing signal, since $\vec{E}_o(\omega) + \vec{E}_o(2\omega)$ cannot give $\vec{E}_o(3\omega)$. Since this is a second order process, we have some effective mixing coefficient d_{mix} (effective). We can determine its form by writing down the expressions in Figs. 10 - 12 for a mixing process.[96]

$$\begin{aligned} P_x(3\omega) &= 2d_{14}\,[E_y(\omega)\,E_z(2\omega) + E_y(2\omega)\,E_z(\omega)] \\ P_y(3\omega) &= 2d_{14}\,[E_x(\omega)\,E_z(2\omega) + E_x(2\omega)\,E_z(\omega)] \\ P_z(3\omega) &= 2d_{14}\,[E_x(\omega)\,E_y(2\omega) + E_x(2\omega)\,E_y(\omega)] \end{aligned} \tag{3.35}$$

Note here $P(3\omega) = P_o(3\omega)$ so $P_z(3\omega) = 0$. Also $E(2\omega) = E_o(2\omega)$ so that $E_z(2\omega) = 0$. These equations reduce then to

$$\begin{aligned} P_{o,x}(3\omega) &= 2d_{14}\,E_{e,z}(\omega,\theta)\,E_{o,y}(2\omega) \\ P_{o,y}(3\omega) &= 2d_{14}\,E_{e,z}(\omega,\theta)\,E_{o,x}(2\omega) \end{aligned} \tag{3.36}$$

where $P_o(3\omega) = \sin\phi\, P_{o,x}(3\omega) - \cos\phi\, P_{o,y}(3\omega)$ and $E_{e,z}(\omega,\theta) = \sin\rho\, \sin\theta\, E(\omega)$. Note the degeneracy factor 2 is in agreement with other authors.[96] Now from Table 3 we have

$$P_o(2\omega) = - d_{14} \sin\theta \sin 2\phi \sin 2\rho\, E^2(\omega) \tag{3.37}$$

and we can calculate the magnitude of $A(2\omega)$ to be[96]

$$A(z_1', 2\omega) = i \frac{2\pi\omega_2}{n_2 c} d_{SHG} A_1^2 \exp[-\tfrac{1}{2}(\alpha_2 + 2\alpha_1) z'] z' \tag{3.38}$$

where $d_{SHG} = d_{14} \sin\theta \sin 2\phi \sin 2\rho$. Now we assume that for the mixing process we have a coherence length ℓ_c, where

$$\vec{\Delta k} = \vec{k}_1 + \vec{k}_2 - \vec{k}_3 = \frac{6\pi}{\lambda} \left[\frac{n_1 + 2n_2}{3} - n_3\right]$$

$$\boxed{\ell_c = \frac{\pi}{\Delta k} = \frac{\lambda}{6\left[\frac{n_1 + 2n_2}{3} - n_3\right]}} \tag{3.39}$$

and that the magnitude of $E(2\omega)$ is constant and given by its value at $(\ell - \frac{1}{2}\ell_c)$, namely

$$A(\ell - \tfrac{1}{2}\ell_c, 2\omega) = i \frac{2\pi\omega_2}{n_2 c} d_{SHG} A^2(\omega) [\ell - \tfrac{1}{2}\ell_c] \exp[-\tfrac{1}{2}(\alpha_2 + 2\alpha_1)\ell] \tag{3.40}$$

Following the same procedure as for the FHG case, we calculate the power at (3ω) due to mixing to be

$$P(3\omega) = \left(\frac{16}{c}\right)^2 \left(\frac{w_3^2}{w_1^6}\right) (16\pi^2) \left[\frac{24\pi^3 \, d_{MIX} \, d_{SHG}}{n_2 n_3 \lambda^2} \, \ell_c (\ell - \tfrac{1}{2}\ell c)\right]^2 (t_1^3 t_3)^2 \, P^3(\omega) \exp\left[-\tfrac{1}{2}(\alpha_2 + 3\alpha_1)\,\ell\right] \tag{3.41}$$

where $d_{SHG} = - d_{14} \sin\theta \sin 2\phi \sin 2\rho$

$d_{MIX} = - 2d_{14} \sin\theta \sin\rho$

2. $\omega + 3\omega \rightarrow 4\omega$

The case of non-phasematched mixing of a THG signal with the fundamental to produce a signal at 4ω can be analyzed similarly. By analogy to Eq. (3.34) we have

$$\vec{E}_e(\omega) + \vec{E}_o(3\omega) \rightarrow \vec{E}_o(4\omega) \tag{3.42}$$

The coherence length for this process is given by

$$\ell_c = \frac{\pi}{\Delta k} = \frac{\pi}{\vec{k}_1 + \vec{k}_3 - \vec{k}_4} = \frac{\lambda}{8\left[\frac{n_{e,1} + 3\, n_{o,3}}{4} - n_{o,4}\right]} \tag{3.43}$$

Here we are concerned with mixing against a signal at 3ω generated in

a type II-THG process. The calculated output power at 4ω is given by

$$P(4\omega) = \left(\frac{16}{c}\right)^3 \left(\frac{w_4^2}{8 w_1}\right) (16\pi^2) \left[\frac{48\pi^3 \, d_{MIX} \, c_{THG}}{n_3 n_4 \lambda^2} \, \ell_c (\ell - \tfrac{1}{2}\ell_c)\right]^2 (t_1^3 t_4)^2 \, P^4(\omega) \times \exp\left[-\tfrac{1}{2}(\alpha_3 + 4\alpha_1)\,\ell\right] \tag{3.44}$$

where $d_{MIX} = -2d_{14} \sin\theta \sin\rho$

$$c_{THG} = \tfrac{1}{2}[(c_{11} - 3c_{18})\sin^2 2\phi \cos^2\theta + c_{16} \sin^2\theta + c_{18} \cos^2\theta] \sin^2\rho \cos\rho$$

At this point it should be noted that the process $2\omega + 2\omega \rightarrow 4\omega$ does not work because all three waves are ordinary waves when we consider mixing of a SHG signal with itself to give FHG. On the other hand, if we have an external source for the 2ω signals we can polarize the input waves to make this mixing process possible as well.

3. Angular Half Widths

We calculate the angular half widths for these two mixing processes by the same procedure used in Eqs. (3.28) to (3.32)

$\omega + 2\omega \rightarrow 3\omega$

$$\Delta\theta_{II\ ext} = \frac{\lambda_1}{2.25\,\ell \tan\rho} \frac{n_o(3\omega)}{n_e(\theta,\omega)} \tag{3.45}$$

and

$\omega + 3\omega \rightarrow 4\omega$

$$\Delta\theta_{II\ ext} = \frac{\lambda_1}{2.25\,\ell \tan\rho} \frac{n_o(4\omega)}{n_e(\theta,\omega)} \tag{3.46}$$

IV. EXPERIMENTAL AND THEORETICAL WORK ON HIGHER ORDER NONLINEAR PROCESSES IN $CdGeAs_2$

A. INTRODUCTION

Since $CdGeAs_2$ has the largest figure of merit for second order nonlinear optics processes,[4] and since, as shown in Section III, it can be phasematched for third and fourth harmonic generation processes, we undertook an experimental and theoretical investigation of these two interactions. The results on THG experiments in $CdGeAs_2$, and the theoretical models used to calculate contributions to the third order susceptibility from bound electrons and free carriers are discussed in Appendix II. This section gives a summary of the application of the Bond Charge Model[99-101] to the calculation of fourth harmonic tensor coefficients. The results of the third harmonic investigation of $CdGeAs_2$ are discussed and the potential power outputs at the third and fourth harmonics of 10.6 μm are examined.

B. THIRD HARMONIC EXPERIMENTS AND THEORY

1. Separation of Components by Symmetry Arguments

One of the principal points made in Appendix II is that nonlinear susceptibilities of various orders arise from different mechanisms in a semiconductor material. In particular, we note that isotropic materials have non-vanishing odd order susceptibility tensors while even order susceptibilities equal zero from symmetry considerations. In particular, for semiconductor materials odd order susceptibilities arise from two sources: electrons localized in crystal bonds, which reflect the symmetry properties

of the crystal lattice, and the free carrier cloud, which has isotropic symmetry. For crystals with $\bar{4}2$ m symmetry, like $CdGeAs_2$, we can compare nonzero third order tensor elements with those of systems with other symmetries. Such a comparison is shown in Fig. 17 where the nonzero third order tensor elements for uniaxial $\bar{4}2$ m symmetry are obtained from Fig. 10. The fact that the c_{16} element is common to the case of $\bar{4}2$ m and isotropic symmetry suggest that this tensor component arises from a component of the crystal with isotropic symmetry, such as the free carrier cloud. The element $c_{11} - 3c_{18}$, however, appears to arise solely from a component reflecting the symmetry properties of the particular crystal class, i.e. the electrons localized in the bonds. From Table 3, moreover, it is apparent that one can separate these tensor components, and hence the bond electron and free carrier effects, by doing different phasematched THG experiments. These points are summarized in Fig. 18. As discussed in Appendix II, we have performed phasematched Type I and Type II THG to measure the third order tensor coefficients. Until now the only measurements of third order susceptibilities in semiconductors have been carried out by mixing experiments ($2\omega_1 - \omega_2 = \omega_3$) in a nonphasematched configuration. Consequently it was not possible to measure the tensor coefficients independently, as we have done in $CdGeAs_2$.

2. Free Carrier Effects for Third Harmonic Generation

In Section III of Appendix II contributions to the third order susceptibility from free carriers are discussed.[107-109] Since we were doing harmonic generation rather than mixing experiments (where frequency differences can get close to inverse relaxation times), the only contribution to the nonlinear

THIRD ORDER TENSOR ELEMENTS

ISOTROPIC SYMMETRY	AXIAL SYMMETRY	CUBIC SYMMETRY	UNIAXIAL SYMMETRY
0	0	$c_{11}-3c_{18}$	$c_{11}-3c_{18}$
0	$c_{16}-c_{18}$	0	$c_{16}-c_{18}$

c_{16} $\Longrightarrow$ NON-ZERO FOR ALL MATERIALS
$\Longrightarrow$ LIKE AVERAGE REFRACTIVE INDEX

$c_{16}-c_{18}$ $\Longrightarrow$ INDICATES DIFFERENT BEHAVIOR BETWEEN z DIRECTION AND xy PLANE
$\Longrightarrow$ LIKE BIREFRINGENCE

$c_{11}-3c_{18}$ $\Longrightarrow$ INDICATES DEPARTURE FROM ISOTROPY
$\Longrightarrow$ PURELY DEPENDENT ON CRYSTAL SYMMETRY

FIGURE 17. Analysis of THG tensor components by symmetry arguments.

SEPARATION OF BOND ELECTRON AND FREE CARRIER EFFECTS BY PHASE MATCHED THG

$c_{im} \Longrightarrow c_{im}^{BE}$ (BOND ELECTRONS) + c_{im}^{FC} (FREE CARRIERS)

$c_{im}^{BE} \Longrightarrow$ SYMMETRY OF CRYSTAL CLASS $\bar{4}2m$

$c_{im}^{FC} \Longrightarrow$ SYMMETRY OF ISOTROPIC ELECTRON CLOUD

TYPE I THG:

$$c_{eff} \propto (c_{11} - 3c_{18})^{BE}$$

TYPE II THG:

$$c_{eff} \propto (c_{11} - 3c_{18})^{BE} + (c_{16} - c_{18})^{BE + FC} + (c_{16})^{BE + FC}$$

FIGURE 18. Bond electron and free carrier contributions to third order susceptibilities.

susceptibility comes from the nonparabolicity of the energy bands.

We have extended the work of Kane[110] and Kildal[4] to the calculation of third order nonlinear susceptibilities in ternary chalcopyrites. The Kane model has been used successfully to describe the third order properties of elementary and binary compounds.[108-115] Details of the calculation of the energy band shapes by our extension of Kane's model are given in Appendix II. It has been demonstrated by several authors that the third order susceptibility due to nonparabolic energy bands is given by[107-109]

$$c_{ijk\ell}(\omega_1\omega_2\omega_3) = \pm \frac{e^4}{24\hbar^4 V\omega_1\omega_2\omega_3(\omega_1+\omega_2+\omega_3)} \sum_k f_o(E_{c,v}) \frac{\partial^4 E_{c,v}}{\partial k_i \partial k_j \partial k_k \partial k_\ell} \tag{4.1}$$

where $f_o(E)$ if the Fermi-Dirac distribution function. Here we pick the + sign and E_c for n-type material, and the - sign and E_v for p-type material. A comparison of the energy band diagrams for chalcopyrite and sphalerite materials is shown in Fig. 19. The parameters used in this model for $CdGeAs_2$ are also listed. As discussed in Appendix II, the results of this free carrier model for p-type $CdGeAs_2$ are

$$c_{16}^{(p)} = -2.5 \times 10^{-27}\ N \qquad c_{18}^{(p)} - c_{16}^{(p)} = 2 \times 10^{-27}\ N$$

$$c_{16}^{(n)} = 1.5 \times 10^{-27}\ N \qquad c_{18}^{(n)} - c_{16}^{(n)} = 6.3 \times 10^{-28}\ N \tag{4.2}$$

where N is the free carrier density. We use the fact that for an isotropic medium, in this case the free carrier cloud, $c_{11} = 3c_{18}$. We derive the following values for c_{11}, c_{16}, and c_{18} from the free carrier model using a carrier concentration of $N = 1.24 \times 10^{16}$ holes/cm^3. (Note:

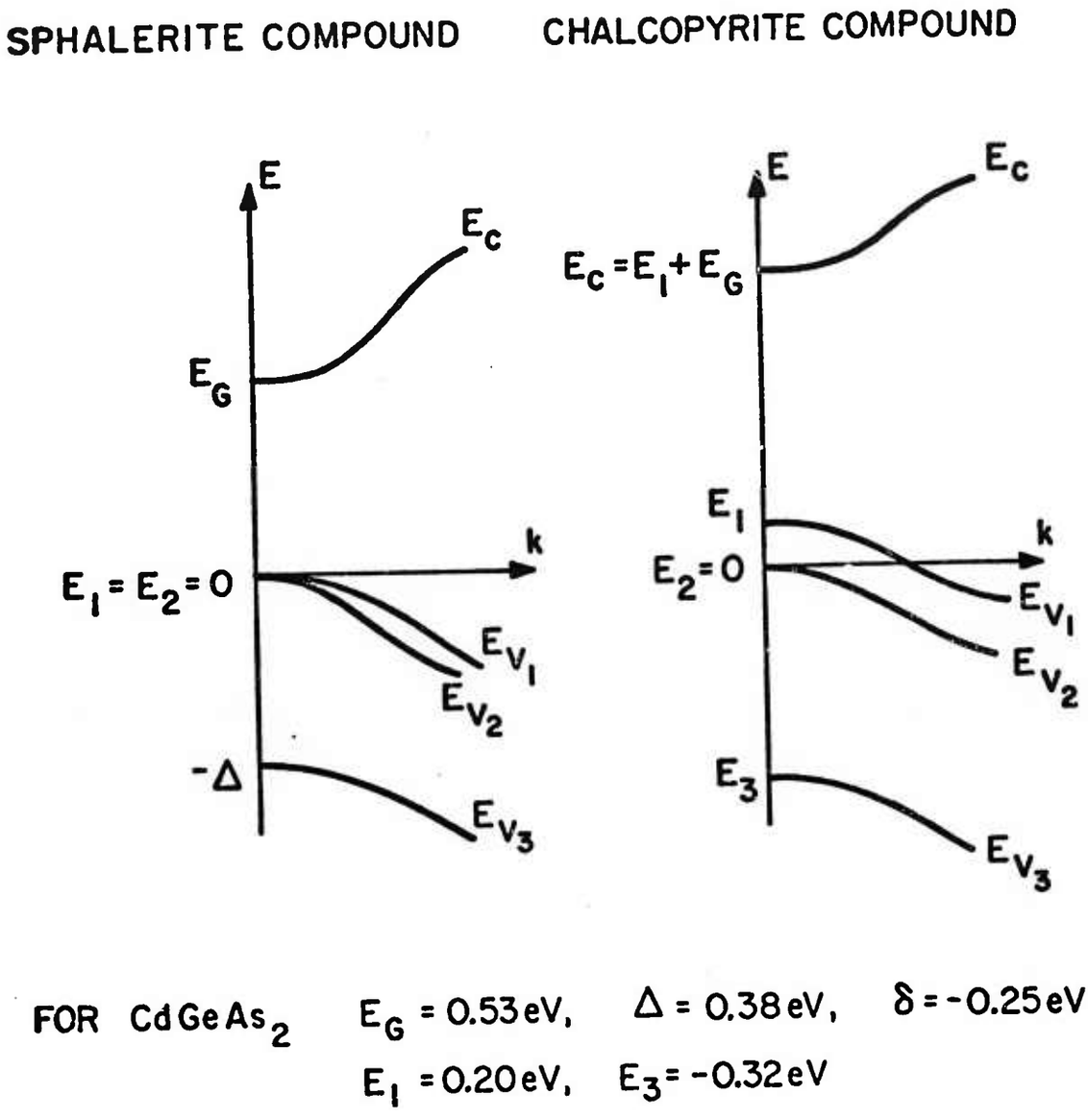

FOR $CdGeAs_2$ $E_G = 0.53\,eV$, $\Delta = 0.38\,eV$, $\delta = -0.25\,eV$

$E_1 = 0.20\,eV$, $E_3 = -0.32\,eV$

FIGURE 19. Band structure of sphalerite and chalcopyrite compounds.

the value $N = 5 \times 10^{16}$ holes/cm^3 given in Appendix II is incorrect).

$c_{11} = -1.49 \times 10^{-11}$ esu

$c_{18} = -0.5 \times 10^{-11}$ esu

$c_{16} = -3.1 \times 10^{-11}$ esu

Free carriers ($N = 1.24 \times 10^{16}$ holes/cm^3)

These should be compared with the results of the Bond Charge Model

$c_{11} = 1.8 \times 10^{-11}$ esu

$c_{18} = 1.3 \times 10^{-11}$ esu

$c_{16} = 1.4 \times 10^{-11}$ esu

Bond Electrons

3. Comparison of Theory and Experiment for Third Harmonic Generation

We can compare the values for the effective c's for Type I and Type II THG by using the expressions in Table 3, keeping in mind that we must use the free carrier and bond electron values in accordance with Fig. 20.

$$\text{Type I}: \quad c_I = -\frac{1}{4}\,(c_{11} - 3c_{18})^{BE} \cos^3\theta_I$$

$$\text{Type II}: \quad c_{II} = \sin^2\rho \cos\rho \left[\frac{1}{2}(c_{11}-3c_{18})^{BE} \cos^2\theta_{II} + (c_{16} \sin^2\theta_{II} + c_{18} \cos^2\theta_{II})^{BE} + FC\right] \qquad (4.3)$$

In our experiments the phasematching angles are $\theta_I = 50^\circ$, $\theta_{II} = 60^\circ$, and $\cos\rho = \frac{1}{\sqrt{3}}$.

The crystals used were cut for maximized ϕ angle in each case. Therefore,

$$c_I = -0.14 \times 10^{-11} \text{ esu}$$

$$c_{II} = -0.53 \times 10^{-11} \text{ esu} \qquad \underline{\text{Calculated}} \tag{4.4}$$

By using the experimental setup shown in Fig. 20, we observe both Type I and Type II THG signals in $CdGeAs_2$. As described in Appendix II we observe a signal at 3ω by nonphasematched mixing of the second harmonic signal with the fundamental $2\omega + \omega = 3\omega$. Since the value for d_{14} of $CdGeAs_2$ is known to be 8.4×10^{-7} esu, by measuring direct Type II THG in the same crystal, we obtain a value for the ratio c_{II}/d_{14}. Finally, by observing Type II THG in one crystal and Type I THG in a second crystal with the same experimental setup, one can get the ratio c_I/c_{II}. A phasematching curve for Type II THG and its $P^3(\omega)$ power dependence are shown in Fig. 21. From these experiments we have determined c_I and c_{II} to be

$$|c_I| \leq 0.6 \times 10^{-11} \text{ esu}$$

$$|c_{II}| = 12.5 \times 10^{-11} \text{ esu} \qquad \underline{\text{Measured}} \tag{4.5}$$

Since our signal to noise ratio was only 2 : 1 in the c_I measurement we must put an error range of $\pm$ 50% on this measurement. It does, nevertheless, compare favorably with the value given in Eq. (4.4) from the Bond Charge Model calculation. However, our measured and calculated c_{II} differ by more than one order of magnitude. There are several reasons to explain this discrepancy, all of which bear further investigation.

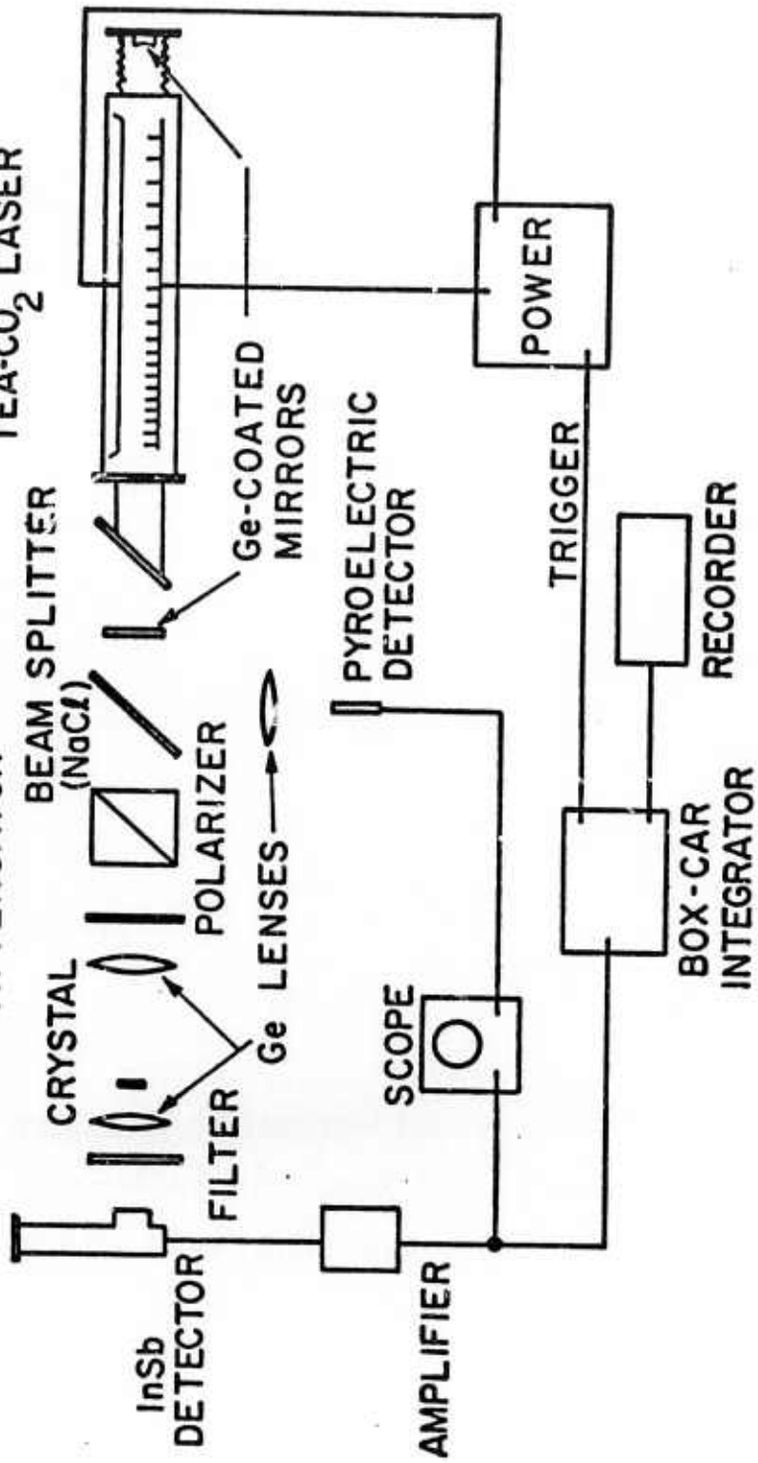

FIGURE 20. Experimental setup for harmonic generation experiments.

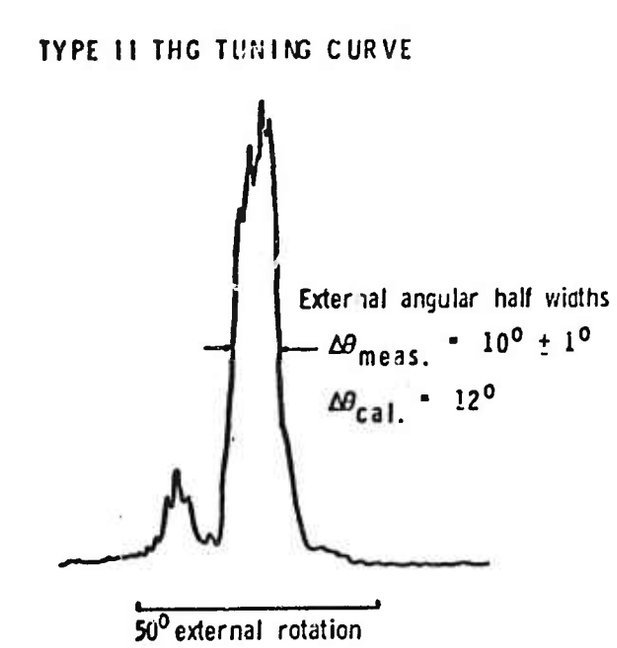

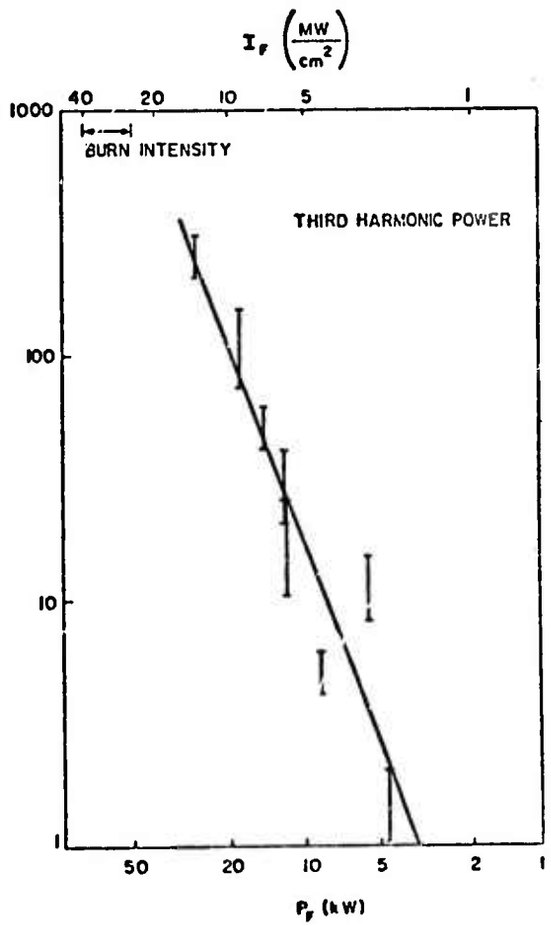

FIGURE 21. THG tuning curve and power dependence.

Since the c_{II} coefficient contains a contribution from free carriers which have been calculated from a modified Kane's model, we might question the accuracy of the carrier concentration measurement. The carrier concentration was measured by the Van de Pauw technique,[116-117] which for bulk samples with possible microcracks and grain boundaries does not have as much accuracy as we would like. It is not unreasonable that our carrier concentration measurement could be wrong by a factor of 2. Since c_{16} and c_{18} in Eq. (4.17) are proportional to N from the form of the equation a factor of 2 error in N gives a factor of 3 error in c_{II}. One can easily attribute part of the error to the experimental measurement process since our crystal must have three angles θ, ϕ and ρ aligned correctly. Moreover, even though we tried to perform this measurement with the laser unmodelocked (and with no mode beating), fluctuations in the laser appear at least three times as large in the third harmonic fluctuations. The d_{14} coefficient of $CdGeAs_2$, as discussed in Appendix II, is accurate to only $\pm$ 40% . The ratio c_{II}/d_{14} is accurate to $\pm$ 25% .

Since the Type II THG tuning curve shown in Fig. 21 compares well with theoretical predictions for the halfwidth, it appears that we were not thermally heating the sample. The angular difference of 12° (internal angle) between Type II SHG and Type II THG, measured in the same material, is in good agreement with the predicted angle difference in Figs. 3.6 & 3.7 . Consequently it does not appear that we were producing additonal free carriers to break phasematching. To change the birefringence by 0.0024 we only need to inject an additional $N = 5 \times 10^{15}$ carriers/cm^3, which would not affect the value of c_{II} as much as indicated in our measurements.

By far the most important point to consider is that our modified Kane model is too simplified a picture. Several workers already observed that Kane's model leads to predicted values of effective masses and third order susceptibilities 2 or 3 times smaller than actually observed. As noted in Appendix II, Cardona[118] in reflectivity and Faraday rotation measurements, and Wynne[119] in third order susceptibility mixing experiments, both observed such deviations of Kane's model's predictions from experiments. In addition, Aspnes[120] has shown that contributions to the second order susceptibility from several points in the Brillouin zone must be considered. He discussed the enhancement of the second order susceptibility from small gap regions throughout the Brillouin zone, rather than only at the direct gap. Much more work on the band structure of $CdGeAs_2$ needs to be done before these points can be clarified.

4. Efficient Harmonic Generation in $CdGeAs_2$

At present all measurements in $CdGeAs_2$ have been made with 200 nsec pulses from TEA-CO_2 lasers. Our 1 nsec system described in Chapter II was not operating well enough to use for measurements. From Table 3 we can derive expressions for the conversion efficiency into the nth harmonic by taking the ratio $I(n\omega)/I(\omega)$.

$$\mathcal{E}(2\omega) = \frac{\pi}{2}\left(\frac{16}{c}\right)(16\pi^2)\left(\frac{2\pi\, d_{eff}\, \ell}{n\lambda}\right)^2 (t_1^2\, t_2)^2\, I(\omega)\, \exp\left[-\tfrac{1}{2}(\alpha_2 + 2\alpha_1)\ell\right]$$

$$\mathcal{E}(3\omega) = \left(\frac{\pi}{2}\right)^2\left(\frac{16}{c}\right)^2(16\pi^2)\left(\frac{3\pi\, c_{eff}\, \ell}{n\lambda}\right)^2 (t_1^3\, t_3)^2 I^2(\omega)\exp\left[-\tfrac{1}{2}(\alpha_3 + 3\alpha_1)\ell\right]$$

$$\mathcal{E}(4\omega) = \left(\frac{\pi}{2}\right)^3\left(\frac{16}{c}\right)^3(16\pi^2)\left(\frac{4\pi\, b_{eff}\, \ell}{n\lambda}\right)^2 (t_1^4\, t_4)^2 I^3(\omega)\exp\left[-\tfrac{1}{2}(\alpha_4 + 4\alpha_1)\ell\right] \qquad (4.6)$$

Here $\mathcal{P}(n\omega)$ is the power conversion efficiency into the nth harmonic and $I(n\omega)$ is the intensity of the nth harmonic. In our experiments, for example, we have measured conversion efficiencies of 2% for SHG and 10^{-4}% for THG in a 2 mm long non-AR coated, p-type crystal with input intensities of 20 MW/cm^2. Kildal[5] has measured a 7% SHG conversion efficiency for a similar 9 mm long p-type crystal and 20 MW/cm^2 input intensity.

Research on $CdGeAs_2$ crystal growth at the Center for Materials Research at Stanford indicates that this material can be made to grow n-type by doping with indium or vanadium. Moreover, crystal growers at both Stanford and Lincoln Laboratories have produced 1 cm long pieces of $CdGeAs_2$. Seeded vertical Bridgeman growth using [111] oriented seeds looks promising as a technique for growing large single crystals. Also, by using 1 nsec pulses and focusing to intensities of 100 MW/cm^2, it is possible to reach 60% SHG and 30% THG conversion efficiencies in 1 cm long crystals. As mentioned in Chapter I, burn densities in p-type Ge for a 1.7 nsec pulse have been measured at 1 GW/cm^2. From the conversion efficiencies quoted above, if the burn density of $CdGeAs_2$ is close to 1 GW/cm^2 one would expect 50 - 80% conversion to second and third harmonic in a 1 cm long crystal with tight focusing. However, Kildal[5] has shown that there is saturation of the SHG signal at high power densities with 200 nsec pulses. The origin of saturation appears to depend on some nonlinear absorption mechanism involving the SHG signal. No free carriers produced by multiphoton absorption were detected; this is the primary saturation mechanism in Te,[121-122] which has a smaller bandgap than $CdGeAs_2$. Further work on the nature of the saturation mechanism in $CdGeAs_2$ is essential, particularly with 1 nsec pulses, in order to fully evaluate its usefulness for high power infrared optics. We have

examined phasematched THG in liquids and gases as an alternative to THG in $CdGeAs_2$, but no experiments have been performed to date.[123]

C. FOURTH HARMONIC THEORETICAL PREDICTIONS

In Section II of Appendix IV the basic approach of the Bond Charge Model is outlined. Starting from Penn's model[102] for the dielectric constant of a semiconductor and Phillip's[103] and Van Vechten's[104] theory for the dielectric properties of semiconductors, Levine[101] developed the Bond Charge Model to calculate second order nonlinear susceptibilities of binary semiconductors. Chemla later extended this model to ternary compounds,[105] and the paper given in Appendix II is a generalization to third order susceptibilities.

In this section we apply the Bond Charge Model to calculate the fourth harmonic tensor coefficients in $CdGeAs_2$. We begin by writing the polarizability of a bond in the language of Phillip's mean energy gap E_g

$$\alpha = \frac{1}{3}(\alpha_{\parallel} + 2\alpha_{\perp}) = (2\alpha_o)^3 \frac{D E_o^2}{E_g^2} \tag{4.7}$$

where $a_o = \hbar^2/me^2 = 5.3 \times 10^{-9}$ cm , $E_o = me^4/2\hbar^2 = 13.6$ ev. D is a correction factor near unity to account for effects of core electrons and E_g is given by

$$E_g^2 = H^2 + C^2 \tag{4.8}$$

The homopolar and heteropolar energy gaps H and C are given in Phillip's

theory by

$$C_{AB} = 1.5\, e^2 \left[\frac{Z_A}{r_A} - \frac{Z_B}{r_B} \right] \exp \left[- \frac{1}{2} k_s (r_A + r_B) \right]$$

$$\frac{1}{H_{AB}^2} \alpha (r_A - r_{CA})^5 + (r_B - r_{CB})^5 \qquad (4.9)$$

where z_A , r_A , r_{CA} are the valence number, covalent radius[106] and the core radius of the A atom in the AB bond, and k_s is a Thomas-Fermi screening constant. Higher order susceptibilities arise from nonlinear variations of the mean bond polarizability α with respect to electric field. We can write the dipole of a bond in terms of a Taylor series expansion of α :

$$P_i = \alpha_{i\ell} (E) E_\ell$$

$$P_i = \left[(\alpha_{i\ell})|_{E=0} + \left(\frac{\partial \alpha_{i\ell}}{\partial E_j} \right) |_{E=0} E_j + \cdots \right] E_\ell \qquad (4.10)$$

The derivative terms give the nonlinear susceptibility components for each bond. For the case of FHG we have

$$\delta_{ijk\ell p} = \frac{1}{3!} \frac{\partial \alpha_{ip}}{\partial E_j \partial E_k \partial E_\ell} \Bigg|_{E=0} \qquad (4.11)$$

As discussed in Appendix II, we assume that we can talk about these higher order polarizabilities in terms of a bond charge[101] q , located at distances r_A and r_B from each atom in the bond. We calculate the variations in α

with electric field by examining the variations in r_A and r_B with electric field. It is shown in Appendix II that

$$\Delta r_A = -\Delta r_B = \frac{\alpha_{||} E_{||}}{g} \qquad E \text{ parallel to bond axis;}$$

$$\Delta r_A = \frac{\alpha_\perp^2 E_\perp^2}{2 r_A q^2} \; ; \; \Delta r_B = \frac{\alpha_\perp^2 E_\perp^2}{2 r_B q^2} \qquad E \text{ perpendicular to bond axis.} \tag{4.12}$$

Since the variations in r_A and r_B are second order in $E_\perp$, we retain only even powers of $E_\perp$. Consequently the odd order derivatives of α_{ij} with respect to $E_\perp$ vanish:

$$\left(\frac{\partial}{\partial E_\perp}\right)^{2p+1} \alpha_{ij} = 0 \tag{4.13}$$

All order derivatives in $E_{||}$ are retained. By using Eq. (4.13) and Kleinman symmetry one can show that the elements of the fourth order susceptibility of a bond are given by

$$\left.\begin{aligned} \delta_{zzzzz} = \delta_{||} &= \frac{1}{6} \frac{\partial^3 \alpha_{||}}{\partial E_{||}^3} \neq 0 \\ \delta_{xxxxx} = \delta_\perp &= \frac{1}{6} \frac{\partial^3 \alpha_\perp}{\partial E_\perp^2} = 0 \\ \delta_{xxzzz} = \delta_{||\perp} &= \frac{1}{6} \frac{\partial^3 \alpha_{xz}}{\partial E_x \, \partial E_z \, \partial E_2} = 0 \end{aligned}\right\} + \text{all permutations} \tag{4.14}$$

By combining expressions Eq. (4.7) through (4.14) as discussed for the case of THG in Appendix II, we obtain an expansion for $\xi_{||}(AB)$ for the fourth order polarizability of the bond between atoms A and B given by the following:

$$\delta_{||}(AB) = \frac{-3\alpha^5}{AE_g^2}\left[\begin{array}{l} 4(2f_h - 1)h_1^3H + 4(2f_i - 1)g_1^3C + 4(6f_i - 1)h_1g_1^2H \\ +4(6f_n - 1)h_1^2g_1C - 8(h_1g_2 + h_2g_1)HC \\ -E_g^2[2(4f_h - 1)h_1h_2 + 2(4f_i - 1)g_1g_2 - 2(h_3H + g_3C)] \end{array}\right] \tag{4.15}$$

where

$$A = (2\,a_o)^3\, D\, E_o^2 \qquad f_i = \frac{C^2}{E_g^2} \qquad f_h = 1 - f_i$$

$$g_1 = \frac{-be^2}{q}\left[\frac{Z_A}{r_A^2} + \frac{Z_B}{r_B^2}\right]\exp\left[-\frac{1}{2}k_s(r_A + r_B)\right] \qquad h_1 = \frac{-25.8}{q}\left[\frac{r_A - r_B}{r_A + r_B)^2}\right] H$$

$$g_2 = \frac{be^2}{q^2}\left[\frac{Z_A}{r_A^3} + \frac{Z_B}{r_B^3}\right]\exp\left[-\frac{1}{2}k_s(r_A + r_B)\right] \qquad h_2 = \frac{-20}{q^2}\left[\frac{1}{(r_A + r_B)^2}\right] H$$

$$g_3 = \frac{-be^2}{q^3}\left[\frac{Z_A}{r_A^4} + \frac{Z_B}{r_B^4}\right]\exp\left[-\frac{1}{2}ks(r_A + r_B)\right] \qquad h_3 = \frac{-103.2}{q^3}\left[\frac{r_A - r_B}{(r_A + r_B)^4}\right] H$$

Here q is the bond charge given by

$$q = -3\left[\frac{2}{n^2} + 0.4(1 - f_i)\right]e \tag{4.16}$$

where n is the index of refraction, f_i the ionicity[103] and the factor 3 arises from the fact that we have a tensor derivation. In $CdGeAs_2$ we must derive the value of the polarizability for the CdAs bond and the GeAs bond, denoted by δ_{11}^{+} and δ_{11}^{-} respectively.

Finally we must sum over the contributions of all bonds in the unit cell of volume V. From Fig. 3.1 we have two nonzero components of the macroscopic FHG tensor. In terms of the parameters τ and σ, which are a measure of the distortion of the unit cell, we can express $b_{1(4)}$ and $b_{1(5)}$ as the geometrical sum over the bond polarizabilities

$$b_{1(4)} = \frac{16}{9\sqrt{3}V}\left[(1 + \frac{4\tau}{3} - \frac{2\sigma}{3})\,\delta_{11}^{+} - (1 + \frac{4\tau}{3} + \frac{2\sigma}{3})\,\delta_{11}^{-}\right]$$

$$b_{1(5)} = \frac{16}{9\sqrt{3}V}\left[(1 - \frac{2\tau}{3} + \frac{\sigma}{3})\,\delta_{11}^{+} - (1 - \frac{2\tau}{3} - \frac{\sigma}{3})\,\delta_{11}^{-}\right] \qquad (4.17)$$

where $\tau = \frac{c}{2a} - 1$, $\sigma = \frac{4x}{a} - 1$, and a and c are the lattice constants. By substituting the expressions Eq. (4.15) for δ_{11}^{+} and δ_{11}^{-} into Eq. (4.17) (using values of the parameters for CdAs and GeAs bonds found by interpolation of values for other bonds,[101,103-106]) we derive the values

$$|b_{1(4)}| = 2.80 \times 10^{-18} \text{ esu}$$

$$|b_{1(5)}| = 0.72 \times 10^{-18} \text{ esu} \qquad \text{Units } cm^{9/2} \,/\, erg^{3/2} \qquad (4.18)$$

This is the central result of this section. The only experimental results on phasematched FGH in any material give a value of $b_{eff} \approx 10^{-21}$ esu for lithium formate.[124] The large nonlinear response of $CdGeAs_2$ is apparent in the three orders of magnitude difference between the two susceptibilities.

Finally we can estimate the conversion efficiencies to be expected for FHG in $CdGeAs_2$ with $10^8 W/cm^2$ input intensity in a 1 nsec pulse. We assume a 1 cm long, AR coated crystal. From Eq. (4.6) we calculate a conversion efficiency of 10^{-8}% for a typical p-type crystal ($\alpha_1 = 0.5\ cm^{-1}$, $\alpha_4 = 7.0\ cm^{-1}$).

For a high resistivity sample ($\alpha_1 \approx 0.01\ cm^{-1}$, $\alpha_4 \approx 4.6\ cm^{-1}$), and an input intensity of $1GW/cm^2$ the conversion efficiency should be about 10^{-4}% for FHG. It appears that FHG in $CdGeAs_2$ will never be a practical source of infrared radiation, but coupled with SHG and THG results, it may provide additional insight into the theoretical models for nonlinear susceptibilities.

V. REFERENCES

1. R.L. Byer, H. Kildal, R.S. Feigelson, "$CdGeAs_2$ A New Nonlinear Crystal Phasematchable at 10.6 μm", Appl. Phys. Letts. vol. 19, p.237, (1971).

2. G.D. Boyd, E. Beuhler, F.G. Storz, J.H. Wernick, "Linear and Non-Linear Optical Properties of Ternary A^{II} B^{IV} C_2^V Chalcopyrite Semiconductors", IEEE Jour. Quant. Elect. vol. QE-8, p.419, (April 1972).

3. H. Kildal, R.F. Begley, M.M. Choy, R.L. Byer, "Efficient Second and Third Harmonic Generation in $CdGeAs_2$", Jour. Opt. Soc. Amer. vol. 62, p.1398, (1972).

4. H. Kildal, "$CdGeAs_2$ and $CdGeP_2$ Chalcopyrite Materials for Infrared Nonlinear Optics", Ph.D. dissertation, Stanford University, Stanford, California. (1972); AFML-TR-72-277.

5. H. Kildal, "Efficient Doubling and cw Difference Frequency Mixing in the Infrared Using the Chalcopyrite $CdGeAs_2$", presented at the Conference on Laser Applications, Washington. D.C.

6. R.L. Byer, "Optical Parametric Oscillators", to be published in Treatise in Quantum Electronics, H. Rabin, C.L. Tang, Editors, Academic Press.

7. D.S. Chemla, R.F. Begley, R.L. Byer, "Experimental and Theoretical Studies of Third Harmonic Generation in the Chalcopyrite $CdGeAs_2$", IEEE Jour. Quant. Elect., vol. QE-10, p.71, (1974).

8. A.F. Gibson, M.F. Kimmett , B. Norris, "Generation of Bandwidth Limited Pulses from a TEA-CO_2 Laser Using p-type Germanium", Appl. Phys. Letts. vol. 24, p.306, (1974).

9. H. Kildal, R.L. Byer, "Comparison of Laser Methods for the Remote Detection of Atmosphere Pollutants", Proc. IEEE, vol. 59, p.1644, (1971).

10. J.A. Hodgeson, W.A. McClenny, P.L. Hanst, "Air Pollution Monitoring by Advanced Spectroscopic Techniques", Science, vol. 182, p.248, (1973).

11. J.C. Phillips, "The Fundamental Optical Spectra of Solids", Solid State Physics, eds. F. Seitz and D. Turnbull, Academic Press, vol. 18, p. 55 (1966).

12. W. Kaiser, C.G.B. Garrett, "Two Photon Excitation in $CaF_2:Eu^{2+}$, Phys. Rev. Letts. vol. 7, p.229, (1961).

13. D. Kleinman, "Laser and Two-photon Processes", Phys. Rev. vol. 125, p. 87, (1962).

14. J.J. Hopfield, J.M. Worlock, K. Park, "Two Quantum Absorption Spectrum of KI", Phys. Rev. Letts. vol. 11, p.414, (1963).

15. D. Frohlick, H. Mahr, "Two Photon Spectroscopy in Arthracene", Phys. Rev. Letts. vol. 16, p.895, (1966).

16. M. Geller, D.E. Altman, F.A. DeTemple, "Two Photon Absorption in Alkali-halides with a Pulsed N_2 Laser", Appl. Phys. Letts. vol. 11, p.221, (1967).

17. J.A. Giordmaine, P.M. Rentzepis, S.L. Shapiro, "Two photon Excitation of Fluorescence by Picosecond Light Pulses", Appl. Phys. Letts. vol. 11, p.216, (1967).

18. J.J. Wynne, "Optical Third Order Mixing in GaAs, Ge, Si, InAs", Phys. Rev. vol. 178, p.1295, (1969).

19. C.B. Moore, "Lasers in Chemistry", Ann. Review Phys. Chem. vol. 22, p. 387, (1971).

20. F.Y. Chang and O.R. Wood, "Optically Pumped Atmospheric Pressure CO_2 Laser", Appl. Phys. Letts. vol. 21, p.19, (1972).

21. H.R. Letterman, H.R. Schlossberg, J. Waldman, "Submillimeter Lasers Optically Pumped Off Resonance", Optics Commun. vol. 6, p.156, (1972).

22. F.Y. Chang, O.R. Wood, "Optically Pumped N_2O Laser", Appl. Phys. Letts. vol. 22, p.93, (1972).

23. L.A. DeTemple, L.J. Plant, P.D. Coleman, "Intense Super-radiant Emission at 496 μm From Optically Pumped Methyl Fluoride", Appl. Phys. Letts. vol. 22, p.644, (1973).

24. R.J. Morgan, A.J. Zelano, L.H. Ngai, "New Submillimeter Laser Lines in Optically Pumped Gas Molecules", Optics Commun. vol. 8, p.46, (1973).

25. F.Y. Chang, O.R. Wood, "Optically Pumped 33 atm CO_2 Laser", Appl. Phys. Letts, vol. 23, p.370, (1973).

26. F.K. Plant, P.D. Coleman, L.A. DeTemple, "New Optically Pumped Far Infrared Lasers", IEEE Jour. Quant. Elect., vol. QE-9, p. 962, (1973).

27. F.Y. Chang, O.R. Wood, "Optical Transfer 42-atm N_2O Laser", Appl. Phys. Letts. vol. 24, p.182, (1974).

28. E.D. Hinkley, K.[illegible] Nill, F.A. Blum, "Infrared Spectroscopy with Tunable Lasers", to be published in Laser Spectroscopy of Atoms and Molecules, H. Walther, editor; Springer-Verlag.

29. R. K. Route, R. S. Feigelson, and R. J. Raymakers, "Growth of $AgGaSe_2$ for Infrared Applications," (to be published).

30. R. Begley, "TEA-CO_2 Laser Systems at Stanford", Microwave Laboratory Report No. 2320.

31. N.N. Sobolev, V.V. Sokovikov, "CO_2 Lasers", Soviet Phys. Uspekhi, vol. 10. p.153, (1967).

32. J.A. Beaulieu, "High Peak Power Gas Lasers", Proc. IEEE, vol. 59, p. 667, (1971).

33. O.R. Wood II, "High Pressure Pulsed Molecular Lasers", Proc. IEEE, vol. 62, p.355, (1974).

34. C.K.N. Patel, "Continuous Wave Laser Action on Vibrational-Rotational Transitions in CO_2", Phys. Rev. vol. 136, p.1187, (1964).

35. M.C. Richardson, A.J. Alcock, K. Leopold, P. Burtyn, "A 300-J Multigigawatt CO_2 Laser", J. Quant. Elect. QE-9, p.236, (1973).

36. A.M. Robinson, "Effect of Inductance on the Small Signal Gain of a Transverse Excitation Atmospheric Pressure Discharge in Carbon Dioxide", J. Quant. Elect. QE-7, p.199, (1971).

37. D.C. Johnson, "Excitation of an Atmospheric Pressure CO_2-N_2-H_e Laser by Capacitor Discharges", J. Quant. Elect. QE-7, p.185, (1971).

38. A.J. Beaulieu, "Transversely Excited Atmospheric Pressure CO_2 Lasers", Appl. Phys. Letts. vol. 16, p.504, (1970).

39. A.K. Laflamme, "Double Discharge Excitation for Atmospheric Pressure CO_2 Lasers", Rev. Sci. Inst. vol. 41, p.1578, (1970).

40. H.M. Lamberton, P.R. Pearson, "Improved Excitation Techniques for Atmospheric Pressure CO_2 Lasers", Electronics Letts, vol. 7, p.141, (1971).

41. P.R. Pearson, H.M. Lamberton, "Atmospheric Pressure CO_2 Lasers Giving High Output Energy per Unit Volume", J. Quant. Elect. QE-8, p.145, (1972).

42. J.L. Lachambre, J. Gilbert, F. Rheault, R. Fortin, M. Blanchard, "Performance Characteristics of a TEA Double Dishcarge Grid Amplifier", J. Quant. Elect. QE-9, p.459, (1973).

43. F.Y. Chang, O.R. Wood, "A Simple Self-mode-locked Atmospheric Pressure CO_2 Laser", J. Quant. Elect. QE-8, p.721, (1972).

44. G. Otis, "High Trigger Current Structure for Double Discharge TEA Lasers", Rev. Sci. Inst. vol. 43, p.1621, (1972).

45. F.W. Johns, J.A. Nation, "A Resistive Electrode, High Energy, Transverse Laser Discharge", Rev. Sci. Inst. vol. 44, p.169, (1972).

46. R. Freiberg, "CO_2 Transverse Discharge Lasers", J. Quant. Elect. QE-6, p.105, (1970).

47. R.K. Gainsworthy, L.E. Mathias, C.H.H. Carmichael, "Atmospheric Pressure Pulsed CO_2 Laser Utilizing Preionization by High Energy Electrons", Appl. Phys. Letts, vol. 19, p.506, (1971).

48. J.P Reilly, "Pulser/Sustainer Electric Discharge Laser", J. Appl. Phys. vol. 43, p.3411, (1972).

49. C.A. Fenstamacher, M.J. Nutter, W.F. Leland, K. Boyer, "Electron Beam Controlled Electrical Discharge as a Method of Pumping Large Volumes of CO_2 Laser Media at High Pressures", Appl. Phys. Letts. vol. 20, p.56, (1972).

50. A. Javan, J.S. Levine, "The Feasibility of Producing Laser Plasmas via Photo-ionization", J. Quant. Elect. QE-8, p.827, (1972).

51. J.S. Levine, A. Javan, "Observation of Laser Oscillation in a 1-atm CO_2-N_2-He Laser Pumped by Electrically Heated Plasma Generated via Photo-ionization", Appl. Phys. Letts. vol. 22, p.55, (1972).

52. H. Seguin, J. Tulip, "Photo-initiated and Photo-sustained Laser", Appl. Phys. Letts. vol. 21, p.414, (1972).

53. O.P. Judd, "An Efficient Electrical CO_2 Laser Using Pre-ionization by Ultraviolet Radiation", Appl. Phys. Letts. vol. 22, p.95, (1973).

54. D.B. Cohn, E.R. Ault, "Photo-initiated Transversely Sustained CO_2 Laser, Appl. Phys. Letts vol. 22, p.138, (1973).

55. N.H. Burnett, A.A. Offenberger, "Simple Electrode Configuration for UV Initiated High Power TEA Laser Discharges", J. Appl. Phys. vol. 44, p.3617, (1973).

56. H.J.J Sequin, J. Tulip, D. McKen, "UV Photo-ionization Density Measurements in TEA Lasers", Appl. Phys. Letts. vol. 23, p.344, (1973).

57. H.J.J. Sequin, J. Tulip, D. McKen, "Enhancement of Photoelectron Density in TEA Lasers Using Additives", Appl. Phys. Letts. vol. 23, p.527, (1973).

58. M.C. Richardson, K. Leopold, A.J. Alcock, "Large Aperture CO_2 Laser Discharges", J. Quant. Elect. QE-9, p.934, (1973).

59. O.P. Judd, and J.Y. Wada, "Investigations of a UV Preionized Electrical Discharge and CO_2 Laser," J. Quant. Elect. QE-10, p.12, (1974).

60. L.J. Denes, J.J. Lowke, "V-I Characteristics of Pulsed CO_2 Laser Discharges", Appl. Phys. Letts. vol. 23, p.130, (1973).

61. A.M. Robinson, "Spatial Resolution of Gain in CO_2 Transversely Excited Pulsed Discharge", J. Appl. Phys. vol. 42, p.4098, (1971).

62. R.W. O'Neil, R.J. Carbone, H. Gunels, H. Kleinman, "TEA Laser Medium Diagnostics", Appl. Phys. Letts. vol. 20, p.461, (1972).

63. T.F. Deutsch, R.I. Rudko, "Spatial and Temporal Dependence of the Gain of a Transversely Excited Pulsed CO_2 Laser", Appl. Phys. Letts. vol. 20, p.423, (1972).

64. L.J. Denes, L.A. Weaver, "Laser Gain Characterization of Near Atmospheric CO_2-N_2-He Glows in a Planar Electrode Geometry", J. Appl. Phys. vol. 44, p.4125, (1973).

65. W.A. Stiehl, P.W. Hoff, "Measurement of the Spectrum of a Helical TEA-CO_2 Laser", Appl. Phys. Letts. vol. 22, p.680, (1973).

66. R. Fostin, A.K. Laflamme, F. Rheault, "Double Discharge TEA Laser Beams", Am. J. Phys. vol. 50, p.583, (1972).

67. M.C. Fowler, "Influence of Plasma Kinetic Processes on Electrically Excited CO_2 Laser Performance", J. Appl. Phys. vol. 43, p.3480, (1972).

68. K.R. Manes, H.J. Seguin, "Analysis of the CO_2 TEA Laser", J. Appl. Phys. vol. 43, p.5073, (1972).

69. D.L. Lyon, "Comparison of Theory and Experiment for a Transversely Excited High Pressure CO_2 Laser", J. Quant. Elect. vol. QE-9, p.139, (1973).

70. G. Girard, M. Hugnet, M. Michon, "High Power Double Discharge TEA Laser Medium Diagnostic", J. Quant. Elect. vol. QE-9, p.426, (1973).

71. B.S. Patel, "Role of Helium in TEA-CO_2 Lasers", J. Quant. Elect. vol. QE-9, p.1160, (1973).

72. A. Girard, H. Pepin, "Performance Characteristics of a TEM_{oo} Mode TEA-CO_2 Oscillator Amplifier System", Optics Communications, vol. 8, p.68, (1973).

73. Y. Pen, J.R. Simson, A. Bernhardt, S. Kiergan, "Generation of a Multigigawatt Nanosecond CO_2 Pulse", J. Quant. Elect. vol. QE-10 p.44, (1974).

74. D.L. Davis, D.L. Smith, J.S. Koval, "Generation of Single Lens Pulses at 10.6 μm", J. Quant. Elect. vol. QE-8, p.846, (1972).

75. R.L. Abrams, D.A. Pinnoir, "Acousto-Optic Properties of Crystalline Germanium", J. Appl. Phys. vol. 41, p.2765, (1970).

76. R.L. Abrams, D.A. Pinnoir, "Efficient Acousto-optic Modulation at 3.39 μm and 10.6 μm in Crystalline Germanium", J. Quant. Elect. vol. 7, p.135, (1971).

77. D.J. Kuizenga, A.E. Siegman, "FM and AM Mode Locking of the Homogeneous Laser - Part I : Theory", J. Quant. Elect. vol. QE-6, p.694, (1970).

78. C. Roundy, "Advances in Pyroelectric Detectors", Ph.D. dissertation, Stanford University, Stanford, Calif. December, 1972.

79. J.P. Kaminov, "Measurements of the Electro-optic Effect in CdS, ZnTe and GaAs at 10.6 Microns", J. Quant. Elect. vol. QE-4, p.23, (1968).

80. S. Namba, "Electro-Optical Effect in Zincblende", J. Opt. Soc. Amer., vol. 51, p.76, (1961).

81. J.E. Kiefer, Ammon Yariv, "Electro-optic Characteristics of CdTe at 3.39 and 10.6 μm", Appl. Phys. Letts. p.26, (1969).

82. C.J. Johnson, "Electro-optic Effect in CdTe at 23.35 and 27.95 Microns", Proc. IEEE, vol. 56, p.1719, (1968).

83. J.R. Bettis, A.H. Guenther, Subnanosecond Jitter Laser Triggered Switching at Moderate Repetition Rates", J. Quant. Elect., QE-6, p.483, (1970).

84. A.H. Guenther, J.R. Bettis, "A Review of Laser Triggered Switching", Proc. IEEE, vol. 59, p.589, (1971).

85. C.J. Peters, "Gigacycle Bandwidth Coherent Light Traveling Wave Phase Modulator", Proc. IEEE, vol. 51, p.147, (1963).

86. J.D. Cobine, Gaseous Conductors, p.178, Dover Press, (1941).

87. G. Balloffet, "Contribution a l'etude des Sources de Lumiere dans l'ultraviolet Lointain et Application a l'analys4 Spectrochimique", Annales de Physique, p.1243, (1960).

88. G.H.C. Freeman, "The Far Ultraviolet Spectra from the Vacuum Sliding Spark", Proc. Phys. Soc. (London), vol. 86, p.117, (1965).

89. J.A.R. Samson, Techniques of Vacuum Ultraviolet Spectroscopy, J. Wiley and Sons, Inc, p.163, (1967).

90. J.E. Midwinter, J. Warner, "The Effects of Phasematching Methods and of Uniaxial Crystal Symmetry on the Polar Distribution of Second Order Nonlinear Optical Polarization", Brit. J. Appl. Phys., 16, 1135, (1965).

91. J.E. Midwinter, J. Warner, "The Effects of Phasematching Methods and of Crystal Symmetry on the Polar Dependence of Third Order Nonlinear Optical Polarization", Brit. J. Appl. Phys., 16, 1667, (1965).

92. D.A. Kleinman, "Nonlinear Dielectric Polarization in Optical Media", Phys. Rev. vol. 126, p.1977, (1962).

93, G.D. Boyd, E. Beuhler, F.G. Storz, J.H Wernick, "Linear and Nonlinear Optical Properties of Ternary A^{II}, B^{IV}, C_2^V Chalcopyrite Semiconductors", IEEE J. Quant. Elect. vol. QE-8, p.419, (1972).

94. J.A. Armstrong, N. Bloembergen, J. Ducuing, P.S. Pershan, "Interaction Between Light Waves in a Nonlinear Dielectric", Phys. Rev. vol. 127, p.1918, (1962).

95. G.D. Boyd, A. Askin, J.M. Dziedzic, D.A. Kleinman, "Second Harmonic Generation of Light with Double Refraction", Phys. Rev. vol. 137, p.A1305, (1965).

96. G.D. Boyd, D.A. Kleinman, "Parametric Interaction of Focused Gaussian Light Beams", Jour. Appl. Phys. vol. 39, p.3597, (1968).

97. D.S. Chemla, "Generation of Second Harmonique des Ordes Lumineous dans les Cristaux Nonlineares", Ann. Telecomm. vol. 27, p.311, (1972).

98. M. Born, E. Wolf, Principles of Optics, Pergamon Press, N.Y. New York, p.36, (1965).

99. B.F. Levine, "Electrodynamical Bond Charge Calculation of Nonlinear Optical Susceptibilities", Phys. Rev. Letts. vol. 22, p.787, (1969).

100. D.S. Chemla, "Dielectric Theory of Tetrahedral Solids: Application to Ternary Compounds with Chalcopyrite Strcuture", Phys. Rev. Letts. vol. 26, p.1441, (1971).

101. a) B.F. Levine, "Electro Dynamical Bond Charge Calculation of Nonlinear Optical Susceptibilities", Phys. Rev. Letts. 22, 787, (1969).

b) "Bond Charge Calculations of Nonlinear Optical Susceptibilities for Various Crystal Structures", Phys. Rev. B, vol. 7, p.2600, (1973).

102. D.R. Penn, "Wave Number Dependent Dielectric Function of Semiconductors", Phys. Rev. vol. 128, p.2093, (1962).

103. a) J.C. Phillips, "A Posteriori Theory of Covalent Bonding", Phys. Rev. Letts. vol. 19, p.405, (1967).

b) "Ionicity of the Chemical Bond in Crystals", Rev. Mod. Phys. vol. 42, p.318, (1970).

104. J.A. Van Vechten, "Quantum Dielectric Theory of Electro-negativity in Covalent Systems, I. Electronic Dielectric Constant, II. Ionization Potentials and Interband Transition Energies", Phys. Rev. vol. 182, p.891, (1969), Phys. Rev. vol. 187, p.1007, (1969).

105. D.S. Chemla, "Dielectric Theory of Tetrahedral Solids", Application to Ternary Compounds with Chalcopyrite Structures", Phys. Rev. Letts. vol. 26, p.1441, (1971).

106. J.A. Van Vechten, J.C. Phillips, "New Set of Tetrahedral Covalent Radii", Phys. Rev. B, vol. 2, p.2160, (1970).

107. P.N. Butcher, F.P. McLean, "The Nonlinear Constitutive Relation in Solids at Optical Frequencies", Proc. Phys. Soc. vol. 81, p.219, (1963).

108. P.A. Wolff, G.A. Pearson, "Theory of Optical Mixing by Mobile Carriers in Semiconductors", Phys. Rev. Letts. vol. 17, p.1015, (1966).

109. S.S. Jha, N. Bloembergen, "Nonlinear Optical Susceptibilities in Group IV and III-V Semiconductors", Phys. Rev. vol. 171, p.891,(1968).

110. E.O. Kane, "Band Structure of Indium Antimonide", J. Phys. Chem. Sol. vol. 1, p.249, (1957),

111. C.K.N. Patel, R.E. Slusher, P.H. Feury, "Optical Nonlinearities due to Mobile Carriers in Semiconductors", Phys. Rev. Letts. vol. 17, p.1011, (1966).

112. P. Kaw, "Optical Mixing by Mobile Carriers in Semiconductors", Phys. Rev. Letts. vol. 21, p.539, (1968).

113. C.C. Wang, N.W. Ressler, "Nonlinear Optical Effects of Conduction Electrons in Semiconductors", Phys. Rev. Lett.. vol. 188, p.1291, (1969).

114. K.C. Rustagi, S.S. Jha, "Effects of Scattering on Optical Nonlinearity due to Carriers in Semiconductors", Phys. Letts. vol. 30a, p.518, (1969).

115. K.C. Rustagi, "Effect of Carrier Scattering on Nonlinear Optical Susceptibility due to Mobile Carriers in InSb, InAs and GaAs", Phys. Rev. vol. B2, p.4053, (1970).

116. L.F. van de Pauw, "A Method of Measuring the Resistivity and Hall Coefficient on Lamellae of Arbitrary Shape", Phillips Tech. Rev. vol. 20, p.220, (1959).

117. L.F. van de Pauw, "A Method of Measuring the Specific Resistivity and Hall Effect of Discs of Arbitrary Shape", Phillips Research Reports, vol. 13. p.1. (1958).

118. M. Cardona, "Electron Effective Masses of InAs and GaAs as a Function of Temperature and Doping", Phys. Rev. vol. 121, p.752, (1961).

119. J.J. Wynne, "Optical Third Order Mixing in GaAs, Ge, Si and InAs", Phys. Rev. vol. 178, p.1295, (1969).

120. D.E. Aspnes, "Energy Band Theory of the Second Order Nonlinear Optical Susceptibility of Crystals of Zinc-Blende Symmetry", Phys. Rev. B. vol. 6, p.4648, (1972).

121. W.B. Gandrud, R.L. Abrams, "Reduction in SHG Efficiency in Tellurium by Photoinduced Carriers", Appl. Phys. Letts. vol. 17, p.302, (1970).

122. C. Schwartz, J.L. Oudar, E. Batifol, "Etude de la Limitation de Generation de Second Harmonique dans le Tellure par l'absorption a Deux Photons", to be published.

123. R. Begley, "Third Harmonic Generation in Liquids and Gases in the Infrared", Microwave Laboratory Report, No. 2321 (1974).

124. Ahkmanov, private communication.

125. F. G. Fumi, "Physical Properties of Crystals: The Direct Inspection Method", Acta. Cryst. vol. 5, p.44, (1952).

126. F. G. Fumi, "The Direct Inspection Method in Systems with a Principal Axis of Symmetry", Acta, Cryst. vol. 5, p.691, (1952).

127. J.F. Nye, Physical Properties of Crystals, Oxford University Press, London, 1957.

128. R. Freschi, F.G. Fumi, "High Order Matter Tensors in Symmetrical Systems", Il Nuovo Cimento, vol. X, p.865, (1953).

129. J.A.R. Coope, R.F. Snider, F.R. McCourt, "Irreducible Cartesian Tensors", J. Chem. Phys., vol. 43, p.2269, (1965).

130. J.A.R. Coope, R.F. Snider, "Irreducible Cartesian Tensors II, General Formulation", J. Math. Phys., vol. 11, p.1003, (1970).

131. J.A.R. Coope, "Irreducible Cartesian Tensors III, Clebsch-Gordon Reduction", J. Math. Phys., vol. 11, p.1591, (1970).

132. J. Jerphagnon, "Invariants of the Third Rank Cartesian Tensor: Optical Nonlinear Susceptibilities", Phys. Rev. B, vol. 2, p.1091, (1970).

133. D.S. Chemla, to be published.

134. J.A. Armstrong, N. Bloembergen, J. Ducuing, P.S. Pershan, "Interactions Between Light Waves in a Nonlinear Dielectric", Phys. Rev. vol. 127, p.1918, (1962).

135. D.A. Kleinman, "Nonlinear Dielectric Polarization in Optical Media", Phys. Rev. vol. 126, p.1977, (1962).

136. J.A. Schouter, Tensor Analysis for Physicists, Oxford University Press, London (1954).

APPENDIX I

CALCULATION OF NONZERO ELEMENTS OF n^{th} RANK SUSCEPTIBILITY TENSORS

In this appendix we examine a very straightforward procedure for determining the nonzero elements of a nonlinear optics susceptibility tensor to any order from one of lower rank. Since most work in the past has required consideration of only $\chi^{(1)}$, $\chi^{(2)}$ and sometimes $\chi^{(3)}$ tensors, the direct inspection method[125-127] has been most often used to simplify the forms of tensors. However, one can easily see that this method can become quite cumbersome for higher rank tensors. The total number of elements in a tensor rank n is 3^n, corresponding to a susceptibility of order $(n-1)$, namely $\chi^{(n-1)}$. For fourth harmonic generation for example, $n = 5$ and $3^5 = 243$ elements. For a possible fifth order process $n = 6$ and $3^6 = 792$ elements. Nevertheless, the direct inspection method has been applied to fifth and sixth order tensors.[128]

From another point of view, one can apply the methods of group theory to the task of expressing a tensor of rank n in terms of its irreducible components of lower ranks,[129-131] This technique has been used successfully in nonlinear optics by Jerphagnon.[132] The use of such techniques, particularly the realization that one can very closely associate the properties of higher rank cartesian tensors with higher order spherical harmonics, leads to a very elegant, but also very practical formulation of higher order tensors for many physical problems.[133] This method moreover, provides the only simple way for finding the exact relationships between the nonzero elements of a tensor of rank n.

In this appendix we simply borrow some points from these more general treatments and consider the case of nonlinear optical susceptibility tensors. There are three classes of symmetry conditions we must consider: the symmetry of the particular crystal class in question; overall permutation symmetry;[134] and Kleinman symmetry.[135] For a tensor of rank n and a harmonic generation process, $n - 1$ of the frequencies involved are the same. Overall permutation symmetry allows one to permute $n - 1$ of the tensor element subscripts without changing the value of the coefficient. For SHG for example

$$d_{ijk} = d_{ikj} \tag{I.1}$$

If all of the frequencies in question are within the transparency range of the material, one often can neglect dispersion in the nonlinear susceptibility. In that case Kleinman symmetry holds, and one can permute all n subscripts. Again for SHG we have

$$d_{ijk} \approx d_{jik} \approx d_{kji} \tag{I.2}$$

For a tensor of rank n, the application of Kleinman symmetry makes the tensor fully symmetric. The total number of independent elements is given by[129]

$$\binom{n+2}{n} = \frac{(n+1)(n+2)}{2}$$

For overall permutation symmetry the tensor is symmetric in only $n - 1$

indices. The total number of independent elements is given by[127]

$$3\binom{n+1}{n-1} = \frac{3n(n+1)}{2}$$

Finally, from above, for the case of no special symmetries there are 3^n independent elements. The factor 3, of course, comes from dealing with a space with three dimensions x, y, z. Table I.1 summarizes the number of independent elements for different symmetry conditions, before the application of the properties of the crystal class. Kleinman symmetry is a very powerful condition for reducing the number of independent tensor elements and it should always be applied <u>first</u> before the symmetry properties of the crystal are considered.

Next, we can write a tensor of rank n in two ways:[136] first it is the tensor product of n vectors

$$b^{(n)}_{ijkl.....p} = t^{(1)}_i \circledast t^{(1)}_j \circledast ..... \circledast t^{(1)}_p \qquad (I.3)$$

Secondly, it can be written as the tensor product of a vector with a tensor of rank (n - 1)

$$b^{(n)}_{ijkl.....p} = t^{(1)}_i \circledast c^{(n-1)}_{jkl.....p} \qquad (I.4)$$

In particular, one can write each higher order nonlinear optics tensor as the tensor product of a vector and the <u>previous lower order</u> tensor.

$$\chi^{(2)}_{ijk} = t_i \circledast \chi^{(1)}_{jk}$$

$$\chi^{(3)}_{ijkl} = t_i \circledast \chi^{(2)}_{jkl} \qquad (I.5)$$

The prescription of this appendix, therefore, is to first apply Eq. (I.4) to generate the appropriate nonzero elements of the n rank tensor, but using the Kleinman symmetry reduced form of the (n-1) rank tensor. Then, the properties of the particular crystal symmetry can be applied to the already much reduced tensor. As a practical example, we can generate the independent elements of $\chi^{(2)}_{ijk}$ and $\chi^{(3)}_{ijk\ell}$. We first note that the linear susceptibility $\chi^{(1)}_{jk}$ has six independent elements

$$(11 \quad 22 \quad 33 \quad 32 \quad 13 \quad 12) \rightarrow \chi^{(1)}_{jk} \tag{I.6}$$

where 1, 2, 3 are short notation for x, y, z. To generate $\chi^{(2)}_{ijk}$ we write

$$\chi^{(2)}_{ijk} = t^{(1)}_{i} \circledast \chi^{(1)}_{jk}$$

$$= (1\ 2\ 3) \times (11 \quad 22 \quad 33 \quad 32 \quad 13 \quad 12) \tag{I.7}$$

If we write down all the possible combinations in the product and keep only the independent ones we have

$$(111\ 112\ 113\ 122\ 123\ 133\ 222\ 223\ 233\ 333) \rightarrow \chi^{(2)}_{ijk} \tag{I.8}$$

Note, there are ten independent coefficients as predicted in Table I.1 for Kleinman symmetry. Using Eq. (I.2) we can determine the coefficients of $\chi^{(3)}_{ijk\ell}$.

$$\chi^{(3)}_{ijk\ell} = t^{(1)}_{i} \circledast \chi^{(2)}_{jk\ell} \tag{I.9}$$

TABLE I.1

INDEPENDENT ELEMENTS OF A TENSOR OF RANK n

Tensor Rank (n)	Susceptibility Order (n-1)	No Symmetry (3^n)	Overall Permutation Symmetry $\frac{3n(n+1)}{2}$	Kleinman Symmetry $\left(\frac{(n+1)(n+2)}{2}\right)$
2	1 (ω)	9	-	6
3	2 (2ω)	27	18	10
4	3 (3ω)	81	30	15
5	4 (4ω)	243	45	21
6	5 (5ω)	729	63	28

Writing out the product and keeping the independent elements gives

$$\begin{pmatrix} 1111 & 1112 & 1112 & 1222 & 2222 & 2223 & 1333 & 2333 & 3333 \\ & 1133 & 1233 & 1122 & 1322 & 1123 & 2233 & & \end{pmatrix} \rightarrow \chi^{(3)}_{ijk\ell} \tag{1.10}$$

Here there are fifteen independent coefficients, again in agreement with Table I.1. At this point we could apply the crystal class symmetry properties, i.e. $\bar{4}2\,m$ symmetry for $CdGeAs_2$ and obtain the final expressions for $\chi^{(2)}_{ijk}$ and $\chi^{(3)}_{ijk\ell}$. We would obtain the tensors shown in Fig. 10. The procedure outlined here was used to calculate the FHG tensor for $CdGeAs_2$ also shown in Fig. 10. The alternative approach of starting with the 243 element general tensor and using the direct inspection method first, proved too awesome to this author. Finally, this technique was used to calculate the nonzero independent elements of the fifth harmonic tensor, although it is not shown in this manuscript.

APPENDIX II

EXPERIMENTAL AND THEORETICAL STUDIES OF THIRD HARMONIC GENERATION IN THE CHALCOPYRITE $CdGeAs_2$

The extraordinarily large third order susceptibility measured for $CdGeAs_2$ in THG experiments provoked a detailed investigation of the origins of higher order nonlinear susceptibilities in semiconductor crystals. The paper provided in this appendix summarizes the essential features, both experimental and theoretical, of the large third order response in $CdGeAs_2$. The three principal results of this paper are the following:

1. All nonlinear optical susceptibilities are due to anharmonic response of electrons. However, by symmetry arguments one can conclude that even order susceptibilities should reflect properties depending on crystal symmetry alone. Consequently they should only involve electrons localized in the crystal bonds. Odd order susceptibilities, on the other hand, are still present in isotropic media. Consequently, the isotropic free carrier cloud should exhibit odd order response, whereas its contribution to even order susceptibilities should be zero. This suggests the interesting possibility of providing direct control over the magnitude of higher order susceptibilities by controlling carrier concentration. For even order susceptibilities we wish to have a high resistivity material to eliminate as many absorption mechanisms as possible. For odd order susceptibilities the situation is not so obvious. Larger free carrier concentrations lead not only to larger nonlinear coefficients, but usually to larger absorption losses as well. At some concentration there is an optimum nonlinear response.

2. $CdGeAs_2$ has enough birefringence to allow both Type I and Type II THG. A careful examination of nonzero elements of third harmonic tensors for various symmetry materials reveals, as discussed in Section IV, that one can separate bond electron from free carrier effects by phasematching experiments alone.

3. The measurement of several higher order nonlinear optical susceptibilities in the same material provides a new technique for studying some properties of electron charge clouds and band structure in semiconductors. All order susceptibilities have contributions from bond electrons, which are proportional to higher order multipole moments. Such an investigation could provide further insight to the models currently used to describe nonlinear optical response, such as the Bond Charge Model or the Bond Orbital Model. Free carriers, on the other hand, are responsive to nonparabolic energy bands and provide a means of testing Kane's Model for energy band shapes, for example. These points have been discussed further in Section IV and are alluded to in the following paper.

Reprinted by permission from
IEEE JOURNAL OF QUANTUM ELECTRONICS
Vol. QE-10, No. 1, January 1974

Experimental and Theoretical Studies of Third-Harmonic Generation in the Chalcopyrite $CdGeAs_2$

DANIEL S. CHEMLA, R. F. BEGLEY, AND ROBERT L. BYER

Abstract—Experimental and theoretical studies of third-harmonic generation (THG) in the chalcopyrite semiconductor $CdGeAs_2$ are presented. The phase-matching configurations for THG are analyzed from the irreducible components point of view. A theory of the bound electron and free-carrier contribution to the third-order susceptibility is presented. The experimental results are given. The effective nonlinear coefficient for type-II THG is mainly due to the free-carrier contribution, and for a hole concentration of 5×10^{18}/cm³ it is measured to be $(13 \pm 6)10^{-13}$ ESU. The practical applications of THG in $CdGeAs_2$ are discussed.

I. Introduction

SINCE the first demonstration of phase-matched second-harmonic generation (SHG) in $AgGaS_2$ [1] the second-order optical effects of the ternary compounds with chalcopyrite structure have been widely studied [2]–[6]. Their large nonlinear susceptibilities together with their natural birefringence make them very attractive for nonlinear optical devices. Nonlinear optical mixing has been recently achieved in $ZnGeP_2$ [7], $AgGaS_2$ [8], [9], and $AgGaSe_2$ [10]. High efficiency second- and third-harmonic generation (THG) has been demonstrated in $CdGeAs_2$ [11], [12].

In addition to its large second-order nonlinearity $CdGeAs_2$ has a correspondingly large third-order susceptibility. In this paper we report both theoretical and experimental studies of the third-order susceptibility of the II–IV–V_2 chalcopyrite compound $CdGeAs_2$.

The third-order susceptibility is a tensor of rank 4 [13]–[15]. In the case of THG this tensor c_{ijkl} is symmetric in the three last indices [16] and a contracted notation can be used. Thus $c_{ijkl} \rightarrow c_{im}$ where m runs from 0 to 9 [16] and the nonlinear polarization can be written as

$$P_i^{3\omega} = c_{ijkl}(3\omega, \omega, \omega, \omega)E_j^{\omega}E_k^{\omega}E_l^{\omega} = c_{im}\mathcal{E}_m. \qquad (1)$$

The Einstein summation convention is assumed and $\mathcal{E}_m$ is a ten-element row matrix defined in Appendix I.

In a crystal, far from the electronic and vibrational absorption regions, the susceptibilities exhibit a very small frequency dependence. Therefore, the Kleinman [17] conjecture is valid and c_{ijkl} is independent of the index permutation so that only 15 of the 81 components are independent.

The intrinsic symmetry of a tensor is better understood when use is made of its decomposition into a sum of irreducible components [18]. The decomposition of the symmetric fourth-rank tensor c_{ijkl} involves [19] a scalar (weight 0, one component) a deviator (weight 2, five com-

Manuscript received August 2, 1973; revised September 26, 1973. This work was supported by the Advanced Research Projects Agency through the Air Force under Contract F33615-72-C-2011. D. S. Chemla's visit to the Microwave Laboratory was made possible through a NATO grant.

D. S. Chemla is with the Microwave Laboratory, W. W. Hansen Laboratories of Physics, Stanford University, Stanford, Calif. 94305. He is on leave of absence from the Centre National d'Etudes des Telecommunications, Bagneux, France.

R. F. Begley and R. L. Byer are with the Microwave Laboratory, W. W. Hansen Laboratories, Stanford University, Stanford, Calif. 94305.

ponents), and a nonor (weight 4, nine components). The scalar: $c^{ijkl} = \sum_{ij} c_{ijij}$ is nonzero for all media and describes the geometrical average of the Cartesian components. The deviator: $c_{ij}{}^{kl} = \sum_{\phi} c_{ij\phi\phi} - 1/3c^{ijkl}\delta_{ij}$ is nonzero for the uniaxial and biaxial crystals and describes a difference of behavior between the crystal axes, analogous to the birefringence. The nonor: $c_{ijkl}{}^{mn} = c_{ijkl} - 1/7 \sum_P \delta_{ij}(\sum_r c_{rrkl}) + 1/35(\delta_{ij}\delta_{kl} + \delta_{ik}\delta_{jl} + \delta_{il}\delta_{jk})(\sum_{r,s} c_{rrss})$ describes the departure from isotropy. In the expression of $c_{ijkl}{}^{mn}$ $\sum_P$ denotes the summation over the distinct permutations of the four indices. The three irreducible components obey different transformation laws and therefore have different contributions to the effective third-order susceptibility under phase-matching conditions.

Because the point group of $CdGeAs_2$ is $\bar{4}2m$, the third-order susceptibility tensor can be written in the contracted notation [20]

$$\begin{bmatrix} c_{11} \cdots c_{16} \cdot c_{16} \cdots \\ \cdot c_{11} \cdot c_{16} \cdots c_{16} \cdot \\ \cdots c_{33} \cdot c_{16} \cdot c_{16} \cdots \end{bmatrix}. \tag{2}$$

According to the Midwinter and Warner classification [20] there can be three types of phase-matched third-harmonic generation (PM-THG) in a crystal belonging to the class $\bar{4}2m$. The corresponding effective nonlinear coefficients for a positive birefringence crystal are [20]

$$c_I = -\tfrac{1}{8}(c_{11} - 3c_{16}) \cos^3\theta \sin 4\phi, \qquad e + e + e \rightarrow o \tag{3a}$$

$$c_{II} = [\tfrac{1}{8}(c_{11} - 3c_{16}) \cos^2\theta \sin^2 2\phi + (c_{16} - c_{14}) \cos^2\theta + c_{14}] \sin^2\alpha \cos\alpha, \qquad e + e + o \rightarrow o \tag{3b}$$

$$c_{III} = [\tfrac{1}{2}(c_{11} - 3c_{16}) \cos\theta \sin 4\phi] \sin\alpha \cos^2\alpha, \qquad e + o + o \rightarrow o \tag{3c}$$

where the angles θ and ϕ define the direction of propagation for phase matching in the crystalographic axes XYZ, and α is the angle between the fundamental field and the XY plane.

The combination $(c_{11} - 3c_{16})$ is a component of the nonor. It characterizes the departure from isotropy in the XY plane. The combination $(c_{16} - c_{14})$ describes the difference between the direction Y and Z and appears in the deviator.

It is well known from the theoretical [13], [21]–[26] and experimental [27]–[30] studies of third-order nonlinear processes in elementary and binary compounds that in semiconductors the third-order susceptibility arises from two distinct contributions:

$$c_{ijkl} = c_{ijkl}{}^{FC} + c_{ijkl}{}^{BE} \tag{4}$$

where $c_{ijkl}{}^{FC}$ is the contribution from the free carriers and $c_{ijkl}{}^{BE}$ is the contribution from the bound electrons.

In the crystal the bound electrons have the symmetry $\bar{4}2m$ and contribute to all the effective nonlinear coefficients. However, the free-carrier gas has a higher symmetry. For example, the free-carrier contribution to the second-order susceptibility vanishes in the dipole approximation even in a noncentric semiconductor. In a crystal with point group $\bar{4}2m$ the free carriers are expected to be isotropic in the XY plane and therefore $c_{11}{}^{FC} = 3c_{16}{}^{FC}$. In type I and type III PM-THG only the bound electrons contribute to the effective nonlinear coefficients, whereas in type II PM-THG both the bound electrons and the free carriers contribute. It should be noted that this result is quite general because in the majority of crystal point groups the free-carrier gas is isotropic or nearly isotropic in the XY plane. The requirement of invariance under axial symmetry on a tensor of rank n is equivalent to the invariance under a rotation $2\pi/m$ with $m > n$. In the case of THG the relevant tensor is of rank 4. The possible phase-matching configurations for the free-carrier gas are the same as for say, an hexagonal crystal. From [20, Table I] it can be seen that in this case type I and type III PM-THG are impossible. In the majority of semiconductors the free-carrier contribution to PM-THG is of type II.

In all the previously reported determination of the third-order susceptibilities of semiconductors only mixing experiments ($\omega_1 + \omega_1 - \omega_2 = \omega_3$ with $\omega_2 \gtrsim \omega_1$) had a substantial coherence length. Thus selective phase matching could not be used to separate the two contributions to c_{ijkl}. The two effects were separated by varying the carrier concentration. In $CdGeAs_2$ both type I ($e + e + e \rightarrow o$) and type II ($e + e + o \rightarrow o$) PM-THG are allowed so that free carrier and bound electron contribution to c_{ijkl} can be separated experimentally for the first time by choice of crystal orientation.

Another aspect of this symmetry analysis is that it provides a useful guide to evaluate the relative magnitude of some irreducible components of unknown high-rank tensors like c_{ijkl}. The irreducible components of lower weight of the tensor c_{ijkl} are a scalar and a deviator. The bound electron contribution is related to the polarizability [22] of the bonds and the free-carrier contribution is related to the derivatives of the energy with respect to the wavevector [13]. From the linear optical and transport properties of the crystal it is easy to form a scalar and a deviator, respectively, related to the bond polarizability and the derivative of the energy. Therefore, an evaluation of the ratio $(c_{16} - c_{14})/c_{16}$ can be given for the two systems of charges within the crystal. For the bound electrons we expect the ratio to be of the order of magnitude of $(\chi_\parallel - \chi_\perp)/\chi_{av}$ where $\chi_\parallel$ and $\chi_\perp$ are the linear susceptibility components. For the free carriers this ratio should be of the same order of magnitude as $(m_\parallel - m_\perp)/m_0$, where $m_\parallel$ and $m_\perp$ are the effective masses of the carriers. For a p-type $CdGeAs_2$ the ratio is of the order of unity, for an n-type material it is of the order of 0.5 according to the effective masses given in [31].

The contribution of the bound electrons is examined in Section II. In that section we generalize the "bond charge model" [32] to a tensor form which enables us to calculate all the components of the third-order polarizability of a tetrahedral bond with axial symmetry.

In Section III we calculate the contribution of the free carriers. This is performed by using Kildal's [31] generalization of Kane's model [33] to crystals with chalcopyrite structure.

In Section IV the experimental work is presented. The effective nonlinear coefficients corresponding to type-I and type-II PH-THG have been compared. c_{14} has been measured relative to d_{14}[3] by comparing PH-THG to the mixing of the laser light with type-II PM-SHG in the same crystal but at different orientation ($\theta_m^{SHG} - \theta_m^{THG} = 11° \pm 1°$) and to d_{14} by comparing PM-THG to PM-SHG.

Finally, the comparison of experimental and theoretical results are discussed. The major practical consequence of our work is to point out the possibility of high conversion-efficiency type-II PM-THG in heavily doped chalcopyrite semiconductors.

II. Theory of the Third-Order Susceptibility of the Bound Electrons in a Tetrahedral Crystal

The most successful recent theory of the dielectric properties of elementary and binary tetrahedral solids is due to Phillips [34] and Van Vechten [35]. Their theory has successfully been extended to multibond tetrahedral solids [36] and is the basis of several models describing the second-order nonlinear susceptibilities of various crystals [32], [37]–[40]. We present in this section a generalization of the bond-charge model [32] to calculate *all the components of the nonlinear optical susceptibilities* of different orders, and we consider in more detail the case of the third-order susceptibility.

To give a good description of all the components of the susceptibilities we have to keep track of the tensor form of the different quantities involved in the theory. The bond interpretation of the Phillips and Van Vechten theory [36] shows that a mean bond polarizability can be macroscopically defined in a way which includes the local field effects by

$$\alpha = \tfrac{1}{3}(\alpha_\parallel + 2\alpha_\perp) = (2a_0)^3 D \frac{E_n^2}{E_g^2}. \tag{5}$$

In (5) $\alpha_\parallel$ and $\alpha_\perp$ are the parallel and transverse components of the axially symmetric bond polarizability tensor, E_g is the Phillips mean energy gap [34], [35]

$$E_g^2 = E_h^2 + C^2 \tag{6}$$

D is a correction factor close to unity which describes the core electron contributions [35], and $a_0 = \hbar^2/me^2$ is the Bohr radius and $E_n = me^4/2\hbar^2$ is the hydrogen ionization energy. In (5) the Penn correction factor has been neglected.

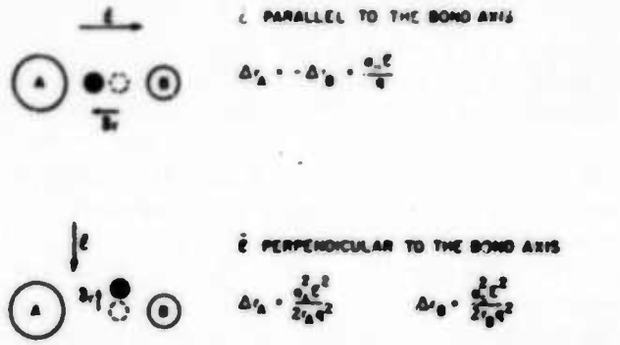

Fig. 1. Variation of the bond-charge position under an applied field.

Following Levine [32] we assume that the nonlinear susceptibilities arise from the variations of the linear susceptibility due to the applied field ϵ. The microscopic dipole of the bond $p_i = \alpha_{ij}(\epsilon)\epsilon_j$ can be written by expanding the linear polarizability [41]

$$\begin{aligned} p_i &= p_i^{(1)} + p_i^{(2)} + p_i^{(3)} + \cdots \\ &= \left\{(\alpha_{ij})_{\epsilon=0} + \left(\frac{\partial \alpha_{ij}}{\partial \epsilon_l}\right)_{\epsilon=0}\epsilon_l \right. \\ &\qquad \left. + \frac{1}{2}\left(\frac{\partial \alpha_{ij}}{\partial \epsilon_l \partial \epsilon_k}\right)_{\epsilon=0}\epsilon_l\epsilon_k + \cdots\right\}\epsilon_j. \end{aligned} \tag{7}$$

This equation gives the relation between the different components of the bond higher order polarizabilities and the derivatives of the linear polarizability components with respect to the applied field

$$\beta_{ijk} = \left(\frac{\partial \alpha_{ij}}{\partial \epsilon_k}\right)_{\epsilon=0} \gamma_{ijkl} = \frac{1}{2}\left(\frac{\partial^2 \alpha_{ij}}{\partial \epsilon_k \partial \epsilon_l}\right)_{\epsilon=0}. \tag{8}$$

It is important to note that the derivatives are evaluated at vanishing field so that the model is dispersionless. Therefore, Kleinman symmetry [17] holds, i.e., β_{ijk}, $\gamma_{ijkl} = \gamma_{jkli} \cdots$ are invariant under permutations of their indices.

It is now necessary to calculate the field dependence of the α_{ij}. In the bond charge scheme [32] the motion of the weakly bound and well-localized bond charge [42], [43] q is responsible for the bond polarizabilities. The homopolar part E_h and the heteropolar part C of the mean energy gap E_g of the biatomic bond AB are functions of the covalent radii [44] of the atoms r_A, r_B.

If we interpret r_A and r_B as the distances between the bond charges and the two atoms, then the variations of α can be calculated through the variations of r_A and r_B. Two configurations have to be considered, as shown in Fig. 1, depending on the direction of the field with respect to the bond axis. First the applied field is parallel to the bond axis, then $\Delta r_A = -\Delta r_B = (\alpha_\parallel \epsilon_\parallel/q)$ are first order in the field. In the second case the field is perpendicular to the bond axis and $\Delta r_A = (\alpha_\perp^2 \epsilon_\perp^2/2r_A q^2)$ and $\Delta r_B = (\alpha_\perp^2 \epsilon_\perp^2/2r_B q^2)$ are second order in the field. Therefore, in the expansion of the linear polarizability in powers of the applied field only the even powers of $\epsilon_\perp$ can appear. Whatever is the dependence of the α_{ij} in the field, their

odd-order derivatives in $\epsilon_\perp$ vanish

$$\left(\frac{\partial}{\partial \epsilon_\perp}\right)^{2n+1} \alpha_{\perp} = 0$$

whereas the odd- and even-order derivatives in $\epsilon_\parallel$ can be nonzero.

This remark together with the Kleinman symmetry [17] conditions allows the *calculations of all the components of the bond hyperpolarizabilities from the knowledge of the mean linear polarizability alone.*

Let us consider in detail the case of the second- and third-order bond polarizabilities. The nonzero components of the polarizabilities of the axially symmetric bond are

$$\beta_\parallel = \beta_{zzz} \qquad \beta_\perp = \beta_{zxx}$$

$$\gamma_\parallel = \gamma_{zzzz} \qquad \gamma_\perp = \gamma_{xxxx} = 3\gamma_{xxyy} \qquad \gamma_{\parallel\perp} = \gamma_{zzxx}.$$

Using (8) and the Kleinman symmetry to rearrange the indices

$$\beta_\perp = \left(\frac{\partial \alpha_{xx}}{\partial \epsilon_z}\right)_{\epsilon=0} = \left(\frac{\partial \alpha_{zz}}{\partial \epsilon_x}\right)_{\epsilon=0} = 0 \tag{9a}$$

$$\gamma_{\parallel\perp} = \frac{1}{2}\left(\frac{\partial^2 \alpha_{xx}}{\partial \epsilon_z^2}\right)_{\epsilon=0} = \frac{1}{2}\left(\frac{\partial^2 \alpha_{zz}}{\partial \epsilon_x^2}\right)_{\epsilon=0} = \frac{1}{2}\left(\frac{\partial^2 \alpha_{zz}}{\partial \epsilon_x \partial \epsilon_z}\right)_{\epsilon=0} = 0. \tag{9b}$$

From the Phillips and Van Vechten theory we know $\alpha = (\alpha_\parallel + 2\alpha_\perp)/3$ and therefore using (5), (8), and (9)

$$\beta_\parallel = 3\left(\frac{\partial \alpha}{\partial \epsilon_\parallel}\right)_{\epsilon=0} \qquad \gamma_\parallel = \frac{3}{2}\left(\frac{\partial^2 \alpha}{\partial \epsilon_\parallel^2}\right)_{\epsilon=0} \qquad \gamma_\perp = \frac{3}{4}\left(\frac{\partial^2 \alpha}{\partial \epsilon_\perp^2}\right)_{\epsilon=0}. \tag{10}$$

The *ab* initio-calculations of Flytzanis and Ducuing [45] have shown that $\beta_\perp/\beta_\parallel \ll 1$. In the bond-charge model this quantity goes to zero. It should be noted that in the previous derivations of the bond second-order polarizabilities [32] the factor 3 arising from the tensor form of α_{ij} and β_{ijk} has been omitted. The fact that the linear polarizability is nearly spherically symmetric is misleading: even if $\alpha \simeq \alpha_\parallel \simeq \alpha_\perp$ their derivatives are completely different. In the following we will use the relation $\alpha \simeq \alpha_\parallel \simeq \alpha_\perp$, but carefully evaluate their derivatives according to (9) and (10).

Let us write the expansion of the homopolar and the heteropolar part of the mean energy gap in the following way,

$$E_h(\epsilon) = E_h + (\alpha\epsilon)h_1 + (\alpha\epsilon)^2 h_2 + \cdots \tag{11a}$$

$$C(\epsilon) = C + (\alpha\epsilon)g_1 + (\alpha\epsilon)^2 g_2 + \cdots. \tag{11b}$$

The quantities h_i and g_i are given in Table I for the two configurations considered. Then expanding the mean linear polarizability by using (5) and (11) gives

$$\alpha(\epsilon) = \alpha - \frac{2}{(2a_0)^3 E_0^2}(h_1 E_h + g_1 C)\alpha^2 \epsilon + \frac{1}{(2a_0)^3 E_0^2}[(4f_h - 1)h_1^2 + (4f_i - 1)g_1^2 + 8(f_i f_h)^{1/2} h_1 g_1 - 2(h_2 E_h + g_2 C)] \times \alpha^4 \epsilon^2 + \cdots \tag{12}$$

where f_i is the ionicity and $f_h = 1 - f_i$. In deriving (12) we have used Levine's [32] definition of E_h, and α is evaluated according to (15).

TABLE I

EXPRESSION OF THE QUANTITIES DEFINING THE DERIVATIVES OF THE HOMOPOLAR AND HETEROPOLAR PART OF THE MEAN BOND ENERGY GAP FOR A DIATOMIC BOND *AB*

ϵ parallel to the bond axis	
$g_1 = -\frac{be^2}{q}\left(\frac{Z_A}{r_A^2} + \frac{Z_B}{r_B^2}\right) \cdot \exp\left(-k_s \frac{r_A + r_B}{2}\right)$	$g_2 = \frac{be^2}{q^3}\left(\frac{Z_A}{r_A^3} - \frac{Z_B}{r_B^3}\right) \cdot \exp -k_s\left(\frac{r_A + r_B}{2}\right)$
$h_1 = -\frac{40}{q}\frac{(r_A - r_B)E_h}{(r_A + r_B)^2}$	$h_2 = -\frac{40}{q^3}\frac{E_h}{(r_A + r_B)^2}$
ϵ perpendicular to the bond axis	
$g_1 = 0$	$g_2 = -\frac{be^2}{2q^3}\left[\frac{Z_A}{r_A^3} - \frac{Z_B}{r_B^3} + \frac{k_s}{2}\left(\frac{1}{r_B} + \frac{1}{r_B}\right)\cdot\left(\frac{Z_A}{r_A} - \frac{Z_B}{r_B}\right)\right] \exp\left(-k_s \frac{r_A + r_B}{2}\right)$
$h_1 = 0$	$h_2 = -\frac{14.3}{q^3}\frac{E_h}{(r_A + r_B)^3}$

The relevant components of the bond polarizabilities are easily calculated from (12), (10), and Table I. Equation (12) has been written in a way which makes directly apparent the ionic, the covalent, and the mixed contributions to the hyperpolarizabilities.

Since the microscopic analogs of the Miller's delta [46] (i.e., β/α^3 and χ/α^4) are very simple functions of macroscopically defined quantities like f_i and r_A and r_B the local field effects [47] are automatically taken into account in our calculations. Levine [32], [38] gives an expression of the bond charge magnitude which gives the best fit with the observed second-order susceptibilities of binary compounds. He uses a scalar model where the different components $\alpha_\parallel$ and $\alpha_\perp$ are not distinguished. For simplicity, we use his result modified to include the factor 3 arising from our tensor treatment.

To calculate the nonlinear susceptibility of the crystal we have to add the contributions of the different bonds

[36], [41]

$$c_{IJKL} = \frac{1}{V} \sum_{s} \cos \theta_{I,i}^{(s)} \cos \theta_{J,j}^{(s)} \cdot \cos \theta_{K,k}^{(s)} \cos \theta_{L,l}^{(s)} \gamma_{i,jkl}^{(s)} \quad (13)$$

where the index (s) covers the different bonds in the unit cell whose volume is V. The capital indices (I, J, K, L) refer to the crystal axis (XYZ), whereas the minor indices $(i, j, k, l)^s$ refer to the bond axis. If, using the axial symmetry of the bond, it is always possible to choose the microscopic axis x^s in the XY plane, then the angles appearing in (13) are simple functions of the polar angle $[\theta^s, \varphi^s]$ of the bond axis z^s, as shown in Fig. 2. The practical calculation of (13) is then simplified by using the operations of the point group of the crystal which gives the directions of equivalent bonds in the unit cell.

The orientations of the two types of bonds of a chalcopyrite compound ABC_2 are simply related to the geometrical factors [36], [41] $\tau = 2 - c/a$ and $\sigma = 4x - 1$. If we use the notation + for AC and − for BC to distinguish between the two types of bonds, then the relevant combinations of components of c_{Im} are

$$c_{11} - 3c_{16} = -\frac{32}{9V}\{[1 - 4(\tau + \sigma)/3]\gamma_{\parallel}^{+} + [1 + 2(\tau + \sigma)/9]\gamma_{\perp}^{+} + [1 - 4(\tau - \sigma)/3]\gamma_{\parallel}^{-} + [1 + 2(\tau - \sigma)/9]\gamma_{\perp}^{-}\} \quad (14a)$$

$$c_{16} - c_{15} = \frac{16}{9V}\{(\tau + \sigma)\gamma_{\parallel}^{+} + (\tau - \sigma)\gamma_{\parallel}^{-}\} \quad (14b)$$

$$c_{16} = \frac{16}{9V}\{[1 - (\tau + \sigma)/3]\gamma_{\parallel}^{+} + 2\gamma_{\perp}^{+} + [1 - (\tau - \sigma)/3]\gamma_{\parallel}^{-} + 2\gamma_{\perp}^{-}\}. \quad (14c)$$

Since the chalcopyrite structure is a superstructure of diamond and sphalerite structures, (14) can also be used for elementary and binary compounds with these structures by putting $\tau = \sigma = 0$.

The expression of the deviator [36] component $(c_{16} - c_{15})$ is to be compared to another deviator [36] $(\chi_{\parallel} - \chi_{\perp})$, i.e., the difference between the parallel and transverse component of the first-order susceptibility. As expected, the two deviators exhibit exactly the same geometrical dependence. Since τ and σ are small (10^{-2} to 10^{-1}) the combination $(c_{16} - c_{15})$ is one or two orders of magnitude smaller than the individual components whatever the values of $\gamma_{\parallel}^{+}$ and $\gamma_{\parallel}^{-}$ are.

In Table II the calculated third-order susceptibilities due to the bound electrons are compared to the experimental determinations for some semiconductors in which this contribution has been isolated [28], [30], and the agreement is good. In the case of $CdGeAs_2$ the model predicts $c_{11} = 1.8 \times 10^{-11}$ ESU; $c_{16} = 1.3 \times 10^{-11}$ ESU; and $c_{15} = 1.4 \times 10^{-11}$ ESU.

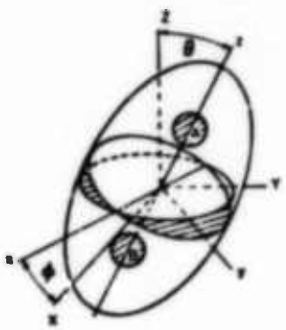

Fig. 2. Orientation of the bond axis in the crystallographic axis.

TABLE II
COMPARISON OF THE EXPERIMENTAL THIRD-ORDER SUSCEPTIBILITIES DUE TO THE BOUND ELECTRONS IN SOME TETRAHEDRAL SEMICONDUCTORS TO THE THEORETICAL VALUES CALCULATED FROM OUR MODEL

Compound	c_{Im} Experimental	c_{Im} Theoretical
Ge[28]	$c_{11} = (10 \pm 5)10^{-11}$ ESU	$c_{11} = 4 \times 10^{-11}$ ESU
	$c_{16} = (6 \pm 3)10^{-11}$ ESU	$c_{16} = 3 \times 10^{-11}$ ESU
Si[28]	$c_{11} = (0.6 \pm 0.3)10^{-11}$ ESU	$c_{11} = 0.9 \times 10^{-11}$ ESU
	$c_{16} = (0.3 \pm 0.15)10^{-11}$ ESU	$c_{16} = 0.65 \times 10^{-11}$ ESU
GaAs[28]	$c_{11} = (0.97 \pm 0.2)10^{-11}$ ESU	$c_{11} = 0.95 \times 10^{-11}$ ESU
	$c_{16} = (0.5 \pm 0.15)10^{-11}$ ESU	$c_{16} = 0.7 \times 10^{-11}$ ESU

Our analysis also provides important information about the physical origins of the nonlinear effects in semiconductors. An alternative of the bond-charge model [32] is the charge-transfer model [40], where the variation of the linear susceptibility is attributed to a transfer of electric charge from one atom to another under the applied field. The two models describe the second-order susceptibility with comparable accuracy. But several difficulties arise in the description of the third-order susceptibility when use is made of the charge transfer model.

First, there is no transfer of electric charges when the field is perpendicular to the bond axis and $\gamma_{\perp}$ vanishes. As a consequence $c_{11} = c_{16}$ for all the sphalerite compounds in disagreement with the experimental results [28], [30].

Furthermore, as only the heteropolar part of the mean energy gap C is charge dependent, there is no covalent or mixed contributions to the nonlinear susceptibility. According to (12) γ is proportional to $(4f_i - 1)$ leading to very small nonlinear susceptibilities for crystal with an ionicity $f_i \approx 0.25$. For example, in the case of gallium arsenide $f_i = 0.27$, the model predicts $c_{11} \approx 2 \times 10^{-13}$ ESU.

The discrepancy should not be attributed to the charge-transfer model itself since it is well known that deformation of the electronic distribution due to a field perpen-

dicular to the bond axis exists. But unfortunately, the formalism of Phillips theory is unable to describe those effects as well as the contribution's second order in Z_α and Z_β when the field is parallel to the bond axis.

III. Theory of the Third-Order Susceptibility of the Free Carriers in a Chalcopyrite Crystal

The other system of charges that has been recognized to make a large contribution to the third-order susceptibility of semiconductors is the free-carrier gas. There are two distinct mechanisms which are responsible for their nonlinear susceptibility: the nonparabolicity of the energy bands [13], [21], [22] (i.e., an energy-dependent effective mass), and an energy-dependent relaxation time [23]–[28]. The two mechanisms have a very different frequency dependence. The second is only important when the inverse of the relaxation time is not negligible compared to the frequencies of the interacting fields. This can occur in the case of mixing experiments [27]–[29] where $\omega_3 = \omega_1 + \omega_1 - \omega_2$ and the difference of frequencies $\omega_1 - \omega_2$ is very small (10^{12} s^{-1}). When only addition of frequencies is considered as in THG ($3\omega = \omega + \omega + \omega$) the effects of carrier scattering become negligible [26] and only the contribution of the nonparabolicity of the energy bands need be considered.

For elementary and binary compounds, the Kane model [31] gives a good description of the energy bands and has been sucessfully used to explain the third-order susceptibility of some semiconductors [13], [21]–[26]. Kildal has recently extended the Kane model to ternary compounds with chalcopyrite structure [31]. The principal feature of Kildal's extension is that in addition to the spin-orbit splitting Δ one has to consider the crystal-field splitting δ due to the tetragonal compression of chalcopyrite compounds. As a result of the two perturbations, the band structure of the chalcopyrite II–IV–V_2 crystal (i.e., containing no noble metal) consists of one conduction band (s-like) and three split-valence bands (p-like). The four bands can be described by four functions $E_m'(k) = E_m(k) + (\hbar^2/2m)k^2$, where the $E_m(k)$ are the solutions of the fourth-order equation

$$E(E - E_1 - E_G)(E - E_1)(E - E_2) - W_\parallel^2 E(E + \tfrac{2}{3}\Delta) - W_\perp^2\left[(E - E_1)(E - E_2) - \frac{\Delta}{3}(E + \delta)\right] = 0. \quad (15)$$

Here $W_\parallel^2 = P^2 k_z^2$, $W_\perp^2 = P^2(k_x^2 + k_y^2)$, $P = -i(\hbar/m) < S|p_z|Z >$ [29], [30], and E_1 and E_2 are solutions of $E_i^2 + (\delta + \Delta)E_i + (2\Delta\delta/3) = 0$.

In the limit $\delta = 0$, (15) reduces to the Kane equation. The band structures of a chalcopyrite compound and of its sphalerite analog are shown in Fig. 3. Fig. 3 also lists the values of the parameters deduced by Kildal [31] to describe the band structure of CdGeAs$_2$.

When the frequencies of the interacting field are small compared to the frequencies associated with the electronic

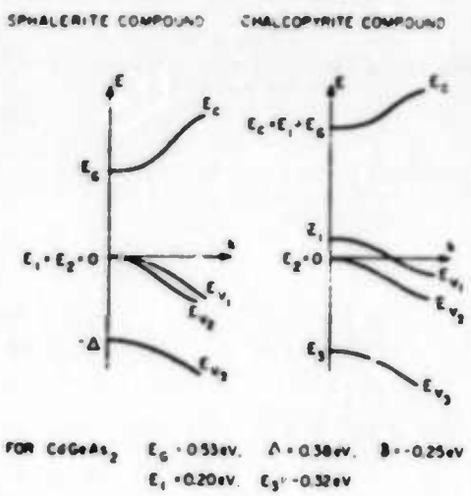

Fig. 3. Schematic of the band structure of a chalcopyrite compound and its sphalerite analog.

transitions, the third-order susceptibility due to the nonparabolicity of the energy band is given by [13], [21], [22]

$$\chi_{ijkl}(\omega_1, \omega_2, \omega_3) = \pm \frac{e^4}{24\hbar^3 i\omega_1\omega_2\omega_3(\omega_1 + \omega_2 + \omega_3)} \cdot \sum_v f_m(E_{v,v}) \frac{\partial^3 E_{v,v}}{\partial k_i \partial k_j \partial k_l} \quad (16)$$

where $f_m(E)$ is the Fermi–Dirac distribution function.

For an n-type material the positive sign and E_c are used, whereas for a p-type compound the negative sign and E_{v_1} are used.

For the elemen ary and binary compounds when the energy gap E_G is small enough so that the deep valence band E_{v_3} is unperturbed, a closed form can be deduced from Kane's model [33] which gives a good description of E_c and E_{v_2}. This close form has been widely used for compounds with very small band gap like InSb. For crystals with a larger band gap the closed form is not valid, and a better description of the band shapes is given by expanding the energy as a function of the wave vector [48]. In the same line we assume the following form for the energy bands of a chalcopyrite compound.

$$E_m(k) = E_m + A_m W_\parallel^2 + B_m W_\perp^2 + C_m W_\parallel^4 + D_m W_\perp^4 + G_m W_\parallel^2 W_\perp^2 + \cdots. \quad (17)$$

In this equation the index m runs over the four energy bands. The coefficients of the expansion are found by inserting (17) into (15). The results are given in Table III.

It should be noted that while the limits of the A_m for $\delta = 0$ are correct, this is not the case of the B_m. To calculate the B_m one has to divide by $E_1E_2 = (2/3)\Delta\delta$, and this process is not valid for δ or Δ going to zero. Therefore, we will assume that in the limit $\delta = 0$, $A_m = B_m$.

The expressions for the coefficients are simple, and due to the fact that (15) is of the second order in $W_\parallel$ and $W_\perp$, the

TABLE III
COEFFICIENTS OF THE EXPANSION OF THE ENERGY BAND AS A FUNCTION OF THE WAVE VECTOR

$$A_1 = \frac{E_1 + \frac{2}{3}\Delta}{(E_2 - E_1)(E_c - E_1)} \qquad B_1 = \frac{E_1 + \delta + \frac{1}{3}\Delta}{2(E_2 - E_1)(E_c - E_1)}$$

$$A_2 = 0 \qquad B_2 = -\frac{1}{2E_c}$$

$$A_3 = \frac{E_3 + \frac{2}{3}\Delta}{(E_c - E_3)(E_1 - E_3)} \qquad B_3 = \frac{E_3 + \delta + \frac{1}{3}\Delta}{2(E_c - E_3)(E_1 - E_3)}$$

$$A_c = \frac{E_c + \frac{2}{3}\Delta}{(E_1 - E_c)(E_3 - E_c)} \qquad B_c = \frac{1}{2E_c} + \frac{E_c + \delta + \frac{1}{3}\Delta}{2(E_1 - E_c)(E_3 - E_c)}$$

$$C_m = A_m S(A_m) \qquad D_m = B_m S(B_m)$$
$$G_m = A_m S(B_m) + B_m S(A_m)$$

where

$$S(A_m) = \sum_{n \neq m} \frac{A_n}{E_m - E_n} \qquad S(B_m) = \sum_{n \neq m} \frac{B_n}{E_m - E_n}$$

Note: $E_m(k) = E_m + A_m W_\parallel^2 + B_m W_\perp^2 + C_m W_\parallel^4 + D_m W_\perp^4 + G_m W_\parallel^2 W_\perp^2$.

coefficients satisfy the interesting relation

$$A_m^2 D_m + B_m^2 C_m = A_m B_m G_m. \tag{18}$$

Since we have only retained the terms in E_m up to the fourth power of the wave vector the fourth derivatives appearing in (16) are constants and the nonlinear susceptibilities are proportional to the number of the free carrier N.

The relevant combinations of coefficients appearing in the effective nonlinear susceptibility are

$$c_{14} = \pm \frac{e^4 N P^4}{18 V(\hbar\omega)^4} G_{c,v} \qquad c_{11} - 3c_{14} = 0$$

$$c_{14} - c_{16} = \mp \frac{e^4 N P^4}{18 V(\hbar\omega)^4} (G_{c,v} - 2D_{c,v}) \tag{19}$$

where $\hbar\omega$ is the energy of the laser photons.

For $CdGeAs_2$ one finds by using Table III and the energies of Fig. 3 and $P^2 = (\hbar^2/2m) \times 20$ eV

$$c_{14}^{v} = -2.5 \times 10^{-37} N \qquad c_{14}^{v} - c_{16}^{v} = 2 \times 10^{-37} N$$
$$c_{14}^{c} = -1.5 \times 10^{-37} N \qquad c_{14}^{c} - c_{16}^{c} = 6.3 \times 10^{-40} N. \tag{20}$$

The particular sample we have used for type-II PM-THG is a p-type crystal with $N = 5 \times 10^{19}$ holes/cm^3 so that

$$c_{14} = -12.5 \times 10^{-11} \text{ESU} \qquad c_{14} - c_{16} = 10 \times 10^{-11} \text{ESU}.$$

TABLE IV
PHASE-MATCHING ANGLES FOR THG AND SHG

Phase-Matching Configuration	SHG I	SHG II	THG I	THG II
θ_m (calculated)	35° ± 7°	55° ± 7°	50° ± 7°	67° ± 7°
θ_m (measured)	32° ± 1°	49° ± 1°	(50°)	60° ± 1°

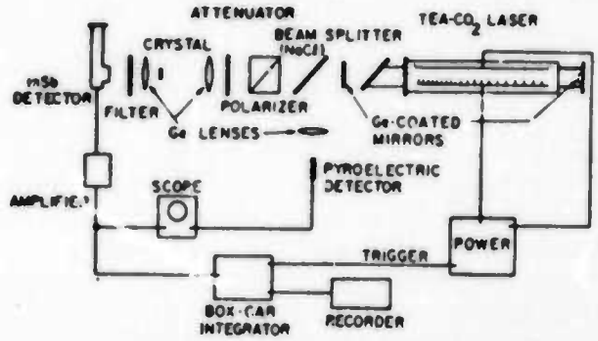

Fig. 4. Schematic of the experimental setup.

The nonlinearities due to the free carriers are about one order of magnitude larger than the nonlinearities due to the bound electrons.

IV. Experiments and Discussion

In this section we present experimental work on the measurement of the third-order nonlinear susceptibility. $CdGeAs_2$ has a birefringence large enough [11], [31] to allow type-I and type-II PM-THG for a fundamental wave length of 10.6 μ. The phase-matching angles calculated [31] from the measured refractive indices [31] are listed in Table IV for both THG and SHG. The difference $\theta_m^{II}(\text{THG}) - \theta_m^{II}(\text{SHG}) = 12°$ is small so that both PM-SHG and PM-THG can be observed in the same sample. Thus the ratio of the third-order and second-order nonlinear coefficients c_{11}/d_{11} can be measured with the same crystal sample. Furthermore, at high power densities a substantial nonphase-matched mixing of the laser radiation with its PM-SHG can be observed. The comparison of the two signals at 3ω gives a simple way to eliminate the detector wavelength response and gives an accurate measurement of the ratio c_{11}/d_{14}[3].

We have examined two samples S_I and S_{II}. S_I was cut for type-I THG and S_{II} for type II. The $CdGeAs_2$ crystals were grown at the Center for Materials Research at Stanford University [49]. The experimental setup is shown in Fig. 4. The electrode structure of the TEA-CO_2 laser is very similar to that described in [50]. The laser operates at a peak power of 50 kW with a pulsewidth of 200 ns in the TEM_{oo} mode, at a repetition rate between 5 and 25 pulses per second (pps). The laser peak output power is stable to better than 10 percent over periods of about 1 h. An internal Brewster window can be rotated to adjust the polarization. During the measurements, the orientation of the

laser polarization and the generated harmonics was carefully checked with an infrared reflection polarizer.

In the first set of experiments S_{II} was examined. The measured phase-matching angles for type-II THG and SHG are given in Table IV. In light of the accuracy of the refractive indices the agreement with the predicted values is satisfactory. It should be noted that there is a better agreement on the difference $\theta_m^{II}(\mathrm{THG}) - \theta_m^{II}(\mathrm{SHG})$.

The signal at 3ω from the direct THG and from the sum generation have a very different behavior. The angular phase-matching tolerance is very acute on the THG, and the half-width of the phase-matching peak $\Delta\theta = 10° \pm 1°$ (outside the crystal) is in good agreement with the predicted value $\Delta\theta = 12° \pm 2°$ for the 1.75-mm crystal. As the crystal is rotated the signal at 3ω goes to zero then increases and has a very broad maximum around $\theta_m^{II}(\mathrm{SHG})$, which can be maximized by translating the slightly wedged sample. By selective use of a sapphire and fused-silica filter we measure the SH and TH signal with a liquid-nitrogen-cooled InSb detector.

The laser is focused with a germanium lens such that the aperture length [51] $l_a = 17$ mm and the length of the focus [52] $l_f = 220$ mm are much larger than the sample thickness $l = 1.75$ mm. The plane-wave analysis is therefore valid [53], and the harmonic power at phase matching can be calculated according to [54]. To calculate the intensity at 3ω due to sum generation we assumed that the field at 2ω is constant over the last coherence length l_c and has the value $E_{2\omega}[l - (1/2)l_c]$, and we assumed that the field at 3ω is mostly radiated in a thin slab of material with a thickness l_c at the output surface of the crystal. The powers at 2ω and 3ω and $2\omega + \omega$ are then given by

$$P_{2\omega}^{\mathrm{SHG}} = \frac{16\pi^2}{c}\frac{16w_1^4}{w_2^4}\left(\frac{2\pi l}{\lambda}\frac{t_1^2 t_2 d_{II}}{n}\right)^2 P_1^2 e^{-(\alpha_2 + 2\alpha_1)l} \tag{21a}$$

and

$$P_{3\omega}^{\mathrm{THG}} = \frac{256\pi^4}{c^3}\frac{16w_1^4}{w_3^4}\left(\frac{3\pi l}{\lambda}\frac{t_1^2 t_3 c_{II}}{n}\right)^2 P_1^3 e^{-(\alpha_3 + 3\alpha_1)l} \tag{21b}$$

$$P_{3\omega}^{\mathrm{MIX}} = \frac{256\pi^2}{c^2}\frac{16w_1^4}{w_3^6}$$

$$\cdot\left(24\pi^2\frac{l_c(l - 1.2l_c)}{\lambda^2}d_M d_{II}\frac{t_1^4 t_2}{n^2}\right)^2 P_1^3 e^{-(2\alpha_1 + \alpha_2 + \alpha_3)l} \tag{21c}$$

where w_n and α_n are the beam waists and the absorption coefficients at the frequency $n\omega$, t_1 is the transmission factor for the laser field at the input surface of the crystal, t_2 and t_3 the transmission factors for the harmonic fields at the output surface, and c_{II}, d_{II}, and d_M are the effective nonlinear coefficients for THG, SHG, and mixing. The angular dependence of the transmission factors has to be taken into account since the incidence angle for PM-SHG is quite large ($\approx 43°$). The absorption coefficients measured for the sample with a CO_2 laser, its SH, and with an He–Ne laser at 3.39 μ are $\alpha_1 = 0.5\ \mathrm{cm}^{-1}$, $\alpha_2 = 1.3\ \mathrm{cm}^{-1}$, $\alpha_3 = 5.7\ \mathrm{cm}^{-1}$.

The measurement of THG to the sum generation leads to $|c_{II}| = (170 \pm 25)|d_{14}|^2$. To compare the THG to the SHG we have to consider the frequency dependence of the sensitivity of the InSb detector. We estimate our particular detector to be twice as sensitive at 5.3 μ as at 3.5 μ. This gives a measured value of $|c_{II}| = (1.6 \pm 0.8)10^{-9}|d_{14}|$ by comparison of PM-THG to PM-SHG. If we use the value 8.5×10^{-9} ESU for the d_{14} (see Appendix II for discussion), the two measurements are in good agreement and give, respectively, $|c_{II}| = 12.2 \times 10^{-11}$ ESU and $|c_{II}| = 13.6 \times 10^{-11}$ ESU. In light of the accuracy of the measurement and of the value of d_{14} we obtain $|c_{II}| = (13 \pm 6)10^{-11}$ ESU.

In the second set of experiments we compared PH-THG in S_I and S_{II}. The experiments were difficult to perform due to the much smaller magnitude of the type-I PM-THG signal. Also mixing of the laser with the non-PM-SHG produces a faint signal at 3.5 μ which could be observed at all angles of incidence. Furthermore, the phase matching for type-I THG and for type-II SHG are very close, and a permanent use of the IR polarizer was necessary. The recorded signal at 3ω showed a broad maximum around $\theta = 50°$, but the signal-to-noise ratio was too poor to surely assign our observation to type-I THG alone. However, an upper limit to the type-I THG coefficient was determined to be $|c_I| < 5 \times 10^{-2}|c_{II}| = 0.6 \times 10^{-11}$ ESU.

Using the theoretical results of Sections II and III and (3) for the expression of the effective nonlinear coefficients gives, for the theoretical values, $c_I = -0.15 \times 10^{-11}$ ESU and $c_{II} = -4 \times 10^{-11}$ ESU. The type-II effective nonlinear coefficient which is mainly due to the free-carrier contribution is between two and four times larger than predicted from the Kane model. Such a difference was already noted for n-type GaAs by Cardona [48] in measurements of the reflectivity and the Faraday rotation as a function of the number of carriers, and by Wynne [29] in measurements of the third-order susceptibility in mixing experiments. These authors also found that the nonparabolicity described by the coefficients of k^4 in the expansion of the energy was larger than predicted by the Kane model, (two times for the results of Cardona and three times for those of Wynne). It should be noted that since the effective masses of the holes on E_{V1} are quite large [31], $m = 0.031\ m$ and $m = 0.77\ m$, the Fermi energy in our sample is small, $E_F = 2$ meV, compared to the splitting, $E_{V1} - E_{V2} = 200$ meV. Therefore, no additional contributions from the lower valence bands E_{V2} and E_{V3} can explain the observed difference.

Reversing the above argument, we can say that the measured value of c_{II} is consistent with a nonparabolicity of the conduction band three times larger than predicted from the Kane model. As for c_I the theoretical value is also smaller than the measured one. The signal that we observed should therefore be attributed to sum generation. The sample used was very thin (1 mm) and when larger crystals are available ($l > 4$ mm) it should be possible to observe type-I PM-THG.

Finally, we would like to discuss briefly the practical use of $CdGeAs_2$ as an IR harmonic generator. Due to the large value of the coefficient c_{11} and the small value of the difference $\theta_m^{II}(THG) - \theta_m^{II}(SHG)$, high conversion efficiency can be obtained for both SHG and THG in the same sample. For example, using a mode-locked CO_2-TEA laser of 0.1 J/pulse, a pulse duration of 1 ns, and a 1-cm-long crystal it is possible to reach 30-percent-THG and 60-percent-SHG conversion efficiency.

IV. Conclusion

We have analyzed the possible THG configurations in chalcopyrite crystal from the point of view of the irreducible components. The bound-electron contribution and the free-carrier contribution to the third-order susceptibility can be experimentally separated by the appropriate THG experiments. We have generalized the bond-charge model to calculate the nonlinear susceptibility of the bound electrons. The results are in good agreement with the experimental determinations. We have used Kildal's extension of the Kane model to chalcopyrite compounds to calculate the free-carrier contribution. Our measurement on $CdGeAs_2$ shows that the nonparabolicity of the first conduction band is about three times larger than predicted. The third-order nonlinear coefficient of $CdGeAs_2$ has a large value $c_{11} = 12.5 \times 10^{-11}$ ESU so that very high conversion efficiency for both SHG and THG can be achieved in this crystal.

Appendix I

Contracted Notation for THG

Throughout this article, we used the notation of Midwinter and Warner [20]. The contracted notation is defined by

m	1	2	3	4	5	6	7	8	9	10
ijk	111	222	333	233	223	133	113	122	112	123.

The nonlinear polarization at the TH frequency is given by

$$\begin{bmatrix} P_1 \\ P_2 \\ P_3 \end{bmatrix} = \begin{bmatrix} c_{11} & c_{12} & c_{13} & c_{14} & c_{15} & c_{16} & c_{17} & c_{18} & c_{19} & c_{110} \\ c_{21} & c_{22} & c_{23} & c_{24} & c_{25} & c_{26} & c_{27} & c_{28} & c_{29} & c_{210} \\ c_{31} & c_{32} & c_{33} & c_{34} & c_{35} & c_{36} & c_{37} & c_{38} & c_{39} & c_{310} \end{bmatrix} \begin{bmatrix} E_1^3 \\ E_2^3 \\ E_3^3 \\ 3E_2E_3^2 \\ 3E_2^2E_3 \\ 3E_1E_3^2 \\ 3E_1^2E_3 \\ 3E_1E_2^2 \\ 3E_1^2E_2 \\ 6E_1E_2E_3 \end{bmatrix}.$$

Appendix II

Second-Order Nonlinear Coefficient of $CdGeAs_2$

The second-order nonlinear coefficient of $CdGeAs_2$ has been measured relative to d_{14} (GaAs).

According to Byer *et al.* [3], $d_{14}(CdGeAs_2)/d_{14}(GaAs) = 3.4 \pm 25$ percent. From Boyd *et al.* [4], $d_{14}(CdGeAs_2)/d_{14}(GaAs) = 2.6 \pm 15$ percent. We use the value $d_{14}(CdGeAs_2) = 3d_{14}(GaAs)$.

The d_{14} coefficient of GaAs has been measured comparatively to Ag_3SbS_3 and CdSe whose coefficients have been measured absolutely.

$$d_{14}(GaAs) = (7.5 \pm 0.3)\, d_{11}(Ag_3SbS_3) \quad [55]$$

$$d_{11}(CdSe) = (0.2 \pm 0.02)\, d_{11}(GaAs) \quad [2]$$

and

$$d_{11}(Ag_3SbS_3) = 0.43\ 10^{-7}\ \text{ESU} \pm 30\ \text{percent} \quad [56]$$

$$d_{11}(CdSe) = 0.53\ 10^{-7}\ \text{ESU} \pm 15\ \text{percent} \quad [57].$$

These sets of values fit well with $d_{14}(GaAs) = 2.8 \times 10^{-7}$ ESU $\pm$ 40 percent, and therefore give $d_{14}(CdGeAs_2) = 8.5 \times 10^{-7}$ ESU.

Acknowledgment

The authors wish to thank C. K. N. Patel and S. E. Harris for suggestions concerning THG in $CdGeAs_2$, R. S. Feigelson for growing the $CdGeAs_2$ crystals at the Stanford Center for Materials Research, and H. Kildal for many early contributions to this work.

References

[1] D. S. Chemla, P. J. Kupecek, D. S. Robertson, and R. C. Smith, "Silver thiogallate a new material with potential for infrared devices," *Opt. Commun.*, vol. 3, pp. 29–31, 1971.

[2] G. D. Boyd, E. Buehler, F. G. Storz, and J. H. Wernick, "Linear and nonlinear optical properties of $ZnGeP_2$ and CdSe," *Appl. Phys. Lett.*, vol. 18, pp. 301–304, 1971.

[3] R. L. Byer, H. Kildal, and R. S. Feigelson, "$CdGeAs_2$ a new nonlinear crystal phase matchable 10.6 μm," *Appl. Phys. Lett.*, vol. 19, pp. 237–240, 1971.

[4] G. D. Boyd, H. Kasper, and J. H. McFee, "Linear and nonlinear optical properties of $AgGaS_2$, $CuGaS_2$, and $CuInS_2$, and theory of the wedge technique for the measurement of nonlinear coefficients," *IEEE J. Quantum Electron.*, vol. QE-7, pp. 563–573, Dec. 1971.

[5] G. D. Boyd, E. Buehler, F. G. Storz, and J. H. Wernick, "Linear and nonlinear optical properties of ternary $A^{II}B^{IV}C_2^V$ chalcopyrite semiconductors," *IEEE J. Quantum Electron.*, vol. QE-8, pp. 419–426, Apr. 1972.

[6] G. D. Boyd, H. M. Kasper, J. H. McFee, and F. G. Storz, "Linear and nonlinear optical properties of some ternary selenides," *IEEE J. Quantum Electron.*, vol. QE-8, pp. 900–908, Dec. 1972.

[7] G. D. Boyd, T. J. Bridges, C. K. N. Patel, and E. Buehler, "Phase matched submillimeter wave generation by difference frequency mixing in $ZnGeP_2$," *Appl. Phys. Lett.*, vol. 21, pp. 553–555, 1972.

[8] C. G. Bethea, "Megawatt power at 1.318 μ in Nd^{3+}:YAG and simultaneous oscillation both at 1.06 and 1.318 μ," *IEEE J. Quantum Electron.* (Corresp.), vol. QE-9, p. 254, Feb. 1973.

[9] D. C. Hanna, V. V. Rampal, and R. C. Smith, "Tunable infrared down conversion in silver thiogallate," *Opt. Commun.*, vol. 8, pp. 151–153, 1973.

[10] R. L. Byer, M. M. Choy, R. L. Herbst, D. S. Chemla, and R. S. Feigelson, "Second harmonic generation and infrared mixing in $AgGaSe_2$," *Appl. Phys. Lett.*, to be published.

[11] H. Kildal, R. F. Begley, M. M. Choy, and R. L. Byer, "Efficient second and third harmonic generation in $CdGeAs_2$," *J. Opt. Soc. Amer.*, vol. 62, p. 1398, 1972.

[12] H. Kildal, "Efficient doubling and cw difference frequency mixing in the infrared using the chalcopyrite $DdGeAs_2$," presented at the Conf. Laser Applications, Washington, D.C.

[13] P. N. Butcher and T. P. McLean, "The nonlinear constitutive relation in solids at optical frequencies," *Proc. Phys. Soc.*, vol. 81, pp. 219–232, 1963.

[14] P. A. Franken and J. F. Ward, "Optical harmonics and nonlinear phenomena," *Rev. Mod. Phys.*, vol. 35, pp. 23–39, 1963.

[15] P. N. Butcher, "Nonlinear optical phenomena," Ohio State Univ. Bull. 200, 1965.

[16] a) P. D. Maker, R. W. Terhune, and C. M. Savage, "Optical third harmonic generation," in *III QEC*, Grivet and Bloembergen, Ed. Paris, France, 1964, pp. 1559–1576.
b) P. D. Maker and R. W. Terhune, "Study of optical effects due to an induced polarization third order in the electric field strength," *Phys. Rev.*, vol. 137A, pp. 801–818, 1965.

[17] D. A. Kleinman, "Nonlinear dielectric polarization in optical media," *Phys. Rev.*, vol. 126, pp. 1977–1979, 1962.

[18] J. Jerphagnon, "Invariants of the third rank Cartesian tensor: Optical nonlinear susceptibilities," *Phys. Rev.*, vol. 2B, pp. 1091–1097, 1970.

[19] J. Jerphagnon and D. S. Chemla, to be published.

[20] J. E. Midwinter and J. Warner, "The effects of phase matching method and of crystal symmetry on the polar dependence of third order nonlinear optical polarization," *Brit. J. Appl. Phys.*, vol. 16, pp. 1667–1674, 1965.

[21] P. A. Wolff and G. A. Pearson, "Theory of optical mixing by mobile carriers in semiconductors," *Phys. Rev. Lett.*, vol. 17, pp. 1015–1017, 1966.

[22] S. S. Jha and N. Bloembergen, "Nonlinear optical susceptibilities in group IV and III-V semiconductors," *Phys. Rev.*, vol. 171, pp. 891–898, 1968.

[23] P. Kaw, "Optical mixing by mobile carriers in semiconductors," *Phys. Rev. Lett.*, vol. 21, pp. 539–541, 1968.

[24] C. C. Wang and N. W. Ressler, "Nonlinear optical effects of conduction electrons in semiconductors," *Phys. Rev. Lett.*, vol. 188, pp. 1291–1293, 1969.

[25] K. C. Rustagi and S. S. Jha, "Effects of scattering on optical nonlinearity due to carriers in semiconductors," *Phys. Lett.*, vol. 30A, pp. 518–519, 1969.

[26] K. C. Rustagi, "Effect of carrier scattering on nonlinear optical susceptibility due to mobile carriers in InSb, InAs and GaAs," *Phys. Rev.*, vol. B2, pp. 4053–4061, 1969.

[27] C. K. N. Patel, R. E. Slusher, and P. H. Fleury, "Optical nonlinearities due to mobile carriers in semiconductors," *Phys. Rev. Lett.*, vol. 17, pp. 1011–1014, 1966.

[28] J. J. Wynne and G. D. Boyd, "Study of optical difference mixing in Ge and Si using a CO_2 gas laser," *Appl. Phys. Lett.*, vol. 12, pp. 191–192, 1968.

[29] J. J. Wynne, "Optical third order mixing in GaAs, Ge, Si and InAs," *Phys. Rev.*, vol. 178, pp. 1295–1303, 1969.

[30] E. Yablanovitch, C. Flytzanis, and N. Bloembergen, "Anisotropic interference of three wave and double two wave frequency mixing in GaAs," *Phys. Rev. Lett.*, vol. 29, pp. 865–868, 1972.

[31] H. Kildal, "CdGeAs, and $CdGeP_2$ chalcopyrite materials for infrared nonlinear optics," Ph.D. dissertation, Stanford Univ., Stanford, Calif., 1972.

[32] a) B. F. Levine, "Electro dynamical bond charge calculation of nonlinear optical susceptibilities," *Phys. Rev. Lett.*, vol. 22, pp. 787–790, 1969.
b) ——, "A new contribution to the nonlinear optical susceptibility arising from unequal atomic radii," *Phys. Rev. Lett.*, vol. 25, pp. 440–449, 1970.
c) ——, "'d' electron effects on bond susceptibilities and ionicities," *Phys. Rev.*, vol. 7B, pp. 2591–2600, 1973.
d) ——, "Bond charge calculation of nonlinear optical susceptibilities of various crystal structures," *Phys. Rev.*, vol. 7B, pp. 2600–2626, 1973.

[33] E. O. Kane, "Band structure of indium antimonide," *J. Phys. Chem. Solids*, vol. 1, pp. 249–261, 1957.

[34] a) J. C. Phillips, "A posteriori theory of covalent bonding," *Phys. Rev. Lett.*, vol. 19, pp. 415–417, 1967.
b) ——, "Covalent bands in crystals I. Element of a structural theory," *Phys. Rev.*, vol. 166, pp. 832–838, 1968.
——, "Covalent bands in crystals II. Partially ionic binding," *ibid.*, vol. 168, pp. 905–911, 1968.
——, "Covalent bonds in crystals III. Anisotropy and quadrupole moments," *ibid.*, vol. 168, pp. 912–917, 1968.
c) ——, "Ionicity of the chemical bond in crystals," *Rev. Mod. Phys.*, vol. 42, pp. 317–356, 1970.

[35] J. A. Van Vechten, "Quantum dielectric theory of electro-negativity in covalent systems, I. Electronic dielectric constant," *Phys. Rev.*, vol. 182, pp. 891–905, 1969.
——, "Quantum dielectric theory of electro-negativity in covalent systems, II. Ionization potentials and interband transition energies," *ibid.*, vol. 187, pp. 1007–1020, 1969.

[36] D. S. Chemla, "Dielectric theory of tetrahedral solids: Application to ternary compounds with chalcopyrite structure," *Phys. Rev. Lett.*, vol. 26, pp. 1441–1444, 1971.

[37] C. Flytzanis, "Etudes des susceptibilities du second ordre des composés III-V et II-VI en utilesant le modele de Phillips," *Compt. Rend.*, vol. 267B, pp. 555–558, 1968.

[38] D. A. Kleinman, "Nonlinear optical susceptibilities of covalent crystals," *Phys. Rev.*, vol. 2B, pp. 3139–3142, 1970.

[39] J. C. Phillips and J. A. Van Vechten, "Nonlinear optical susceptibilities of covalent crystals," *Phys. Rev.*, vol. 183, pp. 709–711, 1969.

[40] C. L. Tang and C. Flytzanis, "Charge transfer model of nonlinear susceptibilities of polar semiconductors," *Phys. Rev.*, vol. 4B, pp. 2520–2524, 1971.

[41] D. S. Chemla, "Proprietes dielectriques lineaires et nonlineaires des cristaux a structure tetraehique. Theories des proprietes dielectrioues des composes a structure tetraehique," *Ann. Telecommun.*, vol. 27, pp. 477–498, 1972.

[42] R. Uno, T. Okano, and K. Yokino, "Electron distribution in GaAs as revealed by the X-ray diffraction," *J. Phys. Soc. Japan*, vol. 25, pp. 437–442, 1970.

[43] J. P. Walter and M. L. Cohen, "Electron charge densities in semiconductors," *Phys. Rev. Lett.*, vol. 26, pp. 17–19, 1971.

[44] J. A. Van Vechten and J. C. Phillips, "New set of tetrahedral covalent radii," *Phys. Rev.*, vol. 2B, pp. 2160–2167, 1970.

[45] C. Flytzanis and J. Ducuing, "Second order optical susceptibilities of III-V semiconductors," *Phys. Rev.*, vol. 178, pp. 1218–1228, 1970.

[46] R. C. Miller, "Optical second harmonic generation in piezoelectric crystals," *Appl. Phys. Lett.*, vol. 5, pp. 17–19, 1969.

[47] J. Ducuing and C. Flytzanis, "Second order optical procession in solids, in optical properties of solids," Abeles, Ed. F. North Holland, 1972, pp. 859–990.

[48] M. Cordona, "Electron effective masses of InAs and GaAs as a function of temperature and doping," *Phys. Rev.*, vol. 121, pp. 752–758, 1961.

[49] R. S. Feigelson and H. W. Swartz, "Solution growth of $CdGeAs_2$," to be published.

[50] A. M. Robinson, "Effect of inductance on small-signal gain of a transverse-excited atmospheric-pressure discharge in carbon dioxide," *IEEE J. Quantum Electron.* (Corresp.), vol. QE-7, pp. 199–200, May 1971.

[51] G. D. Boyd, V. Askin, J. M. Dziedzic, and D. A. Kleinman, "Second harmonic generation of light with double refraction," *Phys. Rev.*, vol. 137, pp. A1305–A1320, 1965.

[52] D. A. Kleinman, A. Ashkin, and G. D. Boyd, "Second harmonic

generation of light by focused laser beams," *Phys. Rev.*, vol. 145, pp. 338–379, 1966.

[53] G. D. Boyd and D. A. Kleinman, "Parametric interaction of focused Gaussian light beams," *J. Appl. Phys.*, vol. 39, pp. 3597–3639, 1968.

[54] D. S. Chemla, "Generation of second harmonique des ondes lumineuses dans les cristaux nonlineaires," *Ann. Telecommun.*, vol. 27, pp. 311–498, 1972.

[55] J. M. McFee, G. D. Boyd, and P. M. Schmidt, "Redetermination of the nonlinear optical coefficients of Te and GaAs by comparison with Ag_3SbS_3," *Appl. Phys. Lett.*, vol. 17, pp. 57–59, 1970.

[56] W. B. Gandrud, G. D. Boyd, J. M. McFee, and F. M. Wehmeir, "Nonlinear optical properties of Ag_3SbS_3," *Appl. Phys. Lett.*, vol. 16, pp. 59–61, 1970.

[57] R. L. Herbst, "Cadmium selenide infrared parametric oscillator," Ph.D. dissertation, Stanford Univ., Stanford, Calif., 1972. (Available as Microwave Laboratory Rep. 2125, pp. 1–88.)

APPENDIX III

Second harmonic generation and infrared mixing in $AgGaSe_2$

R. L. Byer, M. M. Choy, R. L. Herbst, D. S. Chemla[a], and R. S. Feigelson[b]

Microwave Laboratory, W. W. Hansen Laboratories of Physics, Stanford University, Stanford, California 94305
(Received 17 September 1973; in final form 29 October 1973)

We have continuously tuned between 7 and 15 μm by mixing the output of a $LiNbO_3$ parametric oscillator in the chalcopyrite $AgGaSe_2$. We have doubled a CO_2 laser with 2.7% efficiency which agrees very well with the expected efficiency and verifies the high optical quality of the 1.53-cm-long $AgGaSe_2$ crystal. The measured transparency range, indices of refraction, and nonlinear coefficient of $d_{36} = (37 \pm 0.6) \times 10^{-11}$ m/V show that $AgGaSe_2$ is a useful infrared nonlinear material phase matchable over the entire 3–18-μm infrared region.

Since the first demonstration of phase-matched second harmonic generation (SHG) in $AgGaS_2$,[1] the nonlinear properties of the ternary semiconductors with chalcopyrite structure have been widely studied.[2–9] Their large nonlinear susceptibilities together with adequate birefringence to achieve phase matching make them attractive for nonlinear optical devices. Nonlinear mixing has been demonstrated in $ZnGeP_2$,[7] $AgGaS_2$,[8,9] $CdGeAs_2$,[10,11] and recently $AgGaSe_2$.[11,12]

$AgGaSe_2$ single crystals are grown by the vertical Bridgeman method after the starting materials are presynthesized in a carbon boat contained in a sealed quartz crucible. The presynthesized stoichiometric mix with a melting point of approximately 860 °C is then transferred to a quartz crucible coated with pyrolitic carbon for a pregrowth run at 2 mm/h rate through a 40 °C/cm temperature gradient. The top and bottom of the resulting boule are then removed prior to the actual growth run in the same vertical furnace at a slow growth rate of 0.2 mm/h. After growth the crucible is cooled to room temperature at 25 °C/h. The resulting 14-mm-diam single crystals typically show a gallium-rich region near the seed end followed by an approximately 2-cm useful $AgGaSe_2$ single-crystal region and a silver-rich top section. Early crystals showed a precipitate which resulted in a 2-cm^{-1} scatter loss. In recent crystals the scatter loss has been significantly reduced to

Appl. Phys. Lett., Vol. 24, No. 2, 15 January 1974

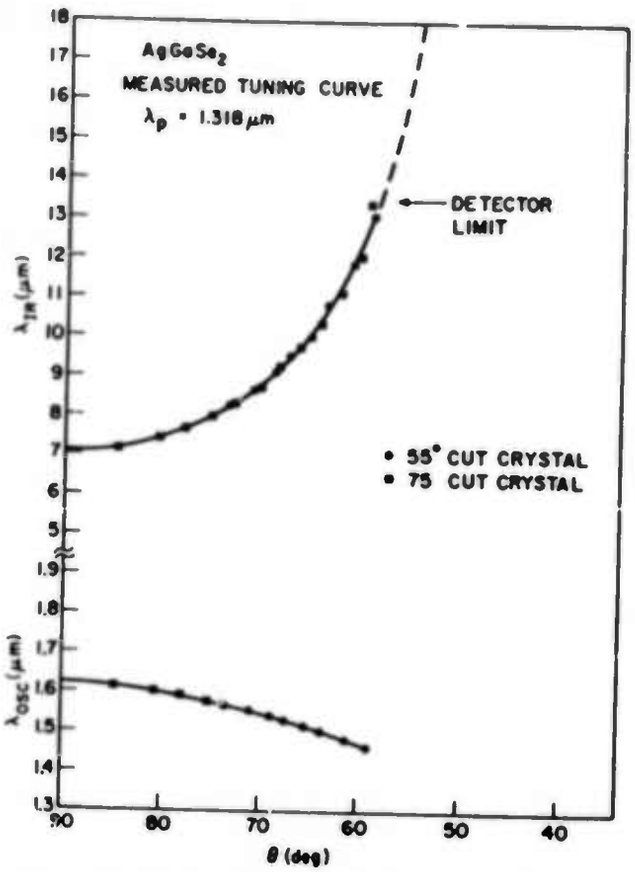

FIG. 1. The 7–15-μm mixing output (λ_{IR}) in angle phase-matched $AgGaSe_2$ pumped by a 1.318-μm Nd:YAG laser mixing with the output of a 0.659-μm pumped $LiNbO_3$ parametric oscillator (λ_{osc}).

near 0.02 cm^{-1} at 10.6 μm. All crystals have high resistivity and good optical transparency from the band gap at 0.71 μm to the two-phonon absorption edge at 18 μm. A particularly attractive feature of $AgGaSe_2$ is the ease with which single crystals can be grown.

We have measured the nonlinear coefficient of $AgGaSe_2$ relative to GaAs at 10.6 μm using the wedge technique.[13–16] The wedge method is suited for small-birefringence large-index materials. For the wedge method the coherence length is given by

$$l_c = \lambda/4(n_{2\omega} - n_\omega) = \tfrac{1}{2}\Delta y \tan\alpha, \qquad (1)$$

where Δy is the wedge translation distance between SHG extrema, α is the wedge angle, and the beam is incident normal to the input face of the wedge. For our crystal samples the coherence lengths are expected to be near 100 μm for GaAs and 200 μm for $AgGaSe_2$ at 10.6 μm.

We used a (001)-oriented $AgGaSe_2$ wedge for the nonlinear susceptibility measurement relative to two GaAs reference samples. One (001)-oriented wedge was cut from GaAs material supplied by Coherent Radiation Laboratories and a second (111)-oriented wedge was cut from Monsanto material; both GaAs samples were chromium compensated to a high resistivity of about 10^7 Ω cm. With the laser polarization parallel to the (110) direction, $E_x = E_y = E_0/\sqrt{2}$ and $P = P_x = \epsilon_0 d_{36} E_0^2$, so the d_{eff} for the (001)-cut GaAs and $AgGaSe_2$ samples are d_{36} and $d_{36} = d_{14}$, respectively. For the (111)-cut GaAs, with the laser polarization along the (111) direction, $E_x = E_y = E_z = E_0/\sqrt{3}$ and $P_x = P_y = P_z = P/\sqrt{3}$, so $P = 2/\sqrt{3} d_{14} E_0^2$ and the d_{eff} in this case is $2/\sqrt{3}\, d_{14}$. The coherence length of GaAs is measured to be 107 ± 2 μm and 109 ± 3 μm for the (001)- and (111)-cut samples. This is in excellent agreement with published values in Refs. 17 and 18 of 107 ± 5 μm and 107 ± 1 μm. The measured coherence length of $AgGaSe_2$ is 237 ± 15 μm which compares favorably with a calculated value of 255 ± 50 μm based on the index data of Boyd *et al.*[6]

The $AgGaSe_2$ nonlinear coefficient measured relative to GaAs is

$$R_1 = d_{36}(AgGaSe_2)/d_{14}(GaAs)001 = 0.33 \pm 25\%,$$

$$R_2 = d_{36}(AgGaSe_2)/d_{14}(GaAs)111 = 0.32 \pm 18\%.$$

These values are in good agreement with the relative measurement by Boyd *et al.*[6] of $d_{36}(AgGaSe_2)/d_{14}(GaAs) = 0.37 \pm 10\%$. Taking $d_{14}(GaAs) = (11.7 \pm 40\%) \times 10^{-11}$ m/V,[16] we obtain $d_{36}(AgGaSe_2) = (3.8 \pm 1.7) \times 10^{-11}$ m/V.

We have also performed phase-matched SHG of 10.6 μm using a 60°-cut $AgGaSe_2$ crystal. The measured phase-matching angle of 57.5° ± 0.5° is in good agreement with the calculated value of 55° ± 4°. The expected phase-matched SHG conversion efficiency is

$$P_{2\omega}/P_\omega = \Gamma^2 l^2 = (2\omega^2 d_{eff}^2/\pi n_\omega^2 n_{2\omega} \epsilon_0 c^3) P_\omega l k_\omega h(B, \xi), \qquad (2)$$

where the powers are defined inside the crystal $d_{eff} = d \sin\theta_{pm}$, l is the crystal length, $k = 2\pi n_\omega/\lambda$, and $h(B, \xi)$ is the Boyd and Kleinman[19] focusing factor which reduces to $l/b = l/w_0^2 k$ in the loose focusing limit. For a low-loss $AgGaSe_2$ crystal 1 cm in length in the loose focusing limit ($l/b < 1$) the calculated SHG conversion efficiency is $\Gamma^2 l^2 = 0.75\%$ at 1 MW/cm^2. Using a TEA CO_2 laser operating in a TEM_{00} mode as a source, we measured the absolute SHG efficiency generated in a high-quality 1.54-cm-long $AgGaSe_2$ crystal. The average input and output powers measured with an Eppley thermopile were 2.82 mW and 76 μW, which corresponds to 1.6 kW of peak power at the fundamental for a 200-nsec pulse width. The experimentally observed conversion efficiency for the incident intensity of 1.68 MW/cm^2 is 2.63%. Using $d_{36} = 38 \times 10^{-12}$ m/V, $l = 1.54$ cm, and $h(B, \xi) = 0.925\, l/b$, which corresponds to the focal spot size of 250 μm, the expected conversion efficiency is 2.76%. This measurement can be considered as a separate absolute determination of the nonlinear coefficient of $AgGaSe_2$. The nonlinear coefficient is found to be

$$d_{36} = (3.74 \pm 0.6) \times 10^{-11} \text{ m/V},$$

which agrees very well with the previous measurement made relative to GaAs and with the recent absolute measurement of Kildal and Mikkelsen[11] of $d_{36} = (3.24 \pm 0.50) \times 10^{-11}$ m/V.

$AgGaSe_2$ phase matches for SHG for fundamental wavelengths between 3 and 13 μm.[6] The SHG efficiency of $AgGaSe_2$ is significantly better than proustite, for example, due to both a factor-of-three increase in the nonlinear coefficient and the small birefringence which

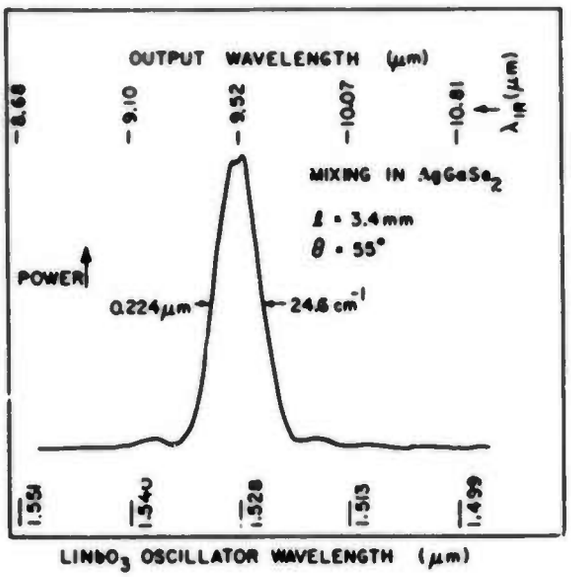

FIG. 2. Phase-matched mixing peak generated in a fixed $AgGaSe_2$ cyrstal pumped with a tunable source.

allows increased interaction lengths without aperture length limitations.

$AgGaSe_2$ has adequate birefringence to phase match over an extended infrared spectral range for tunable wavelength generation by mixing. For mixing, a convenient tunable pump source is a $LiNbO_3$ parametric oscillator[21] mixing with a fixed-frequency Nd:YAG laser. For our experiment we used a collinear geometry. The acoustic Q-switched Nd:YAG laser tuned to 1.32 μm is internally doubled with a $LiIO_3$ crystal to generate 0.659 μm which pumps the temperature-tuned $LiNbO_3$ oscillator. The oscillator output in the 1.5–1.7-μm range mixes in the $AgGaSe_2$ crystal with the remaining collinear 1.32-μm beam which passes through the parametric oscillator. The $AgGaSe_2$ is angle phase matched by rotation on a geared stage.

The mixing efficiency is given by

$$P_{1r}/P_{oec} = (\omega_{1r}/\omega_{oec})\Gamma^2 l^2 \operatorname{sinc}^2(\Delta kl/2), \tag{3}$$

where $\Gamma^2 l^2 = (2\omega_{1r}\omega_{oe}d_{311}^2 l^2/n_p n_{oe} n_{1r} c^3 \epsilon_0) I_p$ and I_p is the pump intensity. For a 1-cm $AgGaSe_2$ crystal and a pump intensity of 1 MW/cm^2 at 1.32 μm, the conversion efficiency is $P_{1r}/P_{oec} = 1.2\%(\omega_{1r}/\omega_{oec})$.

Figure 1 shows the generated mixed output from 7 to 15 μm. Beyond 15 μm our HgCdTe detector is response limited. Figure 2 shows the phase matching peak generated by mixing in a fixed $AgGaSe_2$ crystal pumped by a tunable $LiNbO_3$ parametric oscillator. The characteristic $\operatorname{sinc}^2(\Delta kl/2)$ phase-matching peak width agrees with that calculated from the dispersion of $AgGaSe_2$. The 24.6-cm^{-1} width is the acceptance bandwidth of the mixing crystal which is much greater than the output bandwidth of 2 cm^{-1} determined by the 2-cm^{-1} gain linewidth of the parametric oscillator.

A plot of the phase-matching angle versus $LiNbO_3$ oven temperature showed a nearly linear relation over a wide 7–12-μm spectral range. We therefore used a stepping motor and synchronously rotated the $AgGaSe_2$ crystal to phase match with a 1 °C/min temperature scanned $LiNbO_3$ parametric oscillator. In this way the spectrum between 7 and 12 μm was continuously tuned 8 min.

Figure 3 shows a spectrum of polystyrene as an example of the continuous scanning capability of this source. The spectrum was taken using a dual channel differential boxcar with two HgCdTe detectors. The mixed output is detected with better than a 30-dB signal-to-noise ratio with a peak-to-peak variation of less than 10% at a repetition rate between 10 and 25 pps.

When mixing against 1.32 μm, $AgGaSe_2$ does not have adequate birefringence to phase match at wavelengths shorter than 7 μm. Based on phase-matching calculations using the index of refraction data of Boyd *et al.*,[8] mixing against wavelengths 1.5 μm and longer allows complete coverage of the infrared. As an example, a 1.06-μm pumped $LiNbO_3$ parametric oscillator with degeneracy near 2.12 μm angle tunes over a 1.5–3.7-μm range. $AgGaSe_2$ phase matches for mixing the signal and idler waves to generate 3–18 μm for phase matching angles between 80° and 50°.[12] This example shows the unique phase-matching properties of $AgGaSe_2$ for extended infrared generation by mixing.

In conclusion, we have measured the nonlinear coefficient of $AgGaSe_2$ and demonstrated phase-matched SHG of a CO_2 laser as a verification of crystal quality

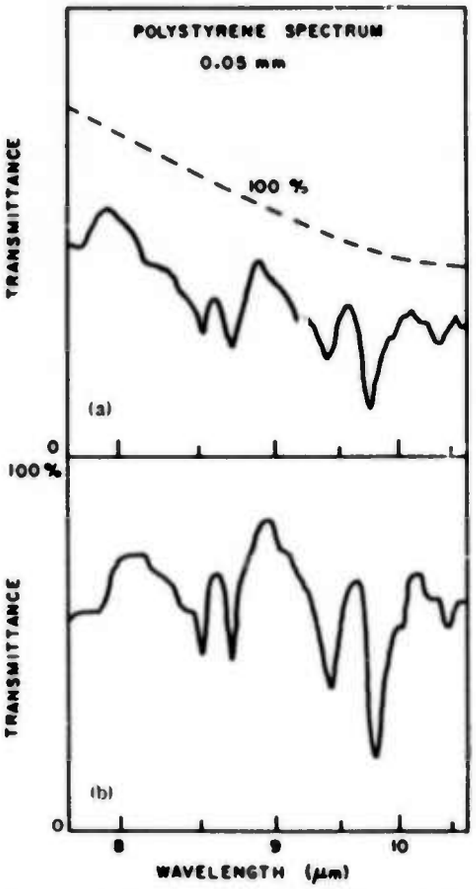

FIG. 3. Spectrum of polystyrene taken with (a) the $AgGaSe_2$ mixer (resolution 2 cm^{-1}) and (b) Perkin Elmer spectrophotometer.

and potential use as a second harmonic generator. Using a $LiNbO_3$ parametric oscillator as source, we have generated continuously tunable output between 7 and 15 μm by mixing in $AgGaSe_2$.

This research was supported in part by the Advance Research Projects Agency of the Department of Defense and monitored by the Air Force Materials Laboratory and in part by the the U.S. Army Research Office, Durham, and Honeywell Research Laboratories.

*Visiting from CNET, Bagneux, France.
†Center for Materials Research, Stanford University.

[1]D.S. Chemla, P.J. Kupeck, D.S. Robertson, and R.C. Smith, Opt. Commun. 3, 29 (1971).
[2]G.D. Boyd, E. Beuhler, and F.G. Storz, Appl. Phys. Lett. 18, 301 (1971).
[3]R.L. Byer, H. Kildal, and R.S. Feigelson, Appl. Phys. Lett. 19, 237 (1971).
[4]G.D. Boyd, H. Kasper, and J.H. McFee., IEEE J. Quantum Electron. QE-7, 563 (1971).
[5]G.D. Boyd, E. Beuhler, F.G. Storz, and J.H. Wernick., IEEE J. Quantum Electron. QE-8, 419 (1972).
[6]G.D. Boyd, H. Kasper, J.H. McFee, and F.G. Storz, IEEE J. Quantum Electron. QE-8, 900 (1972).
[7]G.D. Boyd, T.J. Bridges, C.K.N. Patel, and E. Beuhler, Appl. Phys. Lett. 21, 553 (1972).
[8]C.G. Bethea, IEEE J. Quantum Electron. QE-9, 254 (1973).
[9]D.C. Hanna, V.V. Rampal, and R.C. Smith, Opt. Commun. 8, 151 (1973).
[10]H. Kildal, R.F. Begley, M.M. Choy, and R.L. Byer, J. Opt. Soc. Am. 62, 1398 (1972).
[11]H. Kildal and J.C. Mikkelsen, Opt. Commun. (to be published).
[12]R.L. Byer, M.M. Choy, and R.L. Herbst, Conference on Laser Applications Washington, D.C., 1973 (unpublished); see also R.L. Byer, Proceedings of the First Tunable Laser Spectroscopy Conference, Vail, Colorado, 1973 (unpublished).
[13]J. Jerphagnon, Ph.D. thesis (University of Paris, 1966) (unpublished).
[14]J.J. Wynne and N. Bloembergen, Phys. Rev. 188, 1211 (1969).
[15]D.S. Chemla and P. Kupecek, Rev. Phys. Appl. 6, 31 (1971).
[16]D.S. Chemla, Ph.D. thesis (University of Paris, 1972); Ann. Telecommun. 27, N7-8, 311 (1972).
[17]J.H. McFee, G.D. Boyd, and P.H. Schmidt, Appl. Phys. Lett. 17, 57 (1970).
[18]D.S. Chemla, P.J. Kupecek, and C.A. Schwartz, Opt. Commun. 7, 225 (1973).
[19]D.S. Chemla, R.F. Begley, and R.L. Byer, IEEE J. Quantum Electron. (to be published).
[20]G.D. Boyd and D.A. Kleinman, J. Appl. Phys. 39, 3597 (1968).
[21]R.W. Wallace, Appl. Phys. Lett. 17, 497 (1970).

APPENDIX IV

BOND ORBITAL MODEL FOR SECOND ORDER SUSCEPTIBILITIES

by

M.M. Choy, S. Ciraci* and R.L. Byer

Applied Physics Department
Stanford University
Stanford, California

May 1974

*On leave of absence from The Middle East Technical University, Ankara, Turkey.

BOND ORBITAL MODEL FOR SECOND ORDER SUSCEPTIBILITIES

by

M.M. Choy, S. Ciraci* and R.L. Byer
Applied Physics Department
Stanford University
Stanford, California

ABSTRACT

The Bond Orbital Model for tetrahedral compounds is used self-consistently to calculate the second order susceptibility. No adjustable parameters are used and agreement with experiment is good. The origin of the nonlinearity arises from a charge transfer as a result of the asymmetric polar energy between the anion and the cation. The model correctly predicts an optimum polarity to maximize second order susceptibilities.

*On leave of absence from The Middle East Technical University, Ankara, Turkey.

INTRODUCTION

The understanding of the origin of the nonlinear optical susceptibilities has been the subject of many investigations. This understanding is important in material assesment and prediction of new material characteristics in nonlinear optical devices such as harmonic generators, mixers and parametric oscillators.[1,2] In a more formal approach, quantum mechanical expressions are derived from perturbation expansion involving complex sums of matrix elements and energy denominators.[3,4,5] These fundamental expressions, even when simplified through the use of octupole moment of the ground state charge distribution,[6] or by employing ground state wave functions,[7] are still formidable to use in quantitative predictions. Exact wave functions in solids are often not known to high accuracy and the complete band structure is also required. Other complications from contributions to the nonlinearity from different points in the Brillouin zone can also arise.[8,9] Another approach is to use simple phenomenological models such as the enharmonic oscillator model[10] and Miller's rule.[11] Included in this category are the universal semiconductor model,[12,13] the bond charge model,[14] and the charge transfer model,[15] and the molecular orbital model.[16] The latter three models all draw heavily from the results of Phillip's dielectric theory.[17,18]

In this paper we use an approach based on Harrison's Bond Orbital Model.[19,20] This is a more predictive model and only appeals to essentially two input factors, the dielectric constant and the $E_{2A}(X_4-X_1)$ transition energy to calculate the model parameters. The model predicts useful properties related to valence electrons such as cohesive energy, band structure,[21] etc. Using BOM parameters, we calculate the second order susceptibility in the

optical transparency region of a crystal. The analysis clearly displays the physical origin of the nonlinearity. Perhaps more importantly, by expressing the nonlinearity in terms of the fundamental material parameters of polarity and the bond length, salient characteristics desirable for high optical nonlinearities are distinctly revealed.

II. BOND ORBITAL MODEL

In this section, we outline the BOM so that we can discuss its extension to the calculation of the second order susceptibility. For a more complete discussion of the model and the implications of the approximations involved refer to the original papers.[19,20]

The model is based on a tight-binding approximation of sp^3 hybrid orbitals for tetrahedral compounds. Denoting a sp^3 hybrid orbital on an anion (cation) by $|h^a>$ ($|h^c>$), a bonding orbital is constructed from a linear combination of nearest neighbor hybrids on the anion and its adjacent cation directed along the same bond,

$$|b> = u_a|h^a> + u_c|h^c> \qquad (1)$$

The minimization of the expectation value of the hamiltonian by a standard variation on the u_a and u_c results in a (2×2) secular equation. The solution of the equations gives the eigenvalue and the eigenvectors. They are

$$\epsilon_{b,a} = V_2 < h^c|h^a> \mp \sqrt{V_2^2 + V_3^2} \qquad (2)$$

and

$$u_a = \sqrt{\frac{1 + \alpha_p}{2}} \quad \text{and} \quad u_c = \sqrt{\frac{1 - \alpha_p}{2}} \tag{3}$$

where the polarity is defined by Harrison[19,20] as

$$\alpha_p = \frac{V_3}{(V_2^2 + V_3^2)^{1/2}} \tag{4}$$

Here V_2 and V_3 are the energy parameters defined as:

$$V_2 = - \frac{< h^c | \mathcal{H} | h^a >}{1 - | < h^c | h^a > |^2} \tag{5}$$

for the covalent energy where $< h^c | \mathcal{H} | h^a >$ corresponds to hopping between an anion hybrid and a cation hybrid along the same bond,

$$V_3 = \frac{[< h^c | \mathcal{H} | h^c > - < h^a | \mathcal{H} | h^a >]}{2(1 - | < h^c | h^a > |^2)^{\frac{1}{2}}} \tag{6}$$

for the polar energy where $< h^c | \mathcal{H} | h^c >$ and $< h^a | \mathcal{H} | h^a >$ denote the coulomb integrals at the cation site and the anion site respectively. In addition, there is one more energy parameter $V_1^{a,(c)}$, which is defined as a matrix element of hamiltonian between adjacent anion (cation) hybrids. This is related physically to the atomic s-p splitting and does not come into play in most optical properties.

The dielectric constant, which is the parameter of interest in optical properties, is calculated by considering an isolated bond dipole with an applied electric field.

The field perturbation is treated by adding to the polar energy V_3 the potential energy of the bond dipole in the electric field. Then in the ground state wave function approximation, calculation of the induced polarization by a change of polarity α_p through a change of the polar energy V_3 gives the dielectric constant

$$\epsilon_o = 1 + \frac{N\pi\gamma^2(ed)^2 V_2^2}{3(V_2^2 + V_3^2)^{3/2}} \qquad (7)$$

where N = density of electrons, d = bond length and γ is a parameter defined in the BCM formulation relating microscopic dipole moments to macroscopic linear susceptibilities and is taken to be constant along a row of the periodic table except for correction for carbon row atoms.

To determine the energy parameters Harrison and Ciraci[20] appeal to experimental parameters. The principal optical absorption peak E_{2A} is identified with the bonding and anti-bonding gap

$$\epsilon_a - \epsilon_b = 2\sqrt{V_2^2 + V_3^2}$$

This identification has been shown to be consistent with experiments.

First, the E_{2A} gap of the group IV elemental compounds gives V_2 directly for each row of the periodic table, since $V_3 = 0$ in elemental compounds. The geometric mean is taken for compounds involving two rows. Then using Eq. (7) the dielectric constant gives γ for each row. A value for γ of 1.08 is found for diamond and 1.2 for silicon. When row three

is reached, there are contributions from the polarizable d core electrons as noted by Phillips.[17] This is taken into account by introducing a correction factor θ in addition to γ. γ is taken at the silicon value and a value of $\theta = 1.18$ is obtained for germanium and $\theta = 1.41$ for the tin row. With these values of V_2 and γ, V_3 for any binary compound is derived from its dielectric constant using Eq. (7). This completes the summary of the Bond Orbital Model as originally stated by Harrison.[19]

III. CALCULATION OF $\chi^{(2)}$

The second order susceptibility is defined by expanding the macroscopic polarization in a power series in the field

$$\underset{\sim}{P}(\underset{\sim}{E}) = \chi^{(1)} \underset{\sim}{E} + \underset{\sim}{\chi}^{(2)} : \underset{\sim}{E}\,\underset{\sim}{E} + \ldots \qquad (8)$$

where $\chi^{(1)}$ and $\underset{\sim}{\chi}^{(2)}$ are the field independent susceptibilities. In the independent bond formulation these macroscopic susceptibilities are related to their corresponding microscopic bond polarizabilities through geometrical factors as[21,22]

$$\chi^{(1)}_{IJ} = \frac{1}{V} \sum_{s,i,j} a^{(s)}_{Ii}\, a^{(s)}_{Jj}\, \alpha_{ij} \qquad (9)$$

$$\chi^{(2)}_{IJK} = \frac{1}{V} \sum_{s,i,j} a^{(s)}_{Ii}\, a^{(s)}_{Ji}\, a^{(s)}_{Kk}\, \beta_{ijk} \qquad (10)$$

where a_{Ii} are the direction cosines between the macroscopic crystal axis I and the bond axis frame i. The index s identifies the different bonds in the periodic lattice structural unit whose volume is V. To apply the BOM, confine ourselves to sp^3-bonded tetrahedral compounds with the zinc blende and wurtzite structures. In the former case with crystal class point group $\bar{4}3$ m,

Eqs. (9) and (10) reduce to

$$x_{11}^{(1)} = \frac{4n}{3}(\alpha_{||} + 2\alpha_{\perp}) = \frac{4n}{3}\alpha_{||}(1 + 2\kappa) \qquad (11)$$

$$x_{14}^{(2)} = \frac{4n}{3\sqrt{3}}(\beta_{||} - 3\beta_{\perp}) \qquad (12)$$

where $\kappa = \frac{\alpha_{\perp}}{\alpha_{||}}$ and $\alpha_{||}$ and $\alpha_{\perp}$ are the parallel and perpendicular components of the bond polarizability.

Here $n = 3\sqrt{3}/16\ d^3$ is the number of tetrahedral unit cells per unit volume. In this case $x^{(1)}$ is a scalar, and $x_{14}^{(2)}$ is the only non-vanishing tensor component in Voigts notation. $E_{||}$ is along the bond axis (111) and with axially symmetric $C_{\infty v}$ bonds, the independent non-vanishing components are $\alpha_{||} = \alpha_{zz}$, $\alpha_{\perp} = \alpha_{xx} = \alpha_{yy}$, and $\beta_{||} = \beta_{zzz}$, $\beta_{\perp} = \beta_{xzx} = \beta_{yzy}$. For the case of wurtzite structure the two inequivalent tetrahedra can be obtained from standard zinc blende orientation by simple rotational matrices, the result is[23]

$$-x_{31}^{(2)} = -x_{15}^{(2)} = x_{33}^{(2)} = \frac{2}{\sqrt{3}}x_{14}^{(2)}$$

It can be shown from an abinitio calculation that $\beta_{\perp} << \beta_{||}$.[24] In a bond charge approach, $\beta_{\perp} = 0$ to 1st order.[25] Accordingly, we neglect $\beta_{\perp}$ relative to $\beta_{||}$ in our formulation.

To calculate $\beta_{||}$ we need to determine the variation of the linear polarizability α with an electric field. Physically, we expect a redistribution of charge density in the presence of the field. This manifests itself as an induced dipole as a result of an additional charge transfer. In the context of the BOM there is a change in the bond polarity, α_p, through

a change in the bond-polar energy, V_3. Harrison defines an effective charge on an anion (in units of -e) as

$$Z^* = 4\alpha_p - \Delta Z \tag{13}$$

where ΔZ is half of the nominal valence difference. Then the additional charge incurred by the applied field on a per-bond basis is

$$\Delta Z^* = \frac{\partial \alpha_p}{\partial V_3} \Delta V_3 = \frac{V_2^2}{(V_3^2 + V_2^2)^{3/2}} \Delta V_3 \tag{14}$$

where the main contribution is from the change in polar energy, V_3. The covalent energy, V_2, is constant since the bond length remains fairly undistorted. This is valid in the optical transparency region above the phonon lattice resonance frequencies, where the lattice and the bonds stay relatively stationary compared to the motion of the electronic charge cloud. Here we have to stay below the interband electronic absorption, as the assumption of a bonding state of the hybrid orbitals implies that we are dealing with valence electrons only. In the transparency region the optical response is fairly insensitive to frequency and hence our dispersionless approach should be adequate.

In the formulation of the BCM, when the macroscopic dielectric constant is used to calculate the microscopic bond parameters, the effects of charge distribution scaling and the bond anisotropy are automatically included in the parameter γ. If we let γ^* be the charge distribution scaling and $\kappa = \alpha_{||}/\alpha_{\perp}$ be the anisotropy, then as in the derivation in BCM, the inclusion of the dipole potential energy in an electric field as a change in the polar

energy gives in terms of γ^*

$$\alpha_{||} = \frac{\gamma^{*2} (ed)^2 V_2^2}{2(V_2^2 + V_2^2)^{3/2}} \qquad (15)$$

Putting this into Eq. (11) and comparing the result with Eq. (7) we find that $\gamma^2 = \gamma^{*2} (1 + 2\kappa)$ where $\epsilon = 1 + 4\pi\chi^{(1)}$ has been employed. There is no easy analytical calculation for the bond anisotropy By simple extrapolation on values obtained from Kerr constants on diatomic molecules,[26] we estimate $\kappa \sim 0.5$. Essentially the same estimate was employed previously.[16] With this value for the anistropy factor and the BOM value of 1.2 for γ , γ^* is found to be 0·85.

To introduce the explicit field dependence we note that the induced bond dipole is

$$\Delta p = \gamma^* ed \, \Delta Z^* = \alpha_{||} E_{||} \qquad (16)$$

As explained earlier an electric field induces an additional charge transfer resulting in a change in the polar energy V_3 . The second order polarizability can be related to its linear counterpart by $\alpha_{||}(E_{||}) = \alpha_{||} + \beta_{||} E_{||} + \ldots = \alpha_{||} + \Delta\alpha_{||} + \ldots$ Now $\Delta\alpha_{||} = \beta_{||} E_{||}$ can be calculated from Eq. (15) through a change in polar energy ΔV_3 . Elimination of ΔV_3 through Eq. (14) and Eq. (16) in terms of $E_{||}$ gives

$$\beta_{||} = \frac{3\alpha_p}{ed \ (1 - \alpha_p)^2} \ \alpha_{||}^2 \qquad (17)$$

To convert to experimental macroscopic quantities, Eq. (11) and

Eq. (12) give

$$\chi^{(2)}_{14} = \frac{4\, d^2}{e\gamma^* (2\kappa + 1)^2} \frac{\alpha_p}{(1 - \alpha_p^2)} \left|\chi^{(1)}\right|^2 \qquad (18)$$

where the tetrahedral cell density ($n = 3\sqrt{3}/16\, d^3$) has been used. Since α_p can be calculated from the linear dielectric constant in BOM theory, Eq. (18) shows that $\chi^{(2)}$ can be estimated essentially from just the knowledge of the linear susceptibility alone. This is an important point. The independent bond formulation is only approximate in the sense that correlation effects between neighboring bonds do give rise to local field corrections which are not subject to easy deductive analysis. By appealing to the macroscopic linear susceptibility as an input parameter, most of these local field effects are accounted for in the BOM model.

To demonstrate the dependence of $\chi^{(2)}$ on polarity and to display some underlying physics, we transform Eq. (18) by casting $\chi^{(1)}$ in terms of polarity with the help of Eq. (7). Using the relation[20] $V_2 \propto 1/d^2$ we obtain

$$\chi^{(2)}_{14} \simeq \text{Constant}\ \alpha_p (1 - \alpha_p^2)^2\ d^4 \qquad (19)$$

where the constant contains γ, and is constant for one row in the periodic table.

The dependence of $\chi^{(2)}$ on polarity is shown in Fig. 1, where $\chi^{(2)}/d^4$ is plotted against α_p. The upper boundary corresponds to the fifth row, and the lower one, the third row. Because of differences in geometric factors, we have only included the case of zinc blende. Note the interesting maximum at $\alpha_p \sim 0.44$, corresponding to an ionicity $f_i = 0.28$ in Phillip's model [$f_i = 1-(1 - \alpha_p^2)^{3/2}$]. Tang[15] and Levine[14] have predicted an optimum

value of $f_i \approx 0.17$. However, available experimental data seems to show a peak at around $\alpha_p = 0.45$ ($f_i \tilde{=} 0.3$) in better agreement with our results. The physics of this maximum warrants some comment. In the complete polarity limit of $\alpha_p = 1$, i.e. full ionicity, all excess valence electrons from the cation are transferred to the anion. The anion in turn binds these electrons fairly tightly in its locality, resulting in a big forbidden energy gap characteristic of all ionic compounds. Actually, it can be shown that the energy gap of tetrahedral binary compounds scales linearly with ΔZ[18b]. Thus there is no more charge transfer ($\Delta Z^* \propto V_3^{-3}$) to respond to any applied field and hence the vanishing of $\chi^{(2)}$. In the covalent limit of $\alpha_p = 0$, we approach the transition of zinc blende into the elemental diamond structure and the center of inversion symmetry completely cancels all even order of non-linearities. In a sense, the system overcompensates itself because the gain in the covalent 'bond charge' is completely cancelled by the perfectly symmetric lattice environment. A minor word of caution seems to be appropriate here since we must remember that in actual practice, we have to stay within $f_i < 0.78$ for tetrahedral coordination. Any higher ionicity results in rocksalt structure, a hexa-coordination typical of most ionic compounds.

To further test the accuracy of our analysis we choose materials of roughly equal polarity, i.e. ΔZ = constant, and plot $\log_{10} [\chi^{(2)}_{expt}\ 10^7]$ against $\log_{10} [d]$ in Fig. 2. Lines of slope 4 are drawn and agreement is good with Eq. (18).

Thus for large second order nonlinearities, it is desirable to have a covalency high enough (α_p around 0.44) to give considerable polarizability from charge transfer but low enough such that inversion symmetry is not a detriment. We also want long bond lengths, which, from empirical evidence, means a high atomic number. As high covalency means proximity to Group IV, the above two criteria could be summarized in the context of the periodic table by saying

that for high $\chi^{(2)}_{14}$ we want materials with small ΔZ and high atomic number.

These criteria are well borne out by experimental evidence. The III-V compounds are in general more nonlinear than the II-V and among the III-V themselves, the more metallic elements, InSb and InAs, which are from the fifth rows and fifth and fourth rows respectively, are more nonlinear than GaAs and GaP being compounds from fourth rows and fourth and third rows. In Fig. 3 we plotted $\chi^{(2)}_{14}$ against the average quantum number, $\bar{n}$, introduced first by Mooser and Pearson[27], verifying the above arguments.

However, for any device applications employing the second order nonlinearity, the parameter of interest is the parametric gain coefficient[2] defined by

$$\Gamma^2 = \frac{9.10^8 \omega_1 \omega_2 |\chi^{(2)}|^2 I_3}{8 c^3 n_1 n_2 n_3}$$

where I_3 is the pump intensity and n_i are the refractive indices at ω_i.

From the device standpoint, besides the magnitude of $\chi^{(2)}$, there are also additional transparency factors in the frequency dependence of the gain coefficient. As one goes towards higher atomic numbers one loses ground in the transparancy range as determined by the band gap cut-off frequency. Experimentally, a material is chosen with the smallest band gap consistent with transparency in the wavelength region of interest, as pointed out by Levine.[14] If half the bandgap frequency is taken for both ω_1 and ω_2 to avoid two photon absorption, it turns out that in some cases of high atomic numbers, e.g. InAb and InAs, the increase in $\chi^{(2)}$ is largely offset by frequency factors in the gain expression due to the narrow band gap.

Another parameter which has proven to be very useful as a scale for nonlinearity is the Miller's delta Δ_{ijk}, which is defined by

$$\frac{\chi^{2\omega}_{ijk}}{2} = \Delta_{ijk} \chi^{2\omega}_{ii} \chi^{\omega}_{jj} \chi^{\omega}_{kk}$$

In the context of our model Miller's delta can be obtained by transforming Eq. (18) through use of $\chi^{(1)}$ expressed in polarity α_p and bond length d. We find that $\Delta_{ijk} \alpha \alpha_p d/(1 - \alpha_p)^{5/2}$. Thus we see that for materials of the same average quantum number $\bar{n}$, where the bond length is essentially constant and for materials of the same vertical family i.e. of constant polarity, the Miller's delta should be constant. Essentially a similar conclusion is reached by Tang and Flytzanis,[15] though they employed slightly different parameters, namely the normalized valence difference and the atomic radii difference. In Miller's formulation, which is essentially an anharmonic oscillator model, Miller's delta is found to be a function of the asymmetric potential. Because polarity (charge transfer) is a direct result of the asymmetry between the cation and anion, and bond length also affects the potential, the dependence of Miller's delta on the above BOM parameters is not surprising.

The main results and parameters used are summarized in Tables Ia and Ib. We have chosen the most recent data or that which we believe to be the most reliable. Correlation with experimental values is in general very good. It should be observed that there are two general classes of compounds where the relative discrepancy warrants some discussion. They are the narrow band gap materials for example InSb, InAs and GaSb and the copper compounds.

As pointed out in the original formulation of BOM,[20] the use of the E_{2A} peak for the bonding and anti bonding gap works especially well for the large band gap materials. For narrow band gap materials, the minimum optical gap could be almost an order of magnitude smaller than the E_{2A} gap. For example in InAs $E_o = 0.33$ eV and $E_{2A} = 3.9$ eV so one might expect the Γ point in the Brillouin zone to modify the BOM energy parameters. As a result, the application of the BOM to these compounds is not as successful.

For the copper compounds, it is known that the d-bands are strongly hybridized with the valence s and p bands. These delocalized d electrons at these noble-metal cations have been found experimentally to give an anomalous contribution to the second order nonlinearity.[28,29] This effect is discussed by Levine[14] in his bond charge model and by Tang[16] in terms of an charge redistribution and a reversal of the direction of the bond dipole. Since the BOM deals with the sp^3 electrons, the d-electrons are accounted for phenomenologically and the formulation overestimates the nonlinearity of these compounds. If we stay away from these noble metal compounds and consider compounds where there is no appreciable hybridization of the d-bands, then the BOM predictions agree well with experiment.

IV. SUMMARY AND COMMENTS

Using a more predictive theory, the BOM, we have calculated the second order susceptibility for tetrahedral compounds. Agreement with experiment is good, especially in light of the simplicity of the model.

The approach is self-consistent as the linear susceptibility is used to calculate the second order susceptibility. Compared to other phenomenological models, our approach is more self-contained, as no adjustable parameter is used and all parameters are defined in the BOM.

The physical origin of the nonlinearity is seen to arise from the charge transfer as a result of the asymmetric polar energy between the anion and the cation. Chemical trend considerations reveals an optimum value of polarity for a maximum second order nonlinearity in zinc blende and wurtzite structures. This, together with the bond length dependence gives a rule of thumb estimate on the choice of elements in the periodic table which will result in tetrahedral compounds of high second order nonlinearity. It is found that for these tetrahedral structures, it is desirable to have high covalency and a high metallicity consistent with transparency region of interest. This means that one should stay close to Group IV elements and high atomic numbers. We include the parametric gain parameter in our discussion showing that the band gap is again important through the short wavelength frequency cut-off in the transparency range. The bond orbital model is also quantitatively and qualitatively related to the Miller's rule through the concept of polarity.

ACKNOWLEDGEMENT

We appreciate helpful discussion with Professor W. Harrison. This work has been carried out with support from ARPA Materials Science Division.

REFERENCES

1. S.E. Harris, "Tunable Optical Parametric Oscillators", Proc. IEEE, vol. 57, No. 12, p. 2096-2113, (1969).

2. R.L. Byer, "Optical Parametric Oscillators", to be published in Treatise in Quantum Electronics, H. Rabin and C.L. Tang, eds. Academic Press, (1973).

3. J.A. Armstrong, N. Bloembergen, J. Ducuing and P.S. Pershan, "Interactions Between Light Waves in a Nonlinear Dielectric", Phys.Rev. vol. 127, p.1918-1939, (1962).

4. P.N. Butcher, T.B. McLean, "The Nonlinear Constitutive Relation in Solids at Optical Frequencies", Proc. Phys. Soc. Ser. A., vol. 81, p.219-239, (1963).

5. P.L. Kelley, "Nonlinear Effects in Solids", J. Phys. Chem. Solids, vol. 24, p.607-616, (1963).

6. F.N.H. Robinson, "Nonlinear Optical Coefficients", Bell. Syst. Tech. J., 46, p.913-956, (1967).

7. S.S. Jha and N. Bloembergen, "Nonlinear Optical Susceptibilities in Group IV and III V Semiconductors", Phys. Rev. vol. 171, p.891-898, (1968).

8. D.E. Aspnes, "Energy-band Theory of the Second Order Nonlinear Optical Susceptibility of Crystals of Zinc blende Symmetry", Phys. Rev. vol. B6, p.4648-4659, (1972).

9. M.I. Bell, in Electronic Density of States, L.H. Bennett, Ed. Washington, D.C., NBS, Special Publication 323, (1971).

10. a) C.G.B. Garrett and F.N.H. Robinson, "Miller's Phenomenological Rule for Computing Nonlinear Susceptibilities", IEEE J. Quantum Electronics, vol. QE-2, correspondence, p.328-329, (1966).
b) C.G.B. Garrett, "Nonlinear Optics, Anharmonic Oscillators and Pyroelectricity", IEEE J. Quantum Electronics, vol. QE-4, p.70-84, (1968).

11. R.C. Miller, "Optical Second Harmonic Generation in Piezoelectric Crystals", Appl. Phys. Letts. vol. 5, p.17-19, (1964).

12. D. Penn, "Wave-number-dependent Dielectric Function of Semiconductors", Phys. Rev. vol. 128, p.2093-2097, (1962).

13. D.A. Kleinman, "Nonlinear Optical Susceptibilities of Covalent Crystals", Phys. Rev. vol. B2, p.3139-3142, (1970).

14. B.F. Levine, "Bond Charge Calculation of Nonlinear Optical Susceptibilities for Various Crystal Structures", Phys. Rev. vol. B7, p.2600-2626, (1973).

15. C.L. Tang and C. Flytzanis, "Charge Transfer Model of the Nonlinear Susceptibilities of Polar Semiconductors", Phys. Rev. vol. B4, p.2520-2524, (1971).

16. C.L. Tang, "A Simple Molecular-orbital Theory of the Nonlinear Optical Properties of Group III-V and II-VI Compounds", IEEE J. Quant. Elect. vol. QE-9, p.735-762, (1973).

17. a) J.C. Phillips, "A Posteriori Theory of Covalent Bonding", Phys. Rev. Letts. vol. 19, p.415-417, (1967).

b) J.C. Phillips, "Covalent Bonds in Crystals, I Element of a Structural Theory", Phys. Rev. vol. 166, p.832-838, (1968).
J.C. Phillips, "Covalent Bonds in Crystals, III Anisotropy and Quadrupole Moments", ibid, vol. 168, p.912-917, (1968).

c) J.C. Phillips, "Ionicity of the Chemical Bond in Crystals", Rev. Mod. Phys. vol. 42, p.317-356, (1970).

18. a) J.A. Van Vechten, "Quantum Dielectric Theory of Electro-negativity in Covalent Systems, I Electronic Dielectric Constant", Phys. Rev. vol. 182, p.891-905, (1969),

b) J.A. Van Vechten, "Quantum Dielectric Theory of Electro-negativity in Covalent Systems, II Ionization Potentials and Interband Transition Energies", ibid, vol. 187, p.1007-1020, (1969).

19. W.A. Harrison, "Bond-orbital Model and the Properties of Tetrahedrally Coordinated Solids", Phys. Rev. vol. B8, p.4487-4498, (1973).

20. a) W.A. Harrison and S. Ciraci, "Bond Orbital Model II", Phys. Rev. B. (to be published).

b) S. Ciraci, Ph.D. Thesis, Stanford Univeristy, Stanford, California. (1974).

21. J. Ducuing and C. Flytzanis, "Second Order Optical Processes in Solids", in Optical Properties of Solids, F. Abeles, Ed. F. North Holland, p.859-990, (1972).

22. D.S. Chemla, "Dielectric Theory of Tetrahedral Solids:Application to Ternary Compounds with Chalcopyrite Structures", Phys. Rev. Letts. vol. 26, p.1441-1444, (1971).

23. F.N.H. Robinson, "Relations Between the Components of the Nonlinear Polarizability Tensor in Cubic and Hexagonal II-VI Compounds", Phys. Letts. vol. 26a, p.435-436, (1968).

24. C. Flytzanis and J. Ducuing, "Second Order Optical Susceptibilities of III-V Semiconductors", Phys. Rev. vol. 178, p.1218-1228, (1969).

25. D.S. Chemla, R.F. Begley and R.L. Byer, "Experimental and Theoretical Studies of the Third Harmonic Generation in the Chalcopyrite $CdGeAs_2$", IEEE J. Quant. Elect. vol. QE-10, p.71-81, (1974).

26. K.G. Denbigh, "The Polarizabilities of Bonds", Trans. Faraday Soc., vol. 36, p.936-948, (1940).

27. E. Mooser and W.B. Perason, "On the Crystal Chemistry of Normal Valence Compounds", Acta Cryst. A12, p.1015-1022, (1959).

28. R.C. Miller, S.C. Abrahams, R.L. Barns, J.L. Bernstein, W.A. Nordland and E.H. Turner, "Absolute Signs of the Second Harmonic Generation, Electro-Optic and Piezoelectric Coefficients of CuCl and Zns", Solid State Commun. vol. 9, p.1463-1465, (1971).

29. B.F. Levine, W.A. Nordland and J.W. Shiever, "Nonlinear Optical Susceptibility of AqI", IEEE J. Wuant. Elect. vol. QE-9, p.468-470, (1973).

TABLE Ia

COMPARISON BETWEEN THEORETICAL $\chi_{14}^{(2)}$ (CALC.) AND EXPERIMENTAL $\chi_{14}^{(2)}$ (EXPT.) TOGETHER WITH THE RELEVANT BOM PARAMETERS IN ZINC BLENDE STRUCTURES

Compound	Bond length d [Å]	α_p	$\chi^{(1)}$	$\chi_{14}^{(2)}$(cal) 10^{-7} esu	$\chi_{14}^{(2)}$(expt) 10^{-7} esu
GaP	2.36	0.52	0.65	4.1	5.2 a
GaAs	2.44	0.50	0.79	6.1	6.4 b
GaSb	2.65	0.44	1.07	10.8	20.0 c
InP	2.54	0.58	0.68	6.5	8.0 d
InAs	2.61	0.53	0.90	10.3	17.4 c
InSb	2.80	0.51	1.17	18.3	24.8 c
ZnTe	2.64	0.72	0.50	6.4	7.3 e
ZnSe	2.45	0.72	0.39	3.4	3.7 f
CdTe	2.80	0.76	0.49	8.4	8.0 e
CuCl	2.34	0.75	0.22	1.1	0.2 g
CuBr	2.49	0.79	0.27	2.34	0.4 g
CuI	2.62	0.76	0.36	4.4	0.4 g

TABLE Ib

COMPARISON BETWEEN THEORETICAL $\chi^{(2)}_{33}$ (CALC.) AND EXPERIMENTAL $\chi^{(2)}_{33}$ (EXPT.)

TOGETHER WITH RELEVANT BCM PARAMETERS IN WURTZITE STRUCTURES

Compound	Bond length d [Å]	α_p	$\chi^{(1)}$	$\chi^{(2)}_{33}$(cal) 10^{-7} esu	$\chi^{(2)}_{33}$(expt) 10^{-7} esu
SiC	1.88	0.39	0.45	0.93	0.78 h
ZnO	1.98	0.70	0.24	0.88	0.33 i
Zns	2.34	0.73	0.33	2.64	1.8 f
CdS	2.53	0.77	0.33	3.74	2.1 f
CdSe	2.63	0.77	0.38	5.35	3.8 j

TABLE REFERENCES

a. J.J. Wynne and N. Bloembergen, "Measurement of the Lowest Order Nonlinear Susceptibility in III-V Semiconductors by Second Harmonic Generation with a CO_2 Laser", Phys. Rev. 188, p.1211-1220, (1969).

b. J.H. McFee, G.D. Boyd and P.H. Schmidt, "Redetermination of the Nonlinear Optical Coefficients of Te and GaAs by Comparison with Ag_3SbS_3", Appl. Phys. Letts. 17, p.57-59, (1970).

c. R.K. Chang, J. Ducuing and N. Bloembergen, "Dispersion of the Optical Nonlinearity in Semiconductors", Phys. Rev. Letts. 15, p.415-418,(1965).

d. R. Braunstein and N. Ockman, "Interactions of Coherent Optical Radiation with Solids", Final Report prepared for the Office of Naval Research, Department of the Navy, Washington. D.C. Contract No. NONR-4128100, ARPA Order No. 306-62, August 1964.

e. R.A. Soref and H.W. Moos, "Optical Second Harmonic Generation in ZnS - CdS and CdS - CdSe Alloys", J. Appl. Phys. 35, p.2152-2158, (1964).

f. C.K.N. Patel, "Optical Harmonic Generation in the Infrared Using a CO_2 Laser", Phys. Rev. Letts. 16, p.613-616, (1966).

g. D. Chemla, P. Kupecek, C. Schwartz, C. Schwab and A. Goltzena, "Nonlinear Properties of Cuprous Halides", IEEE J. Quant. Elect. QE-7, 126-132, (1971).

h. S. Singh, J.R. Potopowiez, L.G. Van Uitert and S.H. Wemple, "Nonlinear Optical Properties of Hexagonal Silicon Carbide", Appl. Phys. Letts. 19, p.53-56, (1971).

i. R.C. Miller, "Optical Second Harmonic Generation in Piezoelectric Crystals", Appl. Phys. Letts. 5, p.17-19, (1964).

j. R.L. Herbst, "CdSe Infrared Parametric Oscillator", Ph.D. dissertation, Stanford University, Stanford, California. 1972.

FIGURE CAPTIONS

1. The scaling of $\chi_{14}^{(2)}/d^4$ with α_p, the polarity. The upper boundary corresponds to materials from the fifth row and the lower one from the third row.

2. The dependence of $\chi_{expt}^{(2)}$ on bond length d for materials of roughly constant polarity.

3. A plot of $\chi_{14}^{(2)}$ versus $\bar{n}$, the average quantum number, showing the dependence within a vertical family in the periodic table.

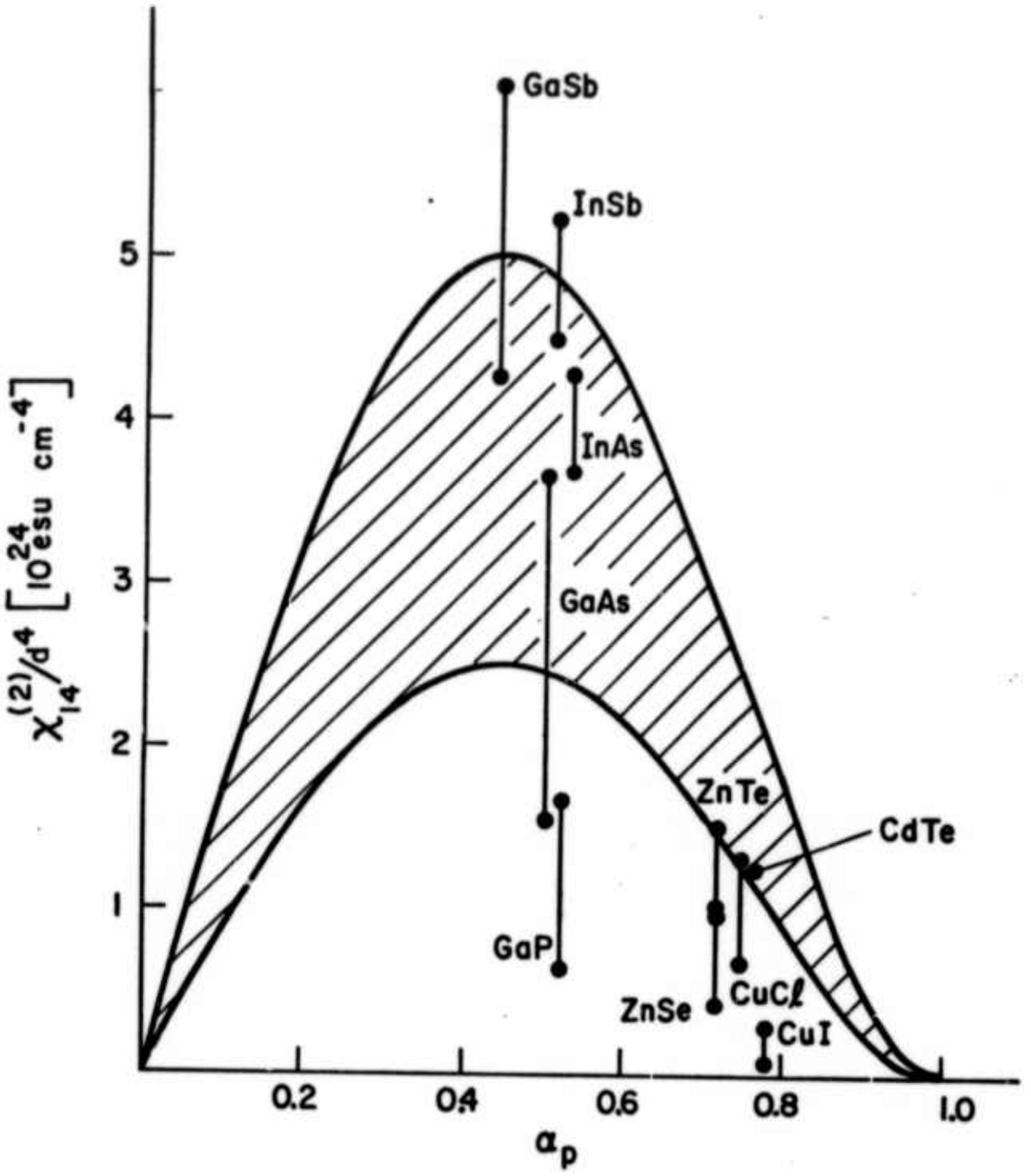
GaSb
InSb
InAs
GaAs
GaP
ZnTe
CdTe
ZnSe
CuCl
CuI
5
4
3
2
1
0.2
0.4
0.6
0.8
1.0
α_p
$\chi^{(2)}_{14}/d^4$ [10^{24}esu cm^{-4}]

FIGURE 1

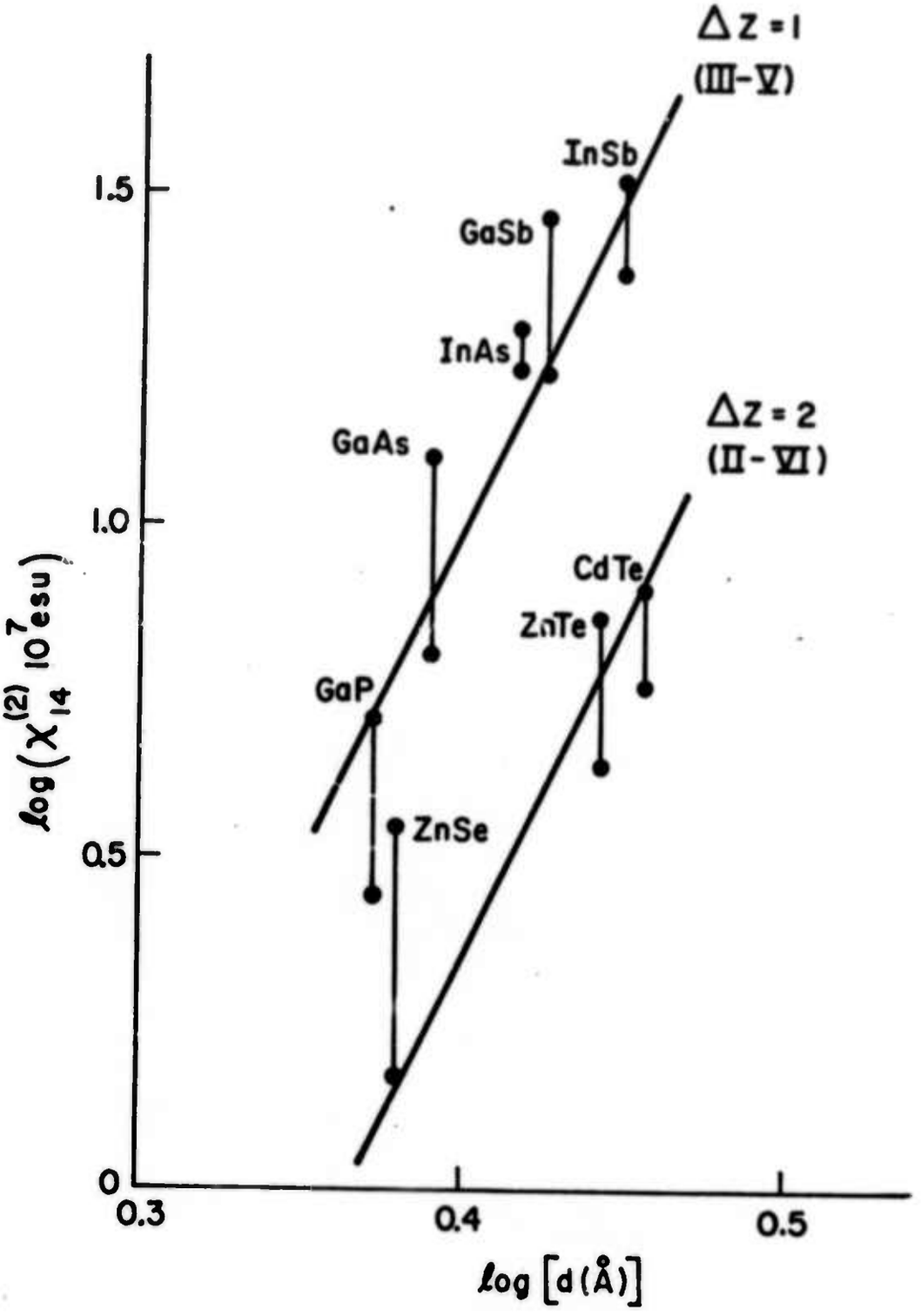
ΔZ = 1
(III-V)
InSb
GaSb
InAs
GaAs
GaP
ZnSe
ΔZ = 2
(II-VI)
CdTe
ZnTe
1.5
1.0
0.5
0
0.3
0.4
0.5
log (χ(2) 14 10^7 esu)
log [d(Å)]

FIGURE 2

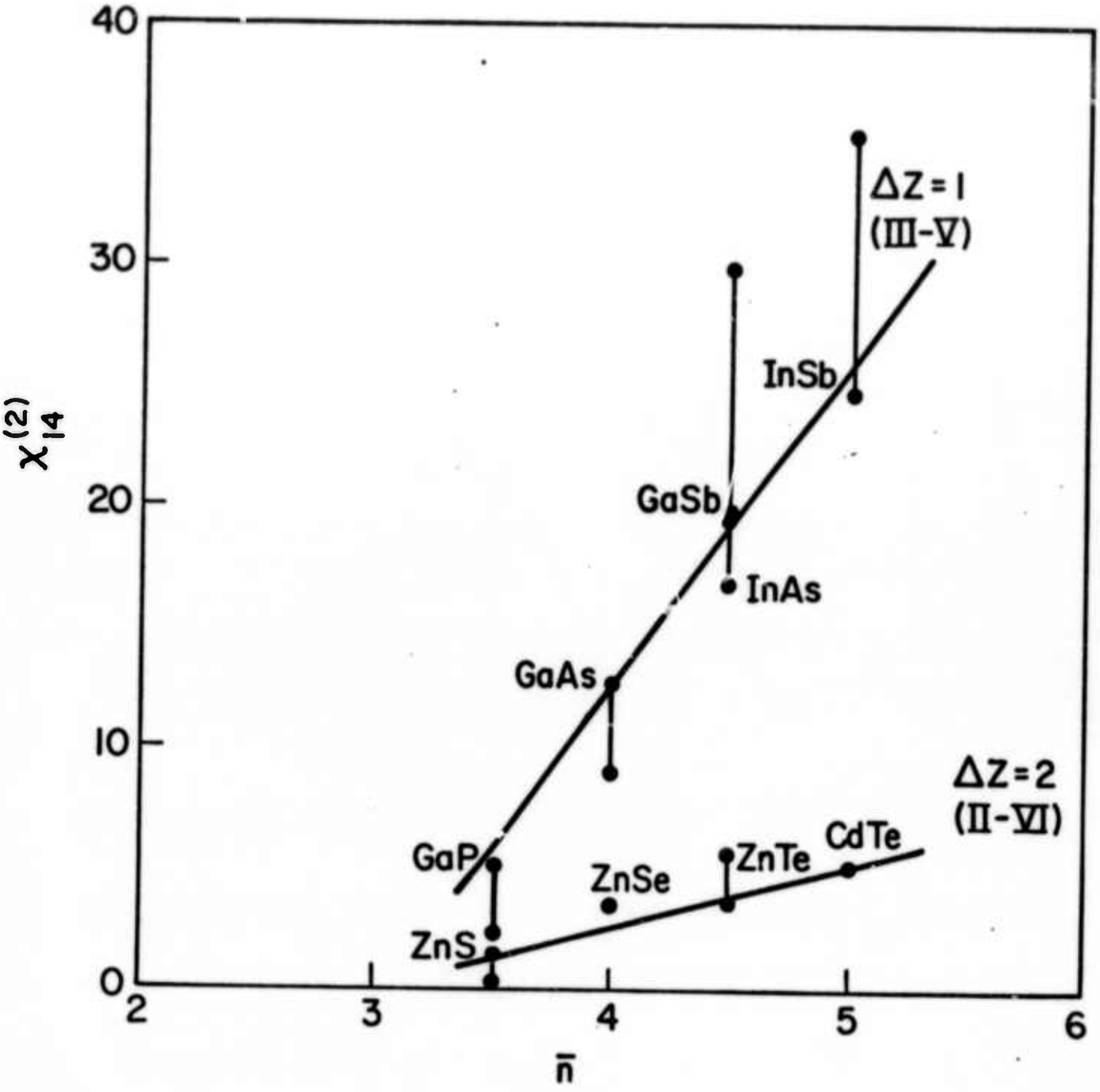
40
30
20
10
0
2
3
4
5
6
$\chi^{(2)}_{14}$
$\bar{n}$
ΔZ=1
(III-V)
InSb
GaSb
InAs
GaAs
ΔZ=2
(II-VI)
GaP
ZnSe
ZnTe
CdTe
ZnS

FIGURE 3